Improved Distribution Feeder and Load Modeling in Power Systems using Electro Magnetic Transient Models

by

Sameer Nekkalapu

A Dissertation Presented in Partial Fulfillment
of the Requirements for the Degree
Doctor of Philosophy

Approved July 2022 by the
Graduate Supervisory Committee:

Vijay Vittal, Chair
John Undrill
Raja Ayyanar
Meng Wu

ARIZONA STATE UNIVERSITY

August 2022

ABSTRACT

With the increasing penetration levels of distributed energy resources along distribution feeders, the importance of load modeling has grown significantly and therefore it is important to have an accurate representation of the distribution system in the planning and operation studies. Although, currently, most of the power system studies are being done using positive sequence commercial software packages for computational convenience purposes, it comes at the cost of reduced accuracy when compared to the more accurate electromagnetic transient (EMT) simulators (but more computationally intensive). However, it is expected, that in the next several years, the use of EMT simulators for large-scale system studies would become a necessity to implement the ambitious renewable energy targets adopted by many countries across the world. Currently, the issue of developing more accurate EMT feeder and load models has yet to be addressed.

Therefore, in the first phase of this work, an optimization algorithm to synthesize an EMT distribution feeder and load model has been developed by capturing the current transients when three-phase voltage measurements (obtained from a local utility) are played-in as input, from events such as sub-transmission faults, to the synthesized model. Using the developed algorithm, for the proposed feeder model, both the load composition and the load parameters have been estimated. The synthesized load model has a load composition which includes impedance loads, single-phase induction motor (SPHIM) loads and three-phase induction motor loads.

In the second phase of this work, an analytical formulation of a 24 V EMT contactor is developed to trip the air conditioner EMT SPHIM load, in the feeder and load model developed in Phase 1 of this work, under low voltage conditions. Additionally, a new

methodology is developed, to estimate and incorporate the trip and reconnection settings of the proposed EMT contactor model to trip, reconnect and stall the SPHIMs in a positive sequence simulator (PSLF) for single-line to ground faults. Also, the proposed methodology has been tested on a modified three-segment three-phase feeder model using a local utility's practical feeder topological and loading information. Finally, the developed methodology is modified to accommodate three-phase faults in the system.

ACKNOWLEDGEMENTS

I would like to first and foremost express my sincerest gratitude to my advisor, Dr. Vijay Vittal, whose encouragement, guidance, and support have motivated me to make significant progress on this research and complete my dissertation. Without his timely inputs and deep insights, this project would not have been possible. I am especially grateful to him for sticking up with me during some of my low times in my graduate studies.

I also credit the success of my PhD degree to Dr. John Undrill for his substantial inputs to my research and for the countless hours discussing the practical issues associated with this work.

I also want to express my gratitude to Dr. Raja Ayyanar and Dr. Meng Wu for their time and consideration in being a member of my graduate supervisory committee.

I would also like to thank Dr. Bo Gong, Mr. Brian Keel and Mr. Ken Brown from the Salt River Project company for providing us the data and the research funding that helped facilitate this work.

I especially want to thank my parents Mr. Ravindra Kumar Nekkalapu and Mrs. Madhavi Nekkalapu for their support of my higher education. I am also grateful to my grandparents, Mr. Mohan Rao Kondrupati and Mrs. Samrajyam Kondrupati for their constant care and guidance throughout my PhD. I would like to thank my uncle and aunt, Mr. Srinivasa R Nalajala and Mrs. Renuka Nalajala, for their hospitality and guidance during various times in my PhD. I also would like to thank my friends and roommates who encouraged me and provided constant support and companionship during this journey to make it a fun and enjoyable ride.

TABLE OF CONTENTS

CHAPTER Page

LIST OF TABLES

Table Page

LIST OF FIGURES

Figure Page

Figure Page

NOMENCLATURE

a	a^{th} node in the local utility feeder data
b	b^{th} node in the local utility feeder data
b_0	Linear Regression Bias
b_1	Fault angle coefficient
b_2	Fault duration coefficient
b_3	Positive sequence feeder head voltage nadir coefficient
c_1, c_2	Unknown constants to model contactor spring force
CIGRE	International Council on Large Electric Systems
D	Power raised to the 3PHIM speed to calculate load torque
DER	Distributed Energy Resource
DFR	Digital Fault Recorder
DG	Distributed Generation
DNN	Deep Neural Network
E	Objective Error function between the square of feeder head measured current and feeder head simulated current
EV	Electric Vehicle
f	Activation function
FA	Fault angle in single-line to ground fault analysis
FA_{3ph}	Fault angle in three-phase fault analysis
FD	Fault duration in single-line to ground fault analysis
FD_{3ph}	Fault duration in three-phase fault analysis

FIDVR	Fault induced delayed voltage recovery
F_g	Contactor gravitational force
F_{mag}	Contactor magnetic force
FN	Positive sequence feeder head voltage nadir normalized using its pre-fault steady state voltage for single-line to ground faults
FN_{3ph}	Positive sequence feeder head voltage nadir normalized using its pre-fault steady state voltage for three-phase faults
g	Acceleration due to gravity
h1	Number of no loaded nodes along the radial line
h2	Number of loaded nodes along the radial line
i	Neuron number
i_c	Coil current
i_s	Shading Coil current
I	Simulated feeder head currents vector
I_m	Measured feeder head currents vector
I_{ma}	Phase A measured feeder head current
I_{mb}	Phase B measured feeder head current
I_{mc}	Phase C measured feeder head current
IMS	Measured total number of feeder segments in which SPHIMs Stalled
IMS_{est}	Estimated total number of segments in which SPHIMs stalled

I_r	RMS current of the faulted phase current
j	Layer number
J	Jacobian vector
k	Iteration number
k_0	Initial load percentage pickup
k_1	First spring constant
k_2	Second spring constant
lo	loaded nodes in the local utility feeder data
m_{ab}	Sparse matrix element obtained from the a^{th} row and b^{th} column
M	Mass of the armature
n	Segment number along the feeder model
n_{ab}	Section number between node a and node b
nl	no-loaded nodes in the local utility feeder data
n_1	Number of main coil turns
n_2	Number of shading coil turns
NV	Neuron value
p	Original parameter of interest in load synthesis procedure
POW	Point-On-Wave
pr	Original parameter in DNNs
pr'	Normalized parameter from pr in DNNs
PSCAD	Power System Computer Aided Design
PSLF	Positive Sequence Load Flow Simulator

R_c	Coil resistance
R_s	Shading Coil resistance
$R_{seg,n}$	Value of resistor used to represent the resistive load in the nth segment of the feeder
R_{0c}	Zero Sequence resistance of the conductor
R_{1c}	Positive Sequence resistance of the conductor
$RMSE_{current}$	Root mean square error of measured current of a particular phase
S_1	Machine rating of 3PHIMs
S_2	Machine rating of SPHIMs
$Scale_1$	Number of motors in 3PHIM load
$Scale_2$	Number of motors in SPHIM load
$Signal_t$	Value that indicates if the contactor is closed (0) or tripped (1) obtained at the t^{th} time step
SPHIM	Single-Phase Induction Motor
ST	Status of the contactor (no tripping, chattering or tripping) for single-line to ground fault analysis
ST_{3ph}	Status of the contactor (no tripping, chattering or tripping) for Three-phase fault analysis
t	Time in secs
T1	Time taken for the EMT contactor to electrically disconnect the load or starts to chatter (after SLG fault is applied in the system)
$T1_{3ph}$	Time taken for the EMT contactor to electrically disconnect the load

	or starts to chatter (after three-phase fault is applied in the system)
T2	Time taken for the EMT contactor to initiate reconnection to the feeder (after SLG fault is applied in the system)
T2	Time taken for the EMT contactor to initiate reconnection to the feeder (after three-phase fault is applied in the system)
$T_{mechanical}$	Load torque of 3PHIMs
TMS	Measured total number of feeder segments in which SPHIMs Stalled
TS	Transient Simulator
VaV1 Segz	Measured terminal voltage (at the '*T1*' time instant after the fault is initiated) at the zth segment contactor in the faulted phase normalized using its pre-fault steady state voltage obtained from PSCAD.
VaV2 Segz	Measured terminal voltage (at the '*T2*' time instant after the fault is initiated) at the zth segment contactor in the faulted phase normalized using its pre-fault steady state voltage obtained from PSCAD.
V1	Feeder head voltage level (in pu) at which the EMT contactor starts to electrically disconnect or starts to chatter (after SLG fault is applied) normalized using its pre-fault steady state voltage.
$V1_{3ph}$	Feeder head voltage level (in pu) at which the EMT contactor starts to electrically disconnect or starts to chatter (after three-phase

	fault is applied) normalized using its pre-fault steady state voltage.
v_c	Voltage excitation of the coil
$V2$	Feeder head voltage level (in pu) at which the EMT contactor starts to electronically reconnect (after the SLG fault is cleared) normalized using its pre-fault steady state voltage.
$V2_{3ph}$	Feeder head voltage level (in pu) at which the EMT contactor starts to electronically reconnect (after the three-phase fault is cleared) normalized using its pre-fault steady state voltage.
W	DNN weights vector
x	Distance between the armature and the stationary part of the EMT contactor
x_c	Contact gap
x_{max}	Maximum distance between the armature and the stationary part of the EMT contactor
x_t	Value of x at t^{th} time step
X	Vector of neuron values of previous layer
X_{0c}	Zero sequence reactance of the conductor
X_{1c}	Positive sequence reactance of the conductor
Y_{train}	Output value given during linear regression training process
Y_{test}	Output value estimated during linear regression testing process
z	z^{th} segment
Z_{eq}	Equivalent impedance of the total radial path

Z_{lo}	Impedance in the lo^{th} loaded section
Z_{nl}	Impedance in the nl^{th} no load section
3PHIM	Three-Phase Induction Motor
α	Step size used in the optimization process
α_1	Step size obtained from the quadratic interpolation step
α_2	Step size obtained from the cubic interpolation step
β	Small perturbation given to calculate numerical Jacobian vector
ε	Infinitesimally small perturbation
ϕ_c	Flux linkage passing through the main coil
ϕ_s	Flux linkage passing through the shading coil
γ	Proportional value in Condition B
γ_0	Perturbation given to calculate parameter sensitivity
η	Permeability of the core
η_0	Permeability of air
η_r	Relative permeability of the core
μ	Set of parameters of interest to be estimated using the optimization Procedure
μ_0	Parameter of interest being estimated using the optimization Procedure
$\mu_{0,\text{ lower bound}}$	Upper bound of μ_0
$\mu_{0,\text{ upper bound}}$	Upper bound of μ_0
μ_{final}	New value of μ_0 at the end of the iteration

μ_{prev}	Value of μ_0 in the previous iteration
μ_{pr}	Mean of total samples of *pr* population
ρ	Tolerance for case convergence criterion
σ_{pr}	Standard deviation of total samples of *pr* population
ω	3PHIM speed
Ω_0	Logit transformed parameter from μ_0

CHAPTER 1

INTRODUCTION

1.1 Background of this research

Load modeling is one of the important features that determines the nature in which the load responds to disturbances in the power system during transient conditions when there is a change in the voltage or frequency in the system network [1]. Although, the importance of the load modeling is widely recognized by the power system researchers and engineers [2], it is of vital importance to update and improve the existing load models to understand the modern distribution system behavior especially due to the emergence of the smart grid technologies such as distributed generation (DG), electric vehicles (EV's), and demand side management [3]. However, due to the following reasons it is very challenging to accurately represent the load behavior in bulk power system studies:

- Continuously varying weather-dependent load composition
- Lack of measurements across most of the feeders in the system
- Varied load responses for different loads due to varying dynamic behavior for the same disturbance event
- Number of loads spread across various nodes in the distribution feeder are too complex to be represented in a computationally feasible manner in a simulation.

In essence, the problem of load modeling becomes a two-step problem – (i) Identifying the load model structure (ii) Identifying the load model parameters and composition. Typically, in the literature, load models are considered to be aggregated models to reduce the computational complexity in the dynamic simulations. However, as mentioned in (i), it is

also important to choose an appropriate feeder structure to distribute the loads across the feeder to represent the reality without losing the computational edge gained from the aggregated load models. Additionally, it is also important to choose different types of load models that capture the aggregated behavior response of various load devices that are typically used in residential and industrial/commercial areas such as air conditioners, refrigerators, water heaters, facility heating/cooling/ventilation, pumps, fans, lighting, and electronic devices such as computers. Finally, an appropriate algorithm must be implemented to estimate the load model parameters and the load composition that captures the distribution system behavior as accurately as possible.

In addition to accurately representing the loads, it is also important to represent the devices that are used for protection of these loads appropriately in power system simulations. For example: 24-V contactors are typically used in the residential feeders to protect the single-phase induction motors (SPHIMs) under low voltage conditions that occur frequently in the distribution system due to the faults that originate in the 69 kV sub-transmission system [4]. Therefore, it is imperative that the impact of the load protection devices on the system response, in the load modeling studies, are also studied in detail. To achieve this, choosing the right model for load protection devices becomes equally important in representing the distribution system in power system studies.

1.2 Goals and Overview:

With the ever-increasing penetration levels of the distributed energy resources (DERs) in the power system, the importance of representing the distribution system as accurately as possible in the transmission operation and planning studies [5] has also been

increasing. Therefore, the overall objective of this work is to develop techniques to improve the current feeder and load models existing in the literature. As mentioned earlier, it is important to have a good representation of both the load models and their protection devices modeled in the simulation studies to accurately represent the distribution system. Based on this, the major goals of the research presented in this work are listed as follows and the relevant literature review (current, past and the research gaps) has been provided in the subsequent chapters as necessary –

- 1. *Load Composition and Load Parameters Estimation:* For the considered feeder model structure from [6], an algorithmic approach to estimate the load composition and the load parameters for the load models assumed in this work has been presented in detail using point-on-wave (POW) voltage and current measurements, at the low voltage end of the 69/12.47 kV substation, obtained from a local utility. The estimated load composition and the load parameters are then validated using new test cases at the same locations, the load composition and parameters are estimated, during both summer and winter conditions. The ability of the proposed algorithm to capture fault induced delayed voltage recovery (FIDVR) type phenomenon has also been discussed in detail.
- 2. *Develop an analytical model for a 24 V EMT contactor for SPHIMs:* An electromagnetic contactor model is typically utilized to switch the load (SPHIMs in this work) or circuit they control which is dependent on the magnetic force generated in the designed contactor based on the voltage excitation provided at its terminals. The set of differential equations that make up this model (mathematical formulation) has

been explored in detail in this work.

- 3. *Comparison between the EMT contactor model and the positive sequence contactor model:* The differences in the performance of the proposed 24 V EMT contactor model compared to a contactor logic (CL) model developed based on its corresponding positive sequence contactor model currently used in the '*cmpldw*' model [7] being used in the industry has been discussed in detail.
- 4. *Estimate the trip and reconnection characteristics of the proposed 24 V EMT contactor:* Typically, the transmission planning engineers, and the local electric utility engineers have access to the system measurements at the low voltage end of the 69/12.47 kV substation from the available digital fault recorders (DFRs) for events that occur at the 230 k, 69 kV and 12. 47 kV level of the system. Therefore, using the developed analytical EMT contactor model, it is important to develop an algorithmic approach to estimate its trip and reconnection characteristics based on the head of the feeder voltage head characteristics. Several regression models have been developed for this purpose and have been discussed in this report.
- 5. *Study the impact of the estimated EMT contactor characteristics on corresponding positive sequence models:* Presently, most of the distribution system studies conducted in industry involve positive sequence modeling. However, the parameters for the contactor models currently being employed for the positive sequence motor loads have not been validated yet. Therefore, the EMT contactor trip and reconnection settings estimated using the developed regression models have been used to trip the 'motorc' model in PSLF to study its impact on the system response.

1.3 Organization of Thesis

This report is organized into six chapters:

The first chapter presents the background of the research presented in this report. Objectives and the overview of the work presented in this report are also discussed in this chapter.

Chapter 2 mainly deals with a novel feeder structure proposed in this work based on [6], where different types of loads, feeder components and the contactor model are used in the distribution feeder model proposed in this work.

Chapter 3 provides an algorithmic approach to estimate the load composition and the load parameters of the proposed distribution feeder and load model using voltage and current measurement data obtained from a local utility at the low side of the 69/12.47 kV substations in both summer and winter loading conditions for both residential and industrial/commercial feeders. The estimated load composition and the load parameters are then validated using four new test cases for the same feeder locations in both summer and winter conditions.

Chapter 4 presents the analytical formulation of the developed EMT contactor model in this work. Comparison between the performance of the proposed EMT contactor model and the contactor logic developed based on the existing positive sequence contactor model is presented. The necessity to represent the EMT contactor trip and reconnection characteristics in the currently used positive sequence contactor models is discussed in detail.

Chapter 5 details the regression models developed in this work to estimate the trip and reconnection settings of the proposed EMT contactor model. The estimated settings are then used to trip the 'motorc' single-phase induction motor model in PSLF to observe the impact of the estimated trip and reconnection settings in a positive sequence simulation environment.

Chapter 6 presents the methodology to utilize a practical feeder data obtained from a local utility to modify the topology and the load distribution of the proposed feeder and load model to validate the results obtained for the algorithm developed in Chapter 5.

Chapter 7 discusses the methodology to estimate the EMT contactor characteristics and the SPHIM stalling behavior for three-phase faults and some recommendations are discussed to improve the proposed methodology as part of future work.

The conclusions from this work have been provided in the Chapter 8 of this report. Possible future works based on the improved feeder and load model are also discussed in this chapter.

CHAPTER 2

FEEDER'S INDIVIDUAL COMPONENTS DESIGN

2.1 Introduction

Until 1980's, the load in the power system had been represented using a constant current model (to represent active power 'P' drawn by the loads) and a constant impedance (to represent reactive power 'Q' drawn by the loads) to reduce the complexity of the distribution system in planning studies. Since then, a load model as a combination of both static load and induction motors such as 'ZIP+IM' [8], 'CLOD' [9] have started to become popular in the literature which is simple in its structure but also able to represent the complex load dynamics of the distribution system more accurately compared to the earlier representation (constant 'I' for 'P' and constant 'Z' for 'Q') of loads. The CLOD model has been presented in Figure 2.1 below –

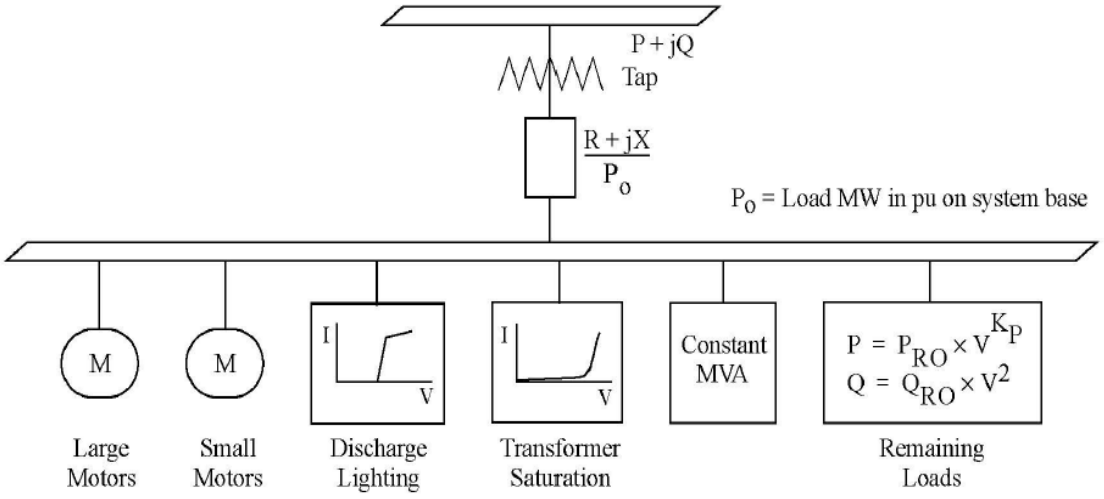

Figure 2.1 CLOD Model Schematic [9]

However, in the late 2000's, it was observed that even this type of representation of the loads is not sufficient to capture FIDVR [10] type events following a number of 230

kV transmission faults in the South California region [11]. The engineers from Southern California Edison (SCE) and Florida Power and Light (FPL) have deduced that the delay in the post-fault voltage recovery in these kinds of events occur due to the stalling of the SPHIMs [12] in the air conditioners in the residential areas near the location of the fault. This is because of the low-inertia in the air-conditioner SPHIMs, and their inability to re-accelerate to their nominal speeds even after the fault is cleared. Therefore, efforts have been made to develop an aggregated representation of a performance based single-phase induction motor, as part of the composite load model '*cmpldw*' [7], which is a set of algebraic equations (developed based on the performance of the many laboratories tested single-phase induction motors) to capture this FIDVR phenomenon.

This composite load model also comprises of an aggregated representation of the three-phase induction motors with varied inertias (high inertia for Motor B, low inertia for Motor A and Motor C) and load torques (constant load torque for Motor A, load torque proportional to motor speed squared for Motor B and Motor C) representing different kinds of three-phase induction motor loads such as commercial ventilation fans, commercial water circulation pumps, central cooling systems used in commercial buildings. Motor A, Motor B and Motor C models are represented as three-phase double-cage induction motors. The composite load model also comprises of the electronic load (represented as a constant PQ load with a constant power factor) and the static load (represented as a ZIP load model). The schematic of the composite load model '*cmpldw*' [7] is presented in Figure 2.2 below. It should be noted that all the aggregated loads in the '*cmpldw*' model have been placed at the end of the feeder (with a feeder equivalent impedance of R_{fdr} + X_{fdr}). Detailed

description of each of its parameters for this model is presented in [7].

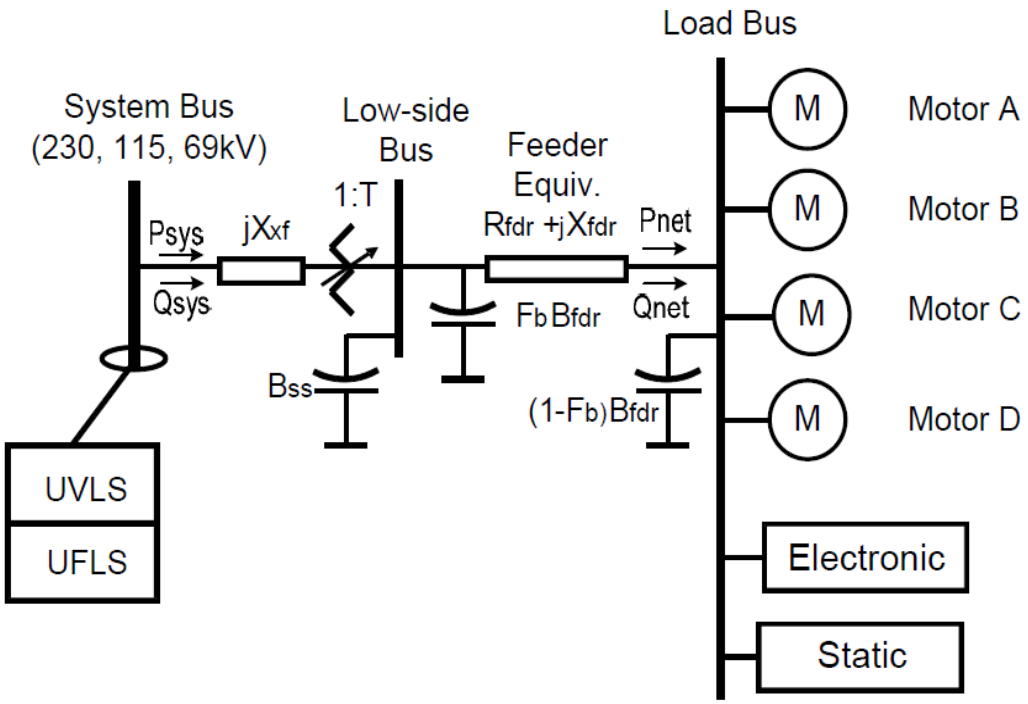

Figure 2.2 '*cmpldw'* Model in [7]

This combination of varied types of load models in the composite load model is important to capture the complex load dynamics and their impact on the power system and is currently being used to conduct transient stabilities to meet the NERC transmission planning standards [13] in the industry.

Therefore, taking this important factor into consideration, a close consultation was conducted with the local utility engineers (who provided the POW measurement data, obtained from the local city substations, for this work) regarding the types of load present on the distribution feeders for which the measurement data is provided. Based on this discussion, it was understood that the data that they provided was for two types of feeder areas (residential and industrial/commercial) under both summer and winter loading

conditions for each type of feeder. As mentioned earlier, it should also be noted that one of the main objectives of this work is to estimate the load composition and the load parameters for the proposed feeder model (whose structural details are discussed in detail in Chapter 3) using POW voltage and current measurements. Therefore, it is important to choose a specific set of electromagnetic transient (EMT) load models to capture the transient behavior of the proposed feeder and load model, as accurately as possible, for the considered POW measurements. Additionally, in Chapter 4 and Chapter 5, the development of a 24-V EMT contactor (for the EMT SPHIMs considered in the proposed feeder model) and the incorporation of its estimated trip and reconnection settings into tripping the single-phase induction motors ('motorc') in the positive-sequence simulation has been discussed in detail. Therefore, it is also important to choose an appropriate contactor model in this work.

Based on the factors discussed above, the following loads, contactor and feeder components have been incorporated into the proposed feeder model in this work. Detailed description for each of these components have also been presented in the sub-sections below -

1. SPHIM loads.
2. 3PHIM loads.
3. Impedance loads.
4. Contactors for SPHIMs
5. Line Impedances

6. Distribution transformers

2.2 Single -Phase Induction Motors

On hot summer days, SPHIMs are the most predominant type of load in residential areas due to the large amount of power consumption from air conditioners. For this reason, a user-defined POW SPHIM model developed in [12] has been used for this work. This motor model is a transient model of air-conditioner compressor single-phase motor. A run capacitor of 40 μF is used in this model. From [12], the load torque of the SPHIM is taken to be a sawtooth waveform, a combination of speed dependent torque (Tspeed) and angle dependent torque (Tav), as depicted in Figure 2.3.

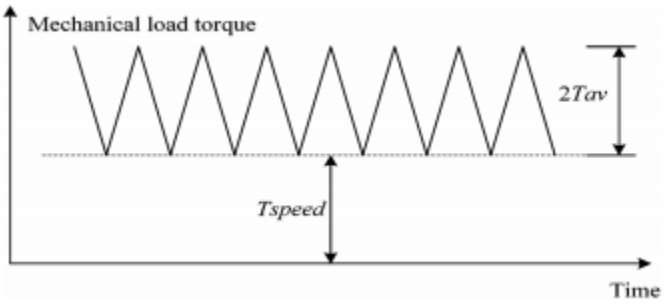

Figure 2.3 Load Torque Profile for SPIM [12]

2.3 Three-Phase Induction Motors

The three-phase induction motor model considered in this work is the double cage squirrel type motor model because of its dominant presence in most of the motors present in a typical distribution feeder. For this model, in PSCAD/EMTDC, torque control mode is used to operate the three-phase induction motors. These are motors which are typically rated at 460 V line-line RMS.

The mechanical torque, in pu, of this motor is modeled using the following equation:

$$T_{mechanical} = k * \omega^{D}$$

Where, k is the initial load percentage pickup factor (0.65 in this case)

ω is the speed of the motor in pu and D can be 0 (such as commercial air conditioners, refrigerators), 1 (such as conveyor belts and reciprocating pumps) or 2 (such as fans, blowers). It should be noted that in this work D = 1 has been chosen to reduce the computational complexity of the considered feeder and load model. Only one (D =1) of the above load torque profiles has been considered in this work based on the suggestion provided by the load modeling task force committee [14]. In [14], it has been recommended to consider D = 1, which is taken to be the average of pumps and fans type of load characteristics, while modeling 3PHIMs in general scenarios with not much information known about the load on the feeder. Additionally, the local utility engineers have also been consulted about the chosen value for D to be 1 based on their expertise and knowledge about the considered feeder and load models in this work. The initial values of the electrical parameters for the considered 3PHIM model [15] chosen for this work has been presented in Chapter 3 in detail.

2.4 Overhead Lines

The feeder model is assumed to have a total maximum voltage drop of 5% across its length, in accordance with the recommendation provided by National Electrical Code (NEC) [6], [16]. Typical overhead line parameters from [17] are used in this model to present the distribution lines, shown in Table 2.1.

Table 2.1 Line Impedances Data [17] Considered in the Feeder Model of this Work

Impedance Type	**Positive Sequence Impedance Value**	**Negative Sequence Impedance Value**	**Zero Sequence Impedance Value**
Resistance (ohm/mile)	0.3	0.3	0.798
Inductive Reactance (ohm/mile)	0.64	0.64	2.04
Capacitive Reactance (Mohm/mile)	0.01	0.01	0.01

2.5 Distribution Transformers

As discussed in [6], for a typical feeder pick-up event, it can be inferred that the first few cycles of the current inrush characteristics do not depend primarily on the type of load present on the feeder and is mainly dependent on the distribution transformer saturation characteristics. In PSCAD [18] simulation, the critical parameters including transformer knee curve characteristics, which is a function of transformer magnetizing current, knee voltage and air core reactance are used to represent saturation in the transformers in this work. These parameters are obtained from [6] using a manually tuned method.

Although, it is necessary to utilize the distribution transformers in the proposed feeder model to step down the voltage from 7.2 kV level to lower load level voltages (115 V (resistive load), 230 V (SPHIMs) and 460 V (3PHIMs)), for the considered SLG fault cases (which are described in greater detail in Chapter 3) in this work, the dynamic behavior of the proposed distribution transformers would be impacted very minimally. This is

because the distribution transformers are fully magnetized at the time of occurrence of the fault and hence the issue of transformer saturation would not be present.

However, for the feeder pick-up case analyzed in [6], in which the feeder of interest (with pre-dominantly industrial load) has been out of service for a significant amount of time (because it got tripped due to a storm in the nearby area) and hence all the loads and the distribution transformers across the feeder are de-magnetized completely by the time the feeder has been reclosed. In the simulations conducted in this case, it was observed that the starting current transients immediately after the closing of the feeder is primarily dependent on the distribution transformer saturation characteristics rather than the load type characteristics.

In this feeder pick-up case, the load models and the feeder structure are the same that has been used in this work. Although, the distribution transformer parameters are not sensitive to the played-in voltages, in this work for the considered transmission fault events, it is important to represent the distribution transformer parameters accurately in the considered feeder and load model to make it realistic and would be useful to study the feeder behavior for feeder pick-up events for the local utilities. It should be noted that a resistor (signifying the distance between the transformer from each segment of the feeder model), whose value is 0.5 ohm, has also been included in series with the distribution transformer to ensure the transformer saturation dies out after a few cycles during the cold load pickup of the feeder. Based on [6], the transformer parameters chosen for this work, to capture the transformer saturation phenomenon, are presented below in Table 2.2.

Table 2.2 Distribution Transformer Parameters

Leakage Reactance	0.02 pu
Air Core Reactance	0.02 pu
Inrush Decay Constant	0.25 sec
Magnetizing Current	2 %
Knee Voltage	1.17 pu
Saturation Enabled	Yes
Voltage Ratio (line to neutral RMS)	7.2 kV/ 265 V

2.6 SPHIM Contactor Models

A 24 V EMT contactor model has been developed in this work to trip the 230 V EMT SPHIMs under low voltage conditions. Unlike the contactor logic (which, the positive sequence contactor models that are typically being used in the industry currently use), a set of differential equations is utilized in the proposed 24 V EMT contactor model in PSCAD to capture the detailed dynamics of a typical 24 V contactor present in the distribution system under low voltage conditions. More details (about this contactor model and the algorithm to estimate its trip and reconnection settings) about this model are discussed in Chapter 4 and Chapter 5 of this report.

CHAPTER 3

FEEDER AND LOAD MODEL SYNTHESIS

3.1 Literature Review

There is a growing need to develop accurate feeder and load models to replicate the behavior of actual distribution systems in transmission planning and operation studies [3], [19]. However, due to the unavailability of accurate load parameters and load composition it is increasingly difficult to model an accurate distribution feeder in power system analysis [20]. In the literature, two types of approaches have been used to estimate the load parameters: component-based approaches and measurement-based approaches. The former approach [21], [22] primarily relies on load surveys whereas the latter approach uses field measurements. A recent survey conducted by CIGRE [23] shows that a majority of 50 utilities on 5 continents adopt measurement-based approaches. Currently, there are two predominant types of measurement-based methods: static load modeling method [24]-[25], which estimates load parameters based on a ZIP (constant impedance, constant current and constant power) model, and composite load modeling method [26]-[27], which expands beyond the ZIP model by including more dynamic load components such as motor models. All these approaches deal with root mean square (RMS) dynamic load models that uses RMS measurements and are typically used in positive sequence transient stability (TS) simulators [28] due to the advantages they offer such as higher computational speed, at large time steps of milliseconds, for grid-level system studies.

In the literature, the most common measurement-based approach to model a distribution feeder is to represent it as an aggregated RMS based composite load model at

the end of the feeder [26] in positive sequence TS simulators. However, this aggregated representation of RMS composite loads is not useful in capturing severe system responses such as fault induced delayed voltage recovery (FIDVR) phenomenon, which may potentially lead to voltage stability concerns [29], [30] in the grid. This FIDVR phenomenon is typically caused by low inertia, air conditioner compressor, single-phase induction motors (SPHIMs) stalling, especially under asymmetric fault conditions [12]. However, positive sequence TS simulators do not accurately capture the impact that the asymmetric fault conditions have on the air conditioners response [31]. Also, based on the laboratory tests conducted in [32], motor stalling depends on the point on the sinusoidal waveform at which the voltage dip is seen at the terminals of the motor and therefore positive sequence TS simulators, that use RMS signals in their analysis, cannot capture this point on wave (POW) phenomenon as EMT simulators do.

Despite the computational burden the EMT dynamic models bring with them in the EMT simulators, network owners and system operators in various countries are progressively using EMT based offline large-scale system studies [33], [34] for which there is an increasing need to develop accurate EMT based dynamic load models in a distribution system [31]. *Currently, a systematic approach to validate the EMT dynamic load models using instantaneous point-on-wave (POW) field measurements, that EMT simulators use, is still missing in the literature and this issue has been addressed in this work.*

These issues are addressed in the proposed model structure proposed in this work and by utilizing POW measurements to capture the FIDVR phenomenon. As mentioned in Chapter 2 of this report, it comprises of feeder sections, distribution transformers, distributed three-phase motor loads, distributed single-phase motor loads, and distributed

resistive loads. It should be noted that the 24 V EMT contactor model (as mentioned in Chapter 2), is added as an additional component from Chapter 3 of this report to the basic feeder and load model considered in this Chapter to further improve the feeder model.

Utility companies typically record feeders' disturbance response through meters at distribution substations. Using these measurements, a POW based technique is introduced in this Chapter. It synthesizes the load and feeder models so that they can accurately capture transient responses when the system is subjected to actual system events such as transmission system faults and feeder pick-up events.

Additionally, none of the works in the literature, provide an approach to estimate the load composition in a distribution feeder at an EMT level analysis. Therefore, using the proposed POW technique, POW voltages measured at the distribution substations during disturbances are played-in to the proposed feeder model to estimate the load composition and the motor load parameters. The estimated parameters of the proposed feeder load models are then adjusted, using a non-linear least squares algorithm, to obtain a good match between the simulated currents and their corresponding currents measured at the substations. The EMT simulator, PSCAD/EMTDC [18], is used to simulate the waveforms obtained from the model response.

3.2 Case Setup

POW voltage measurements, obtained at the distribution substation for events that occurred at the sub-transmission level or along the feeder, are played-in to corresponding residential and industrial/commercial feeder and load models. The detailed description for these events is provided in Table 3.1.

Table 3.1 Event Details of the Test Cases 1-4

	Case 1	**Case 2**	**Case 3**	**Case 4**
Event Type	**Phase-A SLG fault on Substation K Circuit Breaker**	**Phase-A SLG fault on Substation A 69 kV line**	**Phase-A SLG fault on Substation K Circuit Breaker**	**Phase-A SLG Fault on Substation A 69 kV line**
Event Voltage level	69 kV	69 kV	69 kV	69 kV
Time of Event	10:33 AM	5:36 PM	10:33 AM	5:36 PM
Date of Occurrence	8th Aug, 2016	11th Nov, 2016	8th Aug, 2016	11th Nov, 2016
Measurements Location	Substation A	Substation A	Substation B	Substation B
Measurements kV level	12.47 kV	12.47 kV	12.47 kV	12.47 kV
Total Feeder MVA loading	18.33	7.23	23.07	13.59
Voltage Dip % in the Faulted Phase	51%	30%	43%	26%

In this work, the proposed non-linear least squares optimization is first implemented for 4 representative cases to evaluate the efficacy of the approach at different loading conditions, different load classes (residential and industrial/commercial feeders), and during different seasons (summer and winter conditions). From Table 3.1, it can be observed that events corresponding to Case 1 and Case 3 occurred during summer conditions whereas Case 2 and Case 4 occurred in winter. Based on the feeder class information provided by the local utility, it is known that the voltage and currents measurements used for Case 1 and Case 2 are obtained for a residential feeder. Similarly,

the measurements used in this work for Case 3 and Case 4 correspond to an industrial/commercial feeder.

With the proposed algorithmic approach, the load composition and the load parameters obtained for Cases 1- 4, from Table 3.1, are used to estimate the load composition and the motor load parameters. To validate the estimated parameters and load composition, obtained for Cases 1-4, testing has been conducted on 4 new test cases, Cases 5-8, with measurements obtained at the same two substations (Substation A and Substation B) during both summer and winter loading conditions as shown in Table 3.2. From Table 3.1 and Table 3.2, it can be observed that all the events are single line to ground faults that occurred at the 69-kV sub-transmission level and 230-kV transmission level, respectively.

Table 3.2 Event Details of the Test Cases 5-8

	Case 5	**Case 6**	**Case 7**	**Case 8**
Event Type	**Phase-A SLG fault on Substation S Circuit Breaker**	**Phase-C SLG fault on Substation K 230 kV line**	**Phase-A SLG fault on Substation S Circuit Breaker**	**Phase-C SLG Fault on Substation K 230 kV line**
Event Voltage level	230 kV	230 kV	230 kV	230 kV
Time of Event	5:52 AM	10:34 PM	5:52 AM	10:34 PM
Date of Occurrence	17th Jun, 2016	19th Oct, 2015	17th Jun, 2016	19th Oct, 2015
Measurements Location	Substation A	Substation A	Substation B	Substation B
Measurements kV level	12.47 kV	12.47 kV	12.47 kV	12.47 kV
Total Feeder MVA loading	13.71	6.84	19	10.77
Voltage Dip % in the Faulted Phase	18%	21%	18%	21%

The instantaneous voltage and current measurement data are obtained from an electric utility located in the Southwest region of the country, having a sampling frequency of 1921 Hz utilizing Schneider ION 7650 and Schneider ION 8650A meters. The solution time step used in PSCAD is 5 μs. Hence, the voltage measurement data are linearly interpolated in 'Matlab' to achieve a sampling frequency of 200 kHz.

The model representation of Cases 1-8 in PSCAD is shown in Figure 3.1. It can be observed that three-phase feeders (Feeder A, Feeder B and Feeder C) in the actual system, have been represented by a single equivalent aggregated feeder as shown in Figure 3.1. The three-phase voltage measured at the low voltage side of Substation A and Substation B 69/12.47kV transformers are played-in to the aggregated feeder model in PSCAD. The three-phase simulated currents drawn by the aggregated feeder are then compared with their corresponding measured currents.

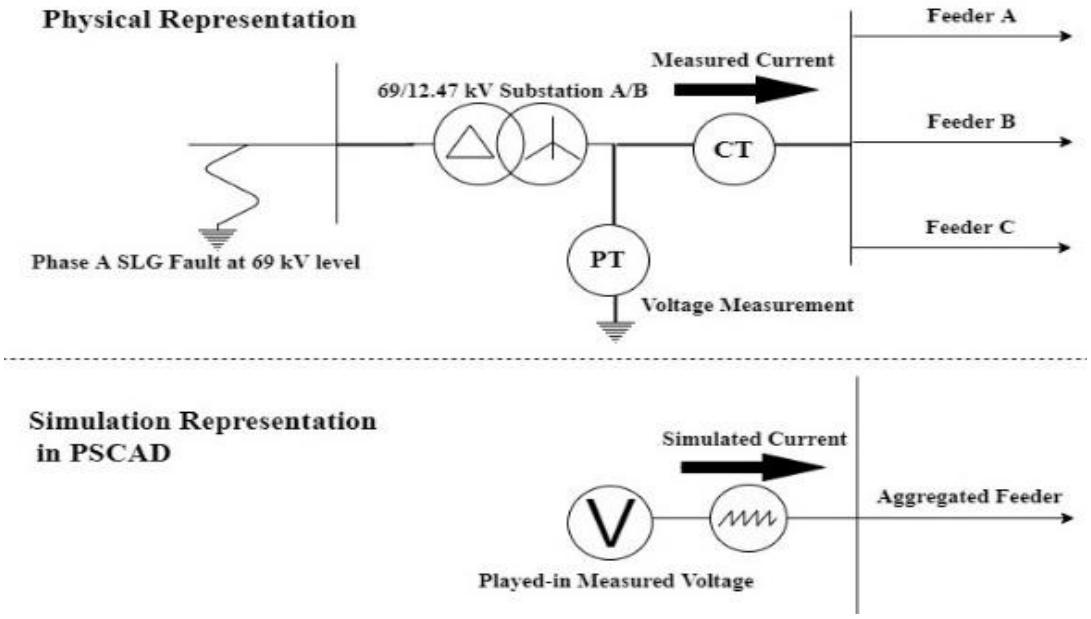

Figure 3.1 Simulation Vs Actual System Representation

For display purposes, the RMS voltages for Case 1 - Case 8 are shown in Figure 3.2 - Figure 3.9 respectively. In Figures 3.10 – 3.12, the POW voltage measurement for phase A (faulted phase), phase B and phase C (non-faulted phases) respectively of Case 1 is presented.

From Figure 3.2, it can be observed that Phase A and Phase B voltages have a nadir at around 50% of the nominal voltage although only Phase A is faulted. The Phase B voltage is affected due to the presence of Δ-Y transformers at the sub-transmission level. In Figure 3.2, from the Phase A voltage, it can be clearly inferred that this fault event is a FIDVR event as the voltage takes a long time to slowly recover to the nominal value. Unlike in Case 1, in Figure 3.3 – Figure 3.9 for Cases 2-8, the voltages recover very quickly, and the voltage nadir is much higher compared to Case 1. This indicates that the event is not a FIDVR type event for the rest of the cases (Cases 2-8).

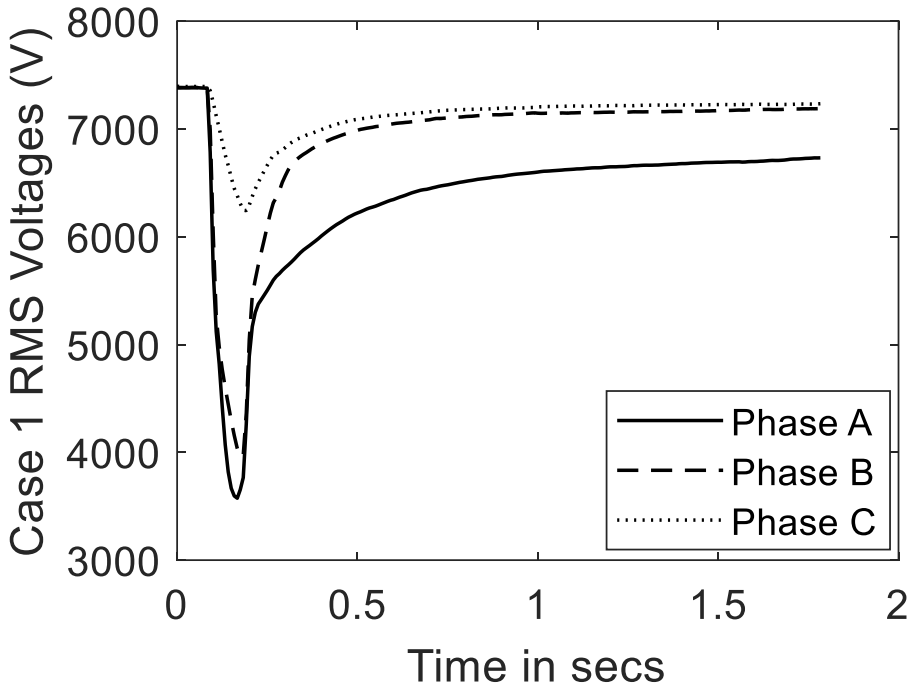

Figure 3.2 Played-in Voltage Measurements (RMS representation) for Case 1

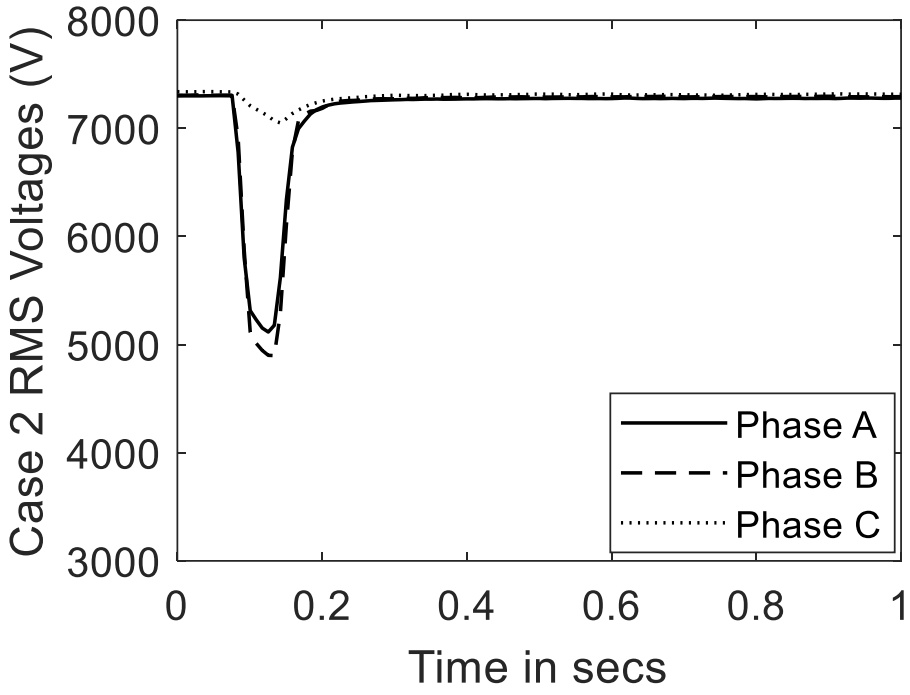

Figure 3.3 Played-in Voltage Measurements (RMS representation) for Case 2

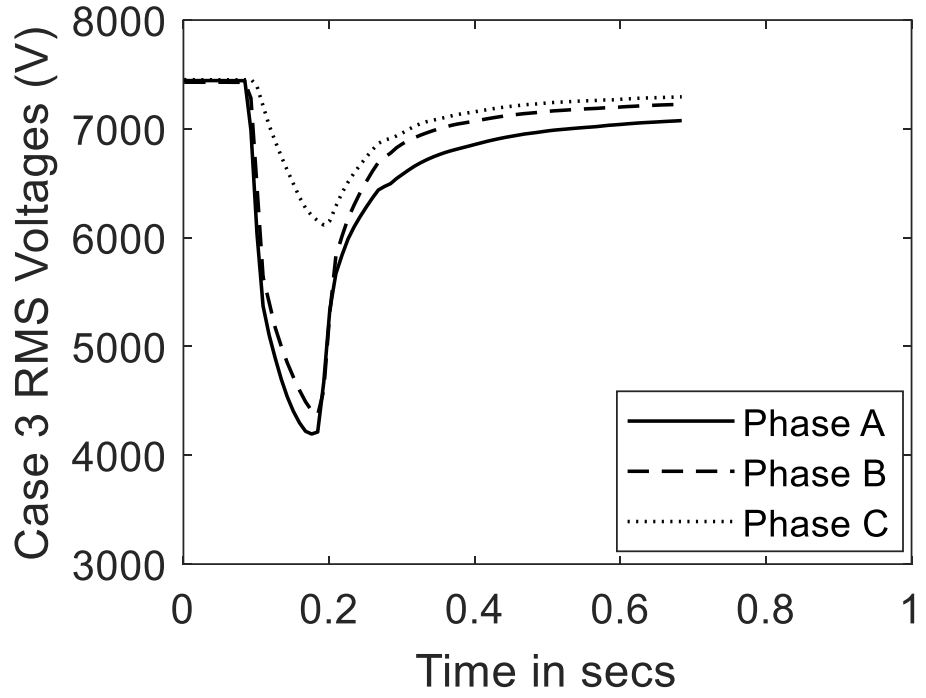

Figure 3.4 Played-in Voltage Measurements (RMS representation) for Case 3

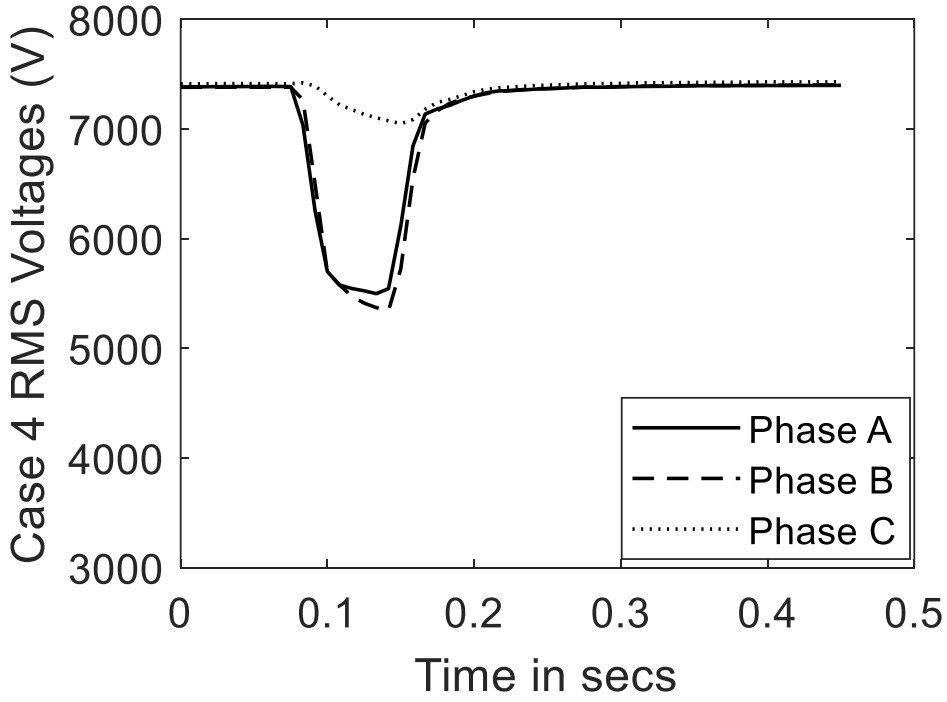

Figure 3.5 Played-in Voltage Measurements (RMS representation) for Case 4

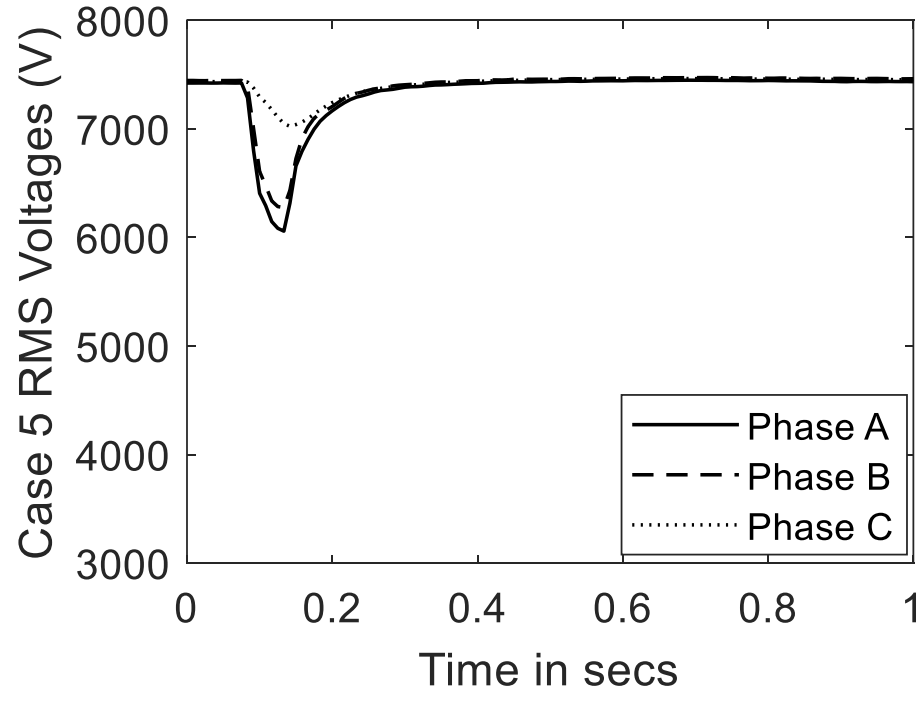

Figure 3.6 Played-in Voltage Measurements (RMS representation) for Case 5

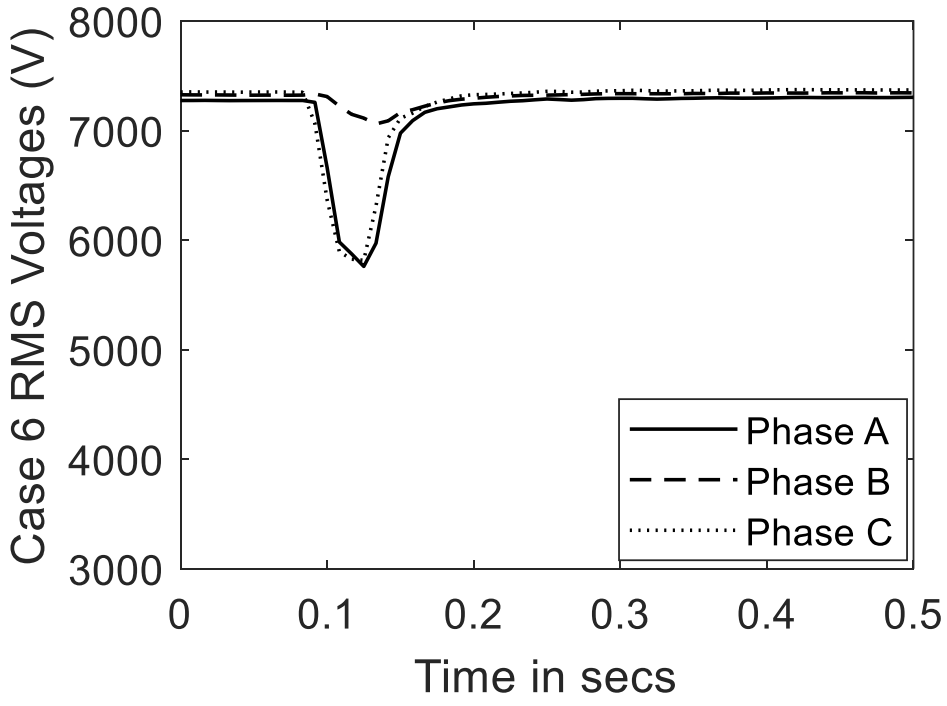

Figure 3.7 Played-in Voltage Measurements (RMS representation) for Case 6

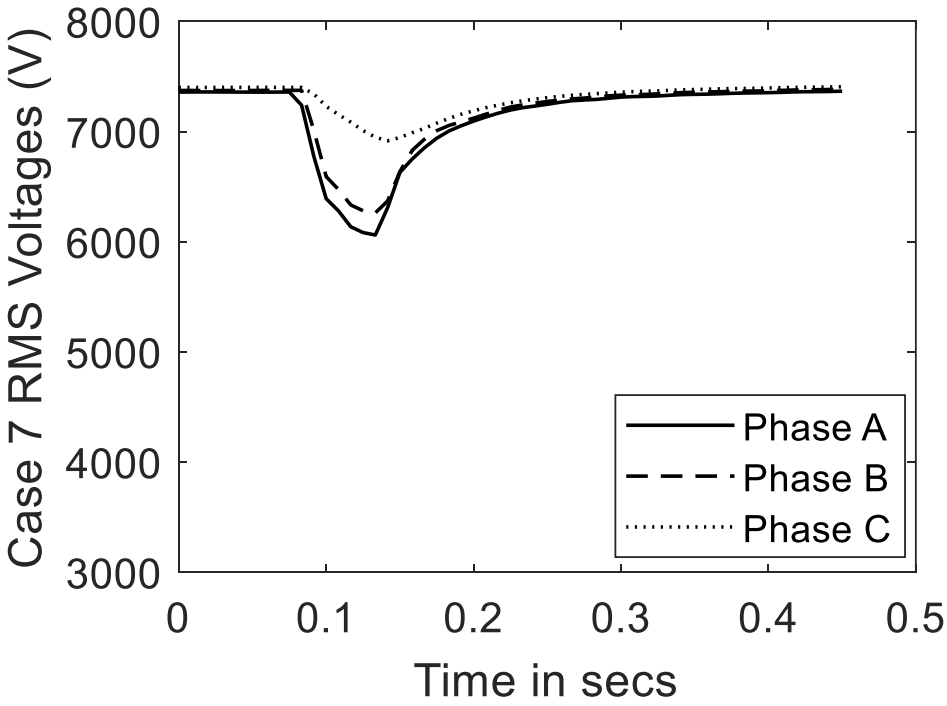

Figure 3.8 Played-in Voltage Measurements (RMS representation) for Case 7

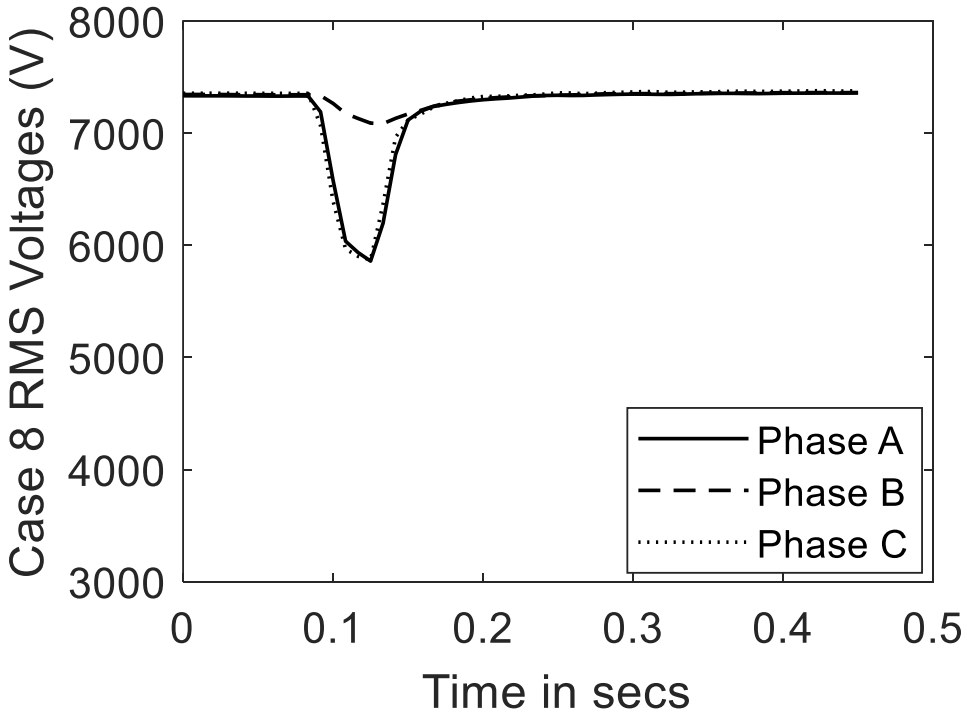

Figure 3.9 Played-in Voltage Measurements (RMS representation) for Case 8

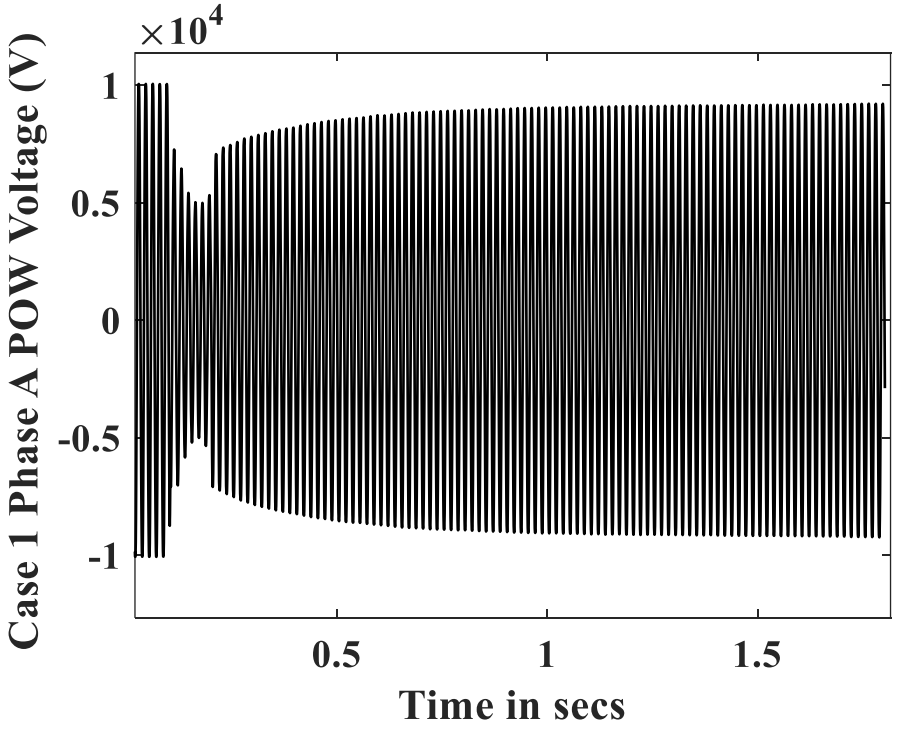

Figure 3.10 POW Played-in Phase A Voltage Measurement for Case 1

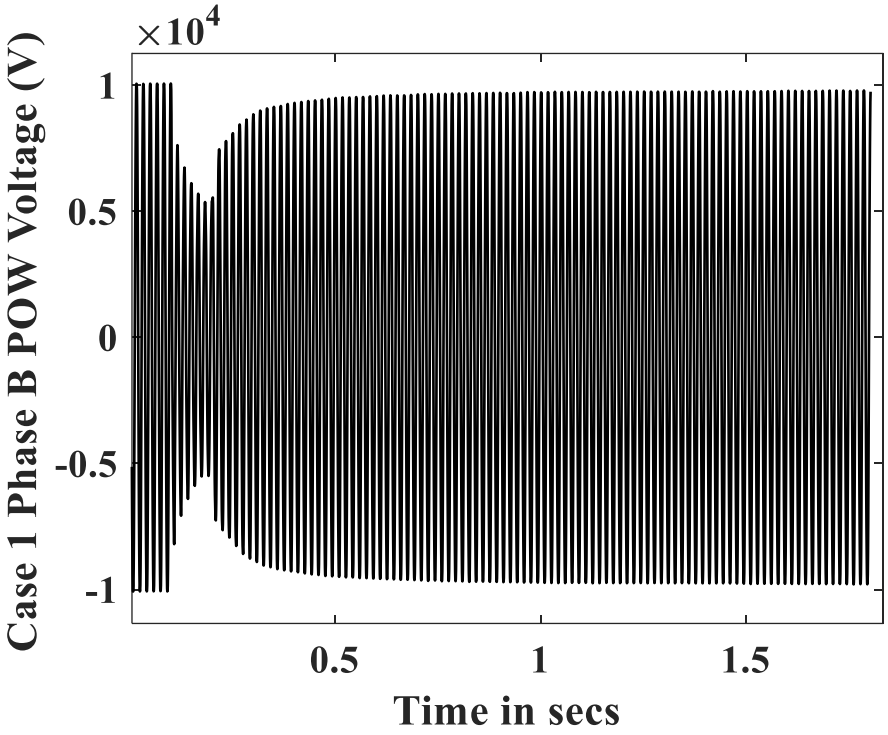

Figure 3.11 POW Played-in Phase B Voltage Measurement for Case 1

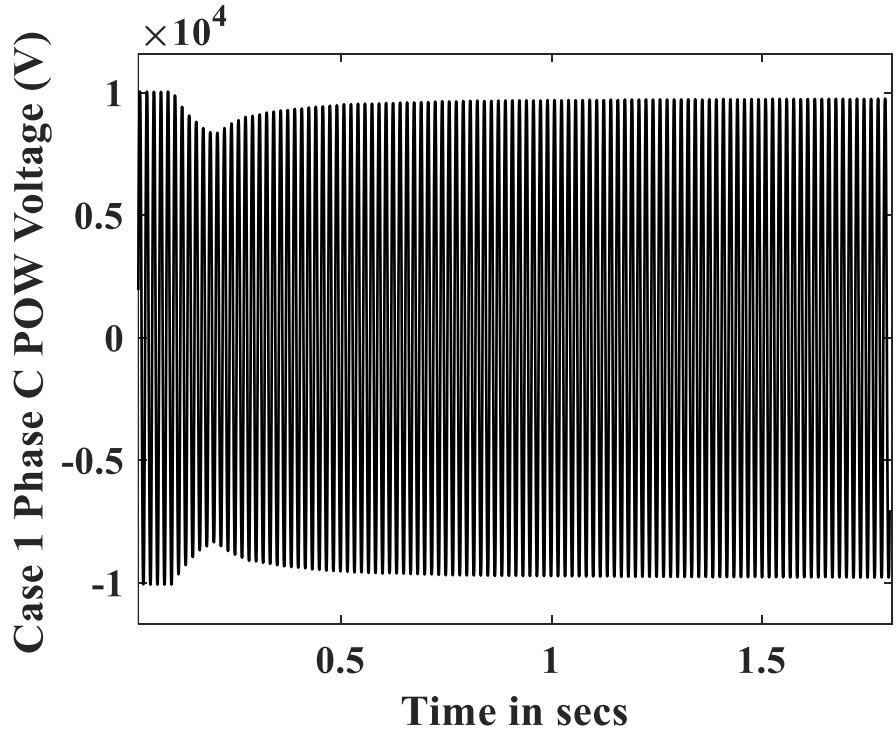

Figure 3.12 POW Played-in Phase C Voltage Measurement for Case 1

3.3 Feeder Model Design

The model depicted in Figure 3.13 is the proposed feeder and load model used in all the simulations conducted in this section. Based on [6], [35], the feeder model is divided into three equal length segments, enabling the capture of the FIDVR phenomenon due to stalling of single-phase induction motors (SPHIMs) at the far end of the feeder for Case 1. A combination of three-phase and single-phase loads along with the representation of the feeder section in each segment is considered. It should be noted that, at the time when measurements for Cases 1-8 were taken, no distributed generation (DG) was present on these feeders and hence they are not considered in this work. The three-phase transformers in the model, at the terminals of three phase motors, are represented by three single-phase transformers (Y-Y three-phase connection). It should also be noted that the impedance load and 3PHIM load are distributed equally in the three segments of the feeder whereas the SPHIM load is distributed in the ratio of 1:1.4:1.4 based on the assumptions that not much residential load is present near the substation, and SPHIMs at the end of the feeder will more likely stall compared to the head of the feeder. It should also be noted that 3-phase capacitor banks have been utilized in this work, at the head of the proposed feeder model, to match the total measured reactive power with their corresponding simulated reactive powers drawn by the feeder model.

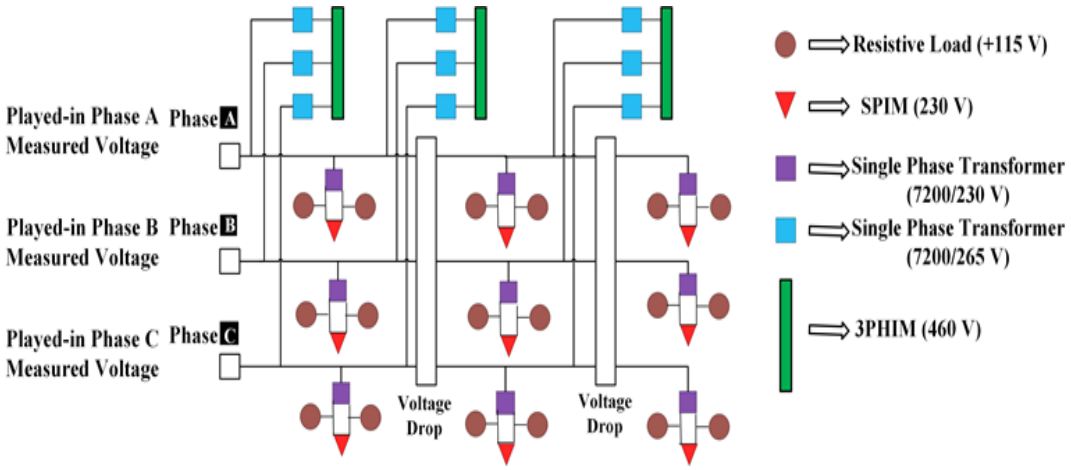

Figure 3.13 Proposed Feeder and Load Model Structure

Note1: *It should be noted that the description of each individual feeder component in Figure 3.13 has already been presented in Chapter 2.*

3.4 Optimization Algorithm

As discussed earlier, one of the main objectives of this work, is to estimate the load composition and the load parameters of the loads considered in Figure 3.13. This is accomplished by playing-in a set of three-phase voltage measurements from Cases 1 - 4 into the head of the proposed feeder and load model to obtain the three-phase simulated currents at the head of the feeder model. The obtained three-phase simulated currents are then matched as closely as possible to their corresponding three-phase measured currents, by tuning the load composition and the load parameters adaptively, using a non-linear least squares optimization technique (Gauss-Newton). This optimization approach has been applied to the motor load (both SPHIMs and 3PHIMs) parameters but not the impedance load (as this type of load does not have any dynamic parameters). More details about the optimization approach have been presented in the following sub-sections below:

3.4.1 Optimization Approach: Objective Function

In this work, a Gauss-Newton, non-linear least squares optimization is used to determine the load composition and the parameters of the motor loads by reducing the root mean square (RMS) error between the measured POW three-phase currents and simulated POW three-phase currents at the head of the feeder. The objective function is defined as shown in (3.1):

$$\arg\min_{\mu} E(\mu) = \left[\left(I_m - I(\mu) \right)^t \left(I_m - I(\mu) \right) \right] \tag{3.1}$$

In (3.1), I_m is the measured current vector at the head of the feeder and $I(\mu)$ is the simulated current (where μ parameter represents the load composition parameters, SPHIM parameters and the 3PHIM parameters) generated in PSCAD by playing-in the POW measured voltages at the head of the feeder. $E(\mu)$ is the objective function that needs to be minimized for each iteration.

The structure of the current vectors I_m and $I(\mu)$ for the considered load models and its composition are discussed below:

All the three-phase currents are augmented into a single vector as shown below:

$$I_m = \left[I_{ma}, I_{mb}, I_{mc} \right]^t, \quad I(\mu) = \left[I_a(\mu), I_b(\mu), I_c(\mu) \right]^t \tag{3.2}$$

Where, I_{ma} is the phase A measured current and $I_a(\mu)$ is the phase A simulated current at the head of the feeder and similarly for the other respective phases.

To obtain the load composition, the optimization procedure is applied on the '*Scale*' parameter (this captures the equivalent representation) of 3PHIMs and SPHIMs simultaneously which is dependent on all three-phase currents. More details about the '*Scale*' parameter (*Scale1* parameter for 3PHIMs and *Scale2* parameter for SPHIMs),

which represents the number of motors, are presented in sub-section 3.4.3.

3.4.2 Optimization Approach: Gradient Calculation, Parameter Updates, Step Size Determination and Convergence Properties

The Gauss-Newton approach is applied one parameter at a time to estimate the load parameters of the SPHIMs and the 3PHIMs using (3), (4) and (5). Since the voltage and current measurements are available in a POW format, as a set of discrete points, representing simulated currents (obtained from the PSCAD as a set of discrete points when instantaneous voltage measurements are played-in) and the measured currents by an analytical continuous function is not possible. Therefore, the first order differential gradient function is implemented by numerically calculating the first order forward difference as shown in (3).

$$J\left(\mu_0\right)=\left(I\left(\mu_0+\beta\right)\right)-I\left(\mu_0\right)/\beta \tag{3.3}$$

where, $J(\mu_0)$ is the gradient column vector corresponding to parameter μ_0, whose dimension is the number of samples of the measured current. β is a small perturbation value whose value is chosen for each parameter by engineering judgement. Values of 0.01 and 0.1 are found to be good choices for β. It should be noted that while estimating the *'Scale'* parameters, to obtain the load composition, two gradient column vectors J as a function of the *'Scale'* parameter for 3PHIMs and SPHIMs has been calculated using (3.3) and then augmented to form a Jacobian matrix.

The increment in parameter μ_0, at each iteration is evaluated using (3.4).

$$\Delta\mu_0=\left(J^t*J\right)^{-1}*J^t*\left(I_m-I\left(\mu_0\right)\right) \tag{3.4}$$

where, J is the gradient vector obtained from (3.3).

Another important feature to consider in this approach, along with the search direction, is the step size of the update of the parameters at each step. The parameters, at the end of each iteration, are updated using (3.5).

$$\mu_{\text{final}} = \mu_{\text{prev}} + \alpha\Delta\mu_0 \tag{3.5}$$

where, μ_{final} is the new value of the parameter obtained at the end of the iteration, μ_{prev} is the value of the parameter from the previous iteration, and α is the step size. It is important to obtain an appropriate value of α during each iteration of the optimization process instead of using a fixed pre-determined value. In this work, the α is determined by a line search technique [36] involving quadratic and cubic interpolations of the known values and derivates of the objective function from (3.1). For each iteration, this procedure is terminated when the sufficient decrease condition shown in (3.6) is satisfied.

$$E\left(\mu_k + \alpha\mu_0\right) \le E\left(\mu_k\right) + C_1\alpha E'\left(\mu_k\right) \tag{3.6}$$

where, C_1 is taken to be 10^{-4} [26] and α is determined by minimizing the quadratic interpolation function and is shown below in (3.7)

$$\alpha = \alpha_1 = E'\left(\mu_k\right) \Big/ 2\left[E\left(\mu_k + \Delta\mu_0\right) - E\left(\mu_k\right) - E'\left(\mu_k\right)\right] \tag{3.7}$$

where, $\alpha_1 = [0,1]$ and $E'\left(\mu_k\right)$ is the gradient of the objective function. If the α_1 obtained from (3.7) does not satisfy (3.6), α is determined by evaluated by minimizing the cubic interpolation function and is shown below in (3.8).

$$\alpha = \alpha_2 = -b + \sqrt{b^2 - 3\alpha E'\left(x_k\right)} \Big/ 3\alpha \tag{3.8}$$

$$\begin{pmatrix} a \\ b \end{pmatrix} = \frac{1}{\alpha_0^2 \alpha_1^2 (\alpha_1 - \alpha_0)} \begin{pmatrix} \alpha_0^2 & -\alpha_1^2 \\ -\alpha_1^2 & \alpha_0^2 \end{pmatrix} \begin{pmatrix} E(x_k + \alpha_1 \Delta\mu_0) - E(x_k) - \alpha_1 E'(x_k) \\ E(x_k + \alpha_0 \Delta\mu_0) - E(x_k) - \alpha_0 E'(x_k) \end{pmatrix} \tag{3.9}$$

where *a* and *b* are calculated from (3.9) and $\alpha_2 = [0, \alpha_1]$. If the α_2 obtained from (3.8) does not satisfy (3.6), this process to determine α_2 is repeated sub-iteratively, in each iteration, until the sufficient decrease condition is satisfied. In (3.9), α_0 and α_1 are the step-size values obtained from the previous two sub-iterations.

It is also important to ensure there would be a reasonable progress on each sub-iteration (Condition A) while also making sure the final obtained value of α would not be too small (Condition B). Therefore, if either Condition A or Condition B is satisfied based on the α_2 value calculated from (3.8), α_2 is updated using (3.10) at the end of the sub-iteration.

$$\alpha_{2,i} = \alpha_{2,i-1}/2 \tag{3.10}$$

Condition A: $\alpha_{2,i-1} - \alpha_{2,i} \leq \Delta$

Condition B: $\alpha_{2,i} \leq \gamma \alpha_{2,i-1}$

where, *i* is the sub-iteration number. Δ is chosen to be 0.05 in this work based on engineering judgement and the value of γ is taken to be 0.1 to ensure there are no drastic changes in the estimated value of the step size obtained in each sub-iteration during the interpolation process [36]. The error function and its gradient in (3.6), (3.7), (3.8) and (3.9) are calculated using the Euclidean norm of their respective vectors.

From [36], the convergence for the proposed algorithm has been guaranteed by satisfying the following conditions:

- Jacobian *J* should have a full rank: Typically, the Jacobian can be rank deficient only if either the parameter being estimated have no impact on the measurements or if there

is linear dependency between columns when two or more parameters have a similar impact on the measurements. In the proposed algorithmic approach, the Jacobian *J* calculated is either having 2 columns dimensionally (while estimating the load composition) or 1 column dimensionally (when estimating the motor load parameters one at a time). In the latter case, as there is only one column corresponding to the parameter of interest, the issue of two parameters having similar impact on the measurements has been eliminated. Also, using (3.16), the sensitivity of each motor parameter has been computed to ensure that all the parameters being estimated do not have zero sensitivity for the considered fault events. Additionally, in the former case (when the Jacobian has two columns), there is no linear dependency between '*Scale1*' and '*Scale2*' parameters because the transient response of 3PHIMs is very different compared to the SPHIMs [37] and both the motor loads have significant impact on the current transient response on the feeder for the considered fault events.

- Step-size should satisfy the Wolfe conditions (sufficient decrease condition and the curvature condition): By using the proposed interpolation line search technique to adaptively estimate the step-size in this work for each iteration, both the Wolfe conditions are being satisfied (sufficient decrease condition is satisfied by using it as a criterion to terminate the line search technique and the curvature condition is satisfied using Condition A and Condition B to ensure there is a significant progress on each sub-iteration of the line search).

3.4.3 Optimization Approach: Choosing Parameter Bounds and Initial Values

While implementing this algorithm, it is important to note that appropriate bounds are considered for the parameters of the motor models to ensure that the parameters

obtained after convergence are realistic. The upper and lower bounds considered for SPHIMs and 3PHIMs are shown in Table 3.3 and Table 3.4 respectively.

The bounds on the SPHIM parameters, as shown in Table 3.5, are obtained using the following criteria:

- Efficiency of SPHIM is assumed to be between 90-95%
- Total motor losses at the rated conditions are calculated for assumed efficiency range.
- Copper losses are assumed to be 60% of the total losses (25% stator copper losses and 35% copper rotor losses).

Typically, the combination of stator reactance and rotor reactance is approximately equal to the sub-transient reactance of the motor. Additionally, sub-transient reactance is usually in the range of 5% - 15% for a SPHIM. Using this assumption, the bounds on rotor and stator reactance have been chosen in this work.

Table 3.3 SPHIM Parameters Bounds

Parameter	**Lower Bound**	**Upper Bound**	**Initial Value**
Rotor Resistance	0.026 pu	0.051 pu	0.034 pu
Inertia Constant	0.031 s	0.1 s	0.043 s
Stator Resistance	0.017 pu	0.034 pu	0.026 pu
Rotor Reactance	0.026 pu	0.06 pu	0.034 pu
Stator Reactance	0.026 pu	0.06 pu	0.043 pu

The SPHIM's considered in this work are used to represent the air-conditioner compressor motors which have very small inertia. Therefore, a 6 cm – 8 cm bound on rotor diameter has been chosen to represent small induction motors in air conditioners. The inertia constant values corresponding to the chosen rotor diameter bounds are presented in

Table 3.3.

Table 3.4 Three-Phase Motor Parameters Bounds

Parameter	**Lower Bound**	**Upper Bound**	**Initial Value**
Inner Rotor Resistance	0.002 pu	0.02 pu	0.009 pu
Outer Rotor Resistance	0.1 pu	0.2 pu	0.15 pu
Inertia Constant	0.1 s	0.35 s	0.15 s
Stator Resistance	0.002 pu	0.05 pu	0.013 pu
Inner Rotor Reactance	0.05 pu	0.2 pu	0.17 pu
Outer Rotor Reactance	0.05 pu	0.25 pu	0.225 pu
Stator Reactance	0.05 pu	0.15 pu	0.067 pu

There are several references available in the literature that provide the parameters of 3PHIMs. Using [38], [39] and [40], the bounds in Table 3.4, for a 460 V dual cage rotor 3PHIM have been chosen in this work.

It is important to have bounds on the load composition percentage for both the motor loads and the impedance load. Based on the feeder class information obtained from the local utility for the considered feeders in this work and references [29], [41], the bounds for the loads, presented in Table 3.5, has been chosen. Using the 'Simple elimination for linear constraints' technique [36], the proposed optimization solves for $Scale_1$ and $Scale_2$ parameters simultaneously in (3.11).

$$Scale_1 S_1 + Scale_2 S_2 + \sum_{n=1}^{3} \frac{V_{seg,n}^2}{2*3*R_{seg,n}} = F_S \tag{3.11}$$

Where, F_S corresponds to the total MVA drawn by the feeder in the faulted phase, $Scale_1$ and $Scale_2$ parameters signify the number of motors of 3PHIM load and SPHIM load respectively connected to the faulted phase. Similarly, S_1 and S_2 correspond to the

machine ratings of the 3PHIMs (50 kVA) and SPHIMs (4.5 kVA) respectively. These ratings of the motors are used to calculate the base impedance of their respective motor parameters. Also, in (3.11), $V_{seg,n}$ is the terminal voltage of the resistive load and $R_{seg,n}$ is the value of the resistor used to represent the resistive load in the nth segment of the feeder respectively. It should be noted that $R_{seg,n}$ is calculated, after each iteration, based on the estimated $Scale_1$ and $Scale_2$ values in each iteration using load balance constraint (3.11).

In this algorithmic approach, it is also important to have a good initial estimation of the parameters of SPHIMs and 3PHIMS. Therefore, the parameters of the motor load models obtained in [12] for SPHIMs and [39]-[40] for 3PHIMs are used as the initial values in this work, within the considered bounds, as shown in Table 3.3 and Table 3.4.

3.4.4 Optimization Approach: Implementing Parameter Bounds

The bounds on the considered parameters cannot be applied as a hard constraint in the Gauss-Newton algorithm. The bounds are implemented, in an interactive environment consisting of a Fortran script and PSCAD, in this work. Therefore, logit transformation has been used to implement bounds on the parameters. In this transformation, the parameter of interest with bounds is transformed into a new parameter with no bounds using (3.12) as shown below.

$$\Omega_0 = \log\left(\frac{\mu_0 - \mu_{0,\text{ lower bound}}}{\mu_{0,\text{ upper bound}} - \mu_0}\right) \tag{3.12}$$

Where, μ_0 is the original parameter, $\mu_{0,\text{ lower bound}}$ the lower bound of the original parameter, $\mu_{0,\text{ upper bound}}$ is the upper bound of the original parameter and Ω_0 is the new transformed parameter and has limits (-∞, ∞).

After the transformation, (3.1) becomes a function of Ω (vector of transformed parameters) as shown in (3.13), which is free of the bound constraints on the parameters.

$$\arg \min_{\Omega} E(\Omega) = \left(I_m - I(\Omega)\right)^t \left(I_m - I(\Omega)\right) \tag{3.13}$$

After the convergence criterion is met, the transformed parameter vector Ω is transformed back to the original parameter vector μ using (3.12).

3.4.5 Optimization Approach: Convergence Criteria

Two convergence criteria are used in this work:

- **Parameter Convergence Criterion**

The main objective of this work is not to obtain a perfect match (zero RMS error) between the measured currents and the simulated currents. Therefore, a small tolerance for the parameters between two consecutive iterations has been chosen as the convergence criterion as shown in (3.14).

$$\Omega_k - \Omega_{k-1} < 10^{-2} \tag{3.14}$$

Where, Ω_k is the transformed parameter in the present iteration k and $\Omega_{k\text{-}1}$ is the transformed parameter in the previous iteration k-1. The convergence criterion used in (3.14) is equivalent to having a tolerance of less than 10^{-3} for the original parameter μ_0 between two successive iterations.

- **Case Convergence Criterion**

The goodness of the fit between the measured currents and their corresponding simulated currents for each phase is verified using (3.15)

$$RMSE_{Current} / Max\ Peak\ Value\ of\ \ Measured\ Current \leq \rho \tag{3.15}$$

Where, $RMSE_{Current}$ is the root mean square error between the measured current vector and its corresponding simulated current vector. It should be noted that in this work, after the proposed optimization technique is applied to obtain the load composition and the motor load parameters, if (3.15) is not satisfied for tolerance ρ chosen to be 0.1 to represent a 10% error per sample between the measured current and its corresponding simulated current, the optimization process is repeated until (3.15) is satisfied.

3.5 Results and Simulations

An interactive implementation of PSCAD (generates simulated currents) and a Fortran script (conducts the optimization procedure) is utilized in this work. The flow chart describing this process is presented below in detail in Figure 3.14.

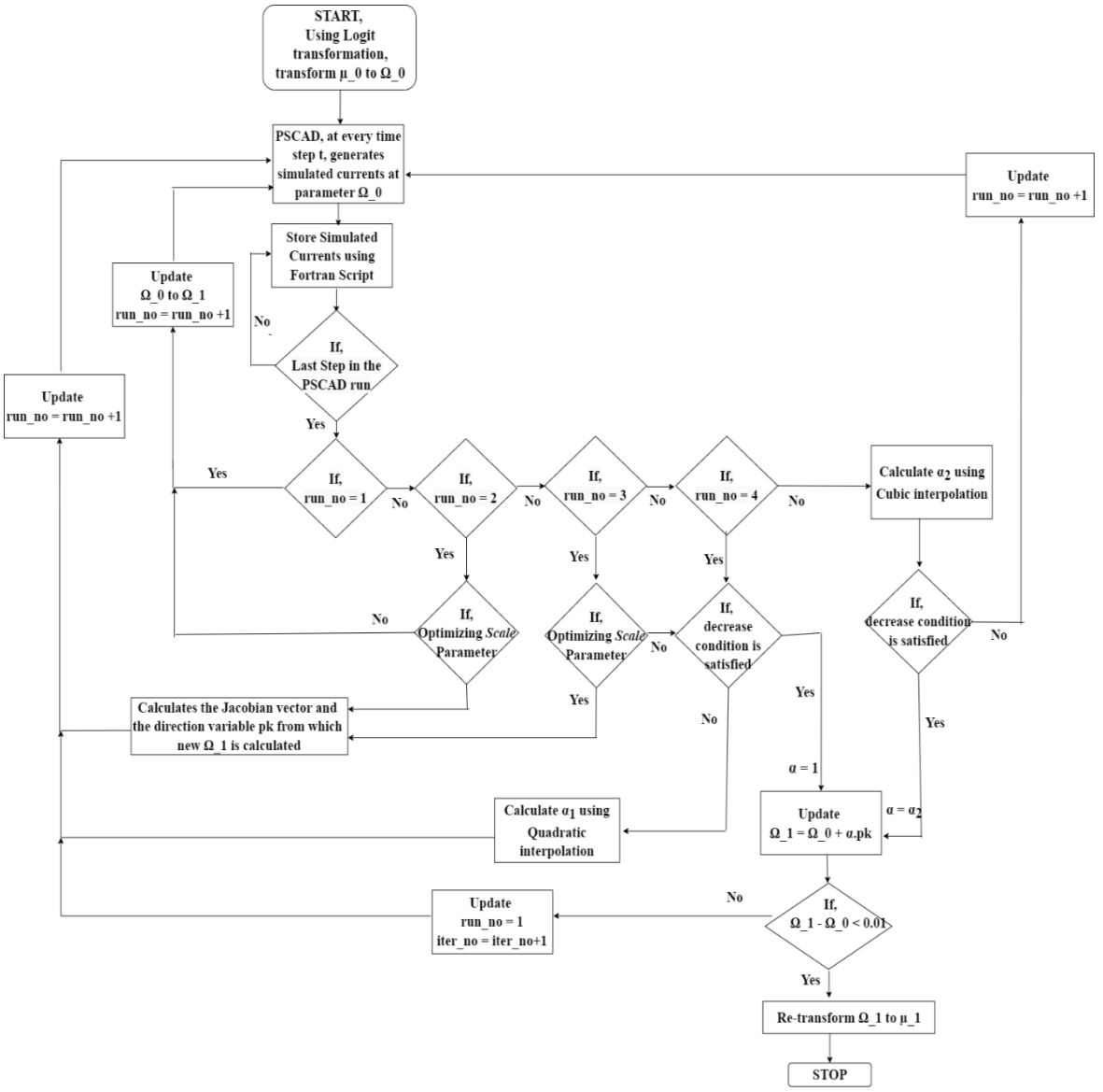

Figure 3.14 Flow Chart Describing the Optimization Procedure

The load compositions obtained for Cases 1-4, using the proposed algorithm for all the cases, are presented in Table 3.5. Based on the sensitivity analysis, the order of parameters given, from top (most sensitive) to bottom (least sensitive) in Table 3.6 and Table 3.7 respectively, for SPHIMs and 3PHIMs is used to conduct the optimization procedure in this work. The sensitivity of each parameter is obtained using (3.16):

$$\partial I/\partial p = \left(I_r\left(p+\gamma_0\right) - I_r\left(p\right)\right)/\gamma_0 \tag{3.16}$$

where, p is the parameter of interest, I_r is the RMS current of the faulted phase at the head of the feeder and $\gamma_0 = \varepsilon p$. Here, ε is an infinitesimally small perturbation.

It can be observed from Table 3.5 that the SPHIM load composition (both % level in the total load and the actual MVA drawn by the SPHIMs) obtained during the summer conditions (Case 1 and Case 3) in both types of feeders is higher compared to the SPHIM composition observed during the winter conditions (Case 2 and Case 4). Whereas, for the 3PHIM load, although the % level in the total load varies from summer to winter conditions significantly, the amount (MVA drawn) of 3PHIM load on the feeder between summer and winter conditions is similar for both feeders. This is to be expected due to the heavy use of air conditioners in the summer weather conditions (during the month of August) and relatively light use during the winter weather conditions (during the month of October and November) whereas the use of 3PHIM loads on both the considered feeders do not have as much seasonal dependance as air conditioner SPHIM load does.

After obtaining the load compositions for Cases 1-4, the proposed optimization procedure to obtain the load parameters, has been applied initially to the type of motor load with major penetration in the feeder and then it is applied to type of motor load with minor

penetration. This is done by assuming the former type of load would have the most impact on the total current at the head of the feeder. Therefore, for Cases 1-2, the optimization approach is first applied to the SPHIM motors and then the 3PHIMs due to the dominant presence of the SPHIM loads in the considered residential feeder and load model and vice-versa for Cases 3-4.

Table 3.5 Final Load Compositions Obtained for Cases 1-4

	SPHIM Load (%, MVA)	**3PHIM Load (%, MVA)**	**Impedance Load (%, MW)**
Case 1	51%, 9.34 MVA	16%, 2.93 MVA	33%, 6.04 MW
Case 2	35%, 2.53 MVA	34%, 2.45 MVA	31%, 2.24 MW
Case 3	23%, 5.3 MVA	38%, 8.76 MVA	39%, 8.99 MW
Case 4	15%, 2.04 MVA	56%, 7.61 MVA	29%, 3.94 MW

Using this procedure, the final converged parameters of the SPHIMs for Case 1-4 are presented in Table 3.6 below:

Table 3.6 Final SPHIM Parameters for Cases 1-4

Parameter	**Case 1**	**Case 2**	**Case 3**	**Case 4**	**Initial Val**
Rotor R pu	0.033	0.051	0.028	0.035	0.034
Inertia s	0.0568	0.0511	0.0769	0.0442	0.043
Stator R pu	0.0256	0.0297	0.034	0.0316	0.026
Rotor X pu	0.035	0.045	0.0595	0.0576	0.034
Stator X pu	0.0575	0.054	0.0595	0.0561	0.043

The final converged parameters for the 3PHIMs for Case 1-4 are shown in Table 3.7. It is observed that the final obtained inertia parameters for the three-phase motors are

low for Case 1 and Case 2 and much higher for Case 3 and Case 4. This is expected because the 3PHIMs in a typical industrial area are larger compared to the 3PHIMs present in residential areas.

Table 3.7 Final 3PHIM Parameters for Cases 1-4

Parameter	**Case 1**	**Case 2**	**Case 3**	**Case 4**	**Initial Val**
Inner Rotor R pu	0.013	0.019	0.02	0.02	0.009
Outer Rotor R pu	0.2	0.2	0.2	0.2	0.15
Inertia s	0.12	0.16	0.25	0.35	0.15
Stator R pu	0.0468	0.0423	0.047	0.05	0.013
Inner Rotor X pu	0.194	0.2	0.2	0.2	0.17
Outer Rotor X pu	0.2396	0.226	0.226	0.229	0.225
Stator X pu	0.139	0.0889	0.069	0.0885	0.067

The final converged parameters for the 3PHIMs for Case 1-4 are shown in Table 3.7. It is observed that the final obtained inertia parameters for the three-phase motors are low for Case 1 and Case 2 and much higher for Case 3 and Case 4. This is expected because the 3PHIMs in a typical industrial area are larger compared to the 3PHIMs present in residential areas.

Overall, the parameters of SPHIMs and 3PHIMs obtained in Case 1 and Case 2 (for residential feeder) are relatively close to each other. Similarly, the parameters of SPHIMs and 3PHIMs obtained for the industrial/commercial feeder (Case 3 and Case 4) are comparable. This indicates that the loading conditions (summer and winter) do not have a very significant impact on the parameters of the motor loads obtained for a particular type of feeder.

From Table 3.8, it can be observed that the proposed algorithmic approach has a

significant improvement on the most severely affected phases (Phase A and Phase B) and a relatively smaller improvement in the least affected phase (Phase C) in all the cases. Additionally, in Cases 1-4, the RMSE per sample after optimizing parameters is within the case convergence criterion threshold as discussed in (3.12). In all the cases, the maximum error per time step (MEPTS) between the measured and simulated current responses has also been observed to have improved significantly when the parameters are optimized from the considered initial estimates. The RMSE values provided here are applied on 3 pre-fault cycles, 6 transient cycles and 11 post-fault steady-state cycles on the current waveforms for all the cases except Case 1 for which the RMSE values are calculated over 78 post-fault steady state cycles to capture the stalled current in the feeder.

Table 3.8 Effectiveness of the Optimization Approach in Cases 1-4

Case/ Phase	**RMSE per sample in Amps (initial parameter estimates)**	**RMSE per sample in Amps (Optimized parameters)**	**RMSE Improvement (%)**	**Max Error per Time Step in Amps (with initial estimates, after optimizing parameters)**
1/A	215.92	150.44	+30%	1026.5, 459.45
1/B	130.93	84.05	+36%	854.6, 371.52
1/C	99.42	90.16	+10%	331.99, 321.75
2/A	228.4	54.25	+76%	1006.1, 200.52
2/B	155.41	52.72	+66%	710.65, 213.21
2/C	49.3	45.28	+8%	181.02, 140.48
3/A	232.53	132.54	+43%	164.62, 98.1
3/B	245.51	148.53	+40%	787.94, 468.7
3/C	160.86	130.48	+19%	185.23, 146.36
4/A	204.45	93.56	+54%	874.29, 461.86
4/B	196.38	99.74	+49%	689.53, 389.74
4/C	77	71.28	+8%	275.93, 256.85

As mentioned earlier, the load parameters and the load compositions obtained from Cases 1-4 have been used to simulate Cases 5-8 respectively. Table 3.9 shows that the parameters estimated from Case 1-4 do in fact give a better estimate of Cases 5-8 than with the initial parameter estimates. As shown in Table 3.9, using the parameters determined from Cases 1-4 produces a significant RMSE improvement in all testing cases except Phase B in Case 6. However, the impact on this phase is minimal (this phase being neither the primary faulted phase nor the secondary affected phase due to Delta-Y transformers). Additionally, in an instantaneous sense, the MEPTS is still observed to have improved slightly for this phase and more significantly for the rest of the cases.

Table 3.9 Use of Estimated Feeder and Motor Parameters for Varying Feeder Operating Conditions in Cases 5-8

Case/Phase	**RMSE per sample in Amps (initial parameter estimates)**	**RMSE per sample in Amps (Optimized parameters)**	**RMSE Improvement (%)**	**Max Error per Time Step in Amps (with initial estimates, after optimizing parameters)**
5/A	113.36	105.34	+7%	632.84, 620.99
5/B	108.47	106.14	+2%	558.28, 433.15
5/C	125.39	98.92	+26%	290.19, 289.2
6/A	88.25	73.22	+17%	486.27, 331.47
6/B	54.1	59.37	-9%	113.73, 110.96
6/C	76.94	67.97	+12%	445.92, 313.63
7/A	161.01	84.54	+48%	673.73, 275.6
7/B	200.35	158.44	+26%	499.74, 478.11
7/C	81.66	62.54	+24%	236.06, 209.49
8/A	92.82	57.99	+37%	402.09, 233.57
8/B	49.22	45.05	+9%	159.44, 128.92
8/C	126.52	53.81	+57%	520.76, 287.49

In Case 1, it was observed that after the optimization, SPHIMs in the third segment stalled (as shown in Figure 3.15), and motors in the second segment took an extended time to reaccelerate for the faulted phase. In the insets of Figure 3.16, the simulations made with the initial parameter estimates did not reproduce the stalled current that occurred when the SPHIMs in segment 3 stalled. The stalling phenomenon observed in the SPHIMs on segment 3 (far end of the feeder) clearly illustrates the need to structure the feeder model and its loads in a distributed manner, as proposed in this work, to capture FIDVR type phenomenon accurately. This would not have been possible if all the motor load is concentrated at a single location, which is the primary assumption in almost all the load modeling works in the literature. Also, from Figures 3.17 – 3.18, it can clearly be seen that the post-fault steady state current is the same as the pre-fault steady state current (which indicates no stalling of the SPHIMs in the non-faulted phases). For Case 1, it should also be noted that although phase B played-in voltage (as shown in Figure 3.11) is similarly affected as the phase A played-in voltage (as shown in Figure 3.10) during the fault, the recovery (after the fault is cleared) is much faster in the former case. This clearly indicates that the SPHIMs reaccelerated in phase B back to their nominal speeds (no stalling). This is to be expected because the stalling phenomenon of the SPHIMs is also dependent on the point on the wave at which the fault is initiated which led to the phase A SPHIMs in the proposed feeder and load model to stall but not in phase B (even though both the phases are similarly affected due to the presence of the Delta-Wye 69/12.47 kV transformers in the sub-transmission level of the system).

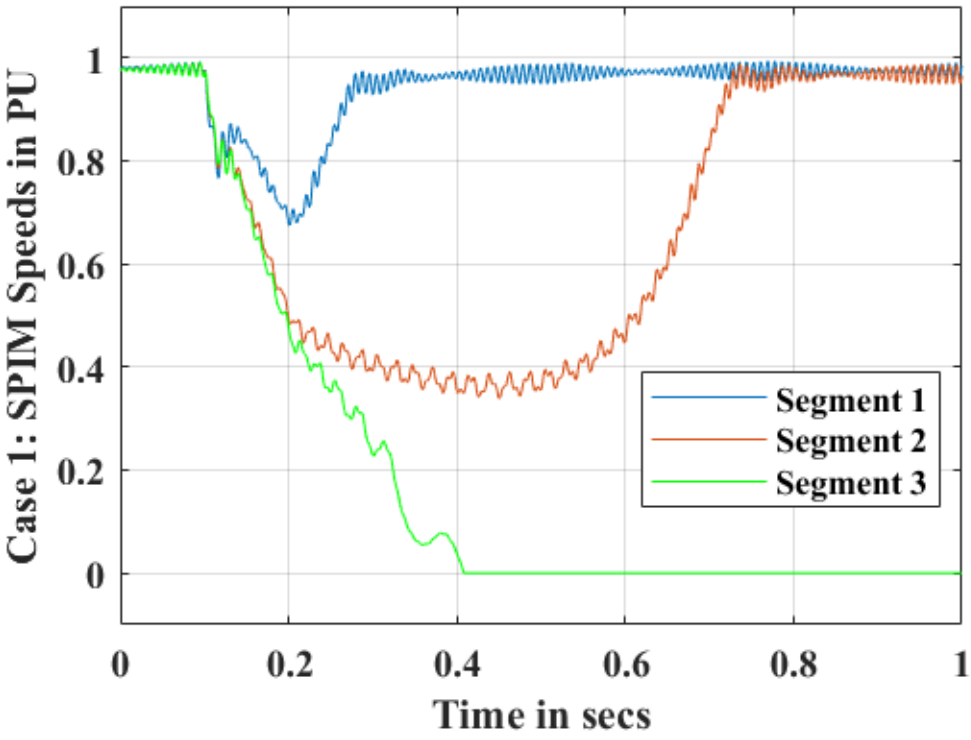

Figure 3.15 Demonstration of SPHIM Stalling in Case 1 in the Faulted Phase A

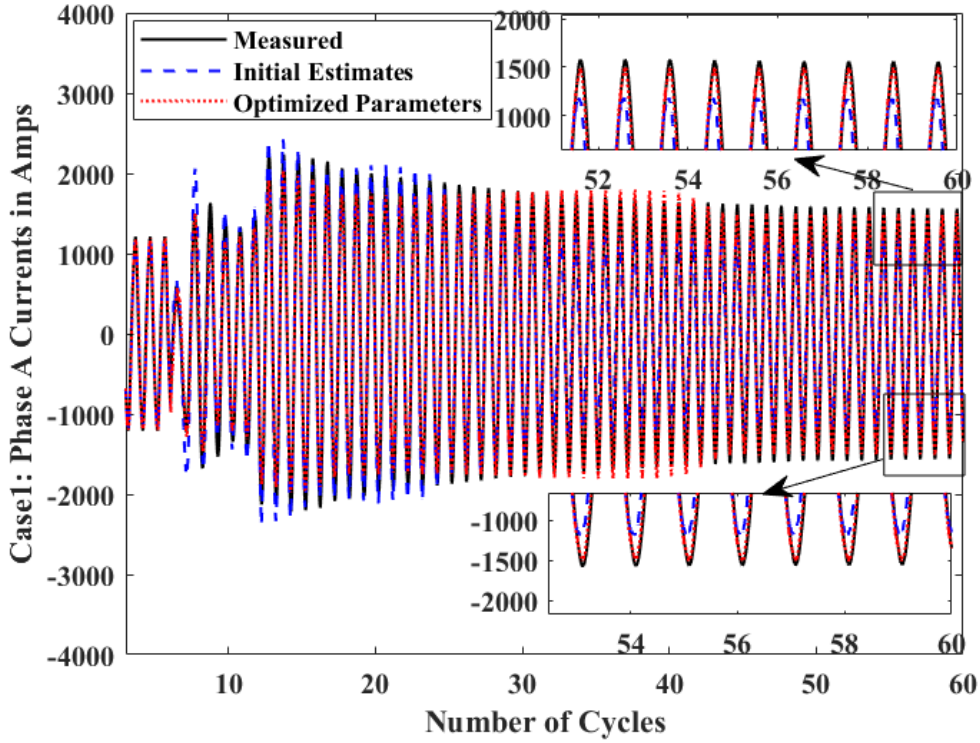

Figure 3.16 Evidence of Stalled Current on Faulted Phase A Current of Case 1

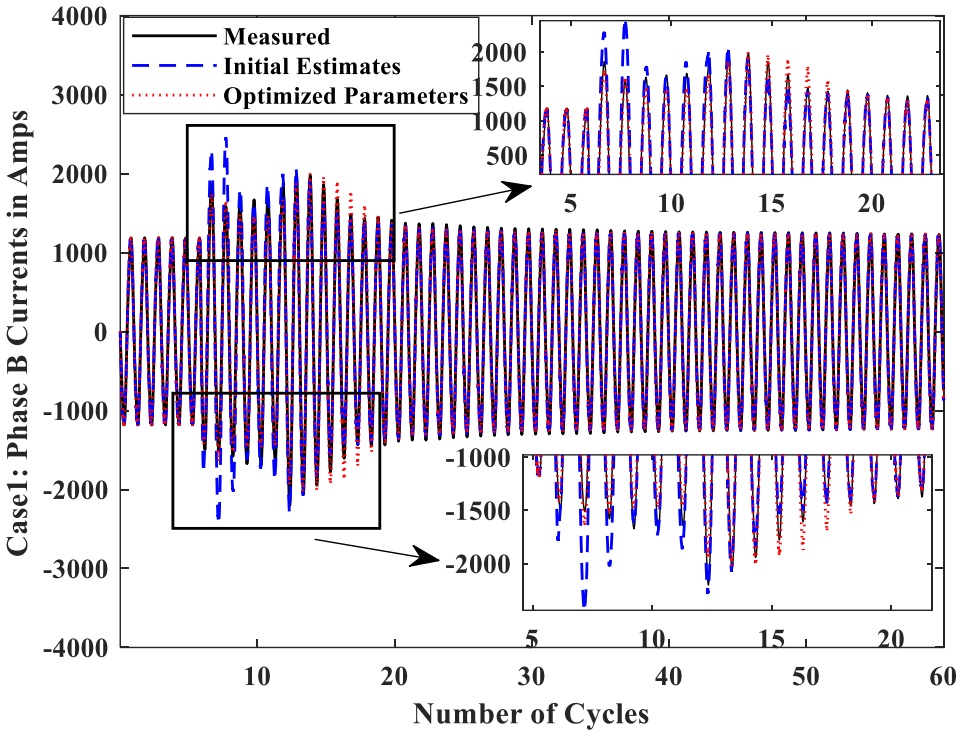

Figure 3.17 Impact of Optimization Approach on Phase B Current of Case 1

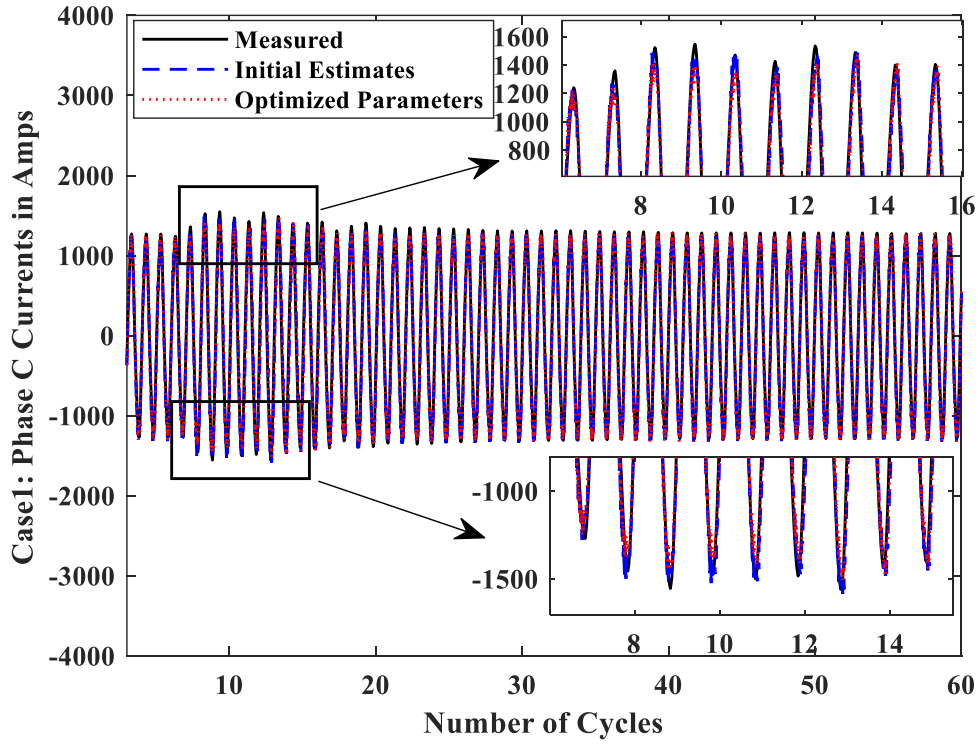

Figure 3.18 Impact of Optimization Approach on Phase C Current of Case 1

Figure 3.19, Figure 3.20, and Figure 3.21 demonstrate the qualitative improvement in the simulated currents matching their respective measured currents, in Case 4, when the optimization algorithm is employed to estimate the parameters of the load models. In these figures, during the time period between the 5^{th} cycle (when the fault occurs as indicated by the vertical solid black line indicated in Figures 3.19 - 3.24) and the 10^{th} cycle (when the fault is cleared), it can be observed that there is a significant improvement, in both magnitude and phase, in the simulated current response in all three phases when the optimization approach is used. However, in the steady state, after 11^{th} cycle, there does not seem to be much impact of the optimization algorithm on the simulated current responses. This is expected because parameters such as rotor resistance and motor inertia have a significant impact on the transient response during a fault and immediately when a fault is cleared. However, in steady state, the impact of parameter sensitivity is much less pronounced. Overall, it can be concluded that the proposed optimization approach is effective in capturing the measured currents with very little-known feeder information by making reasonable assumptions using engineering judgement about the initial estimates of both load composition and the load parameters.

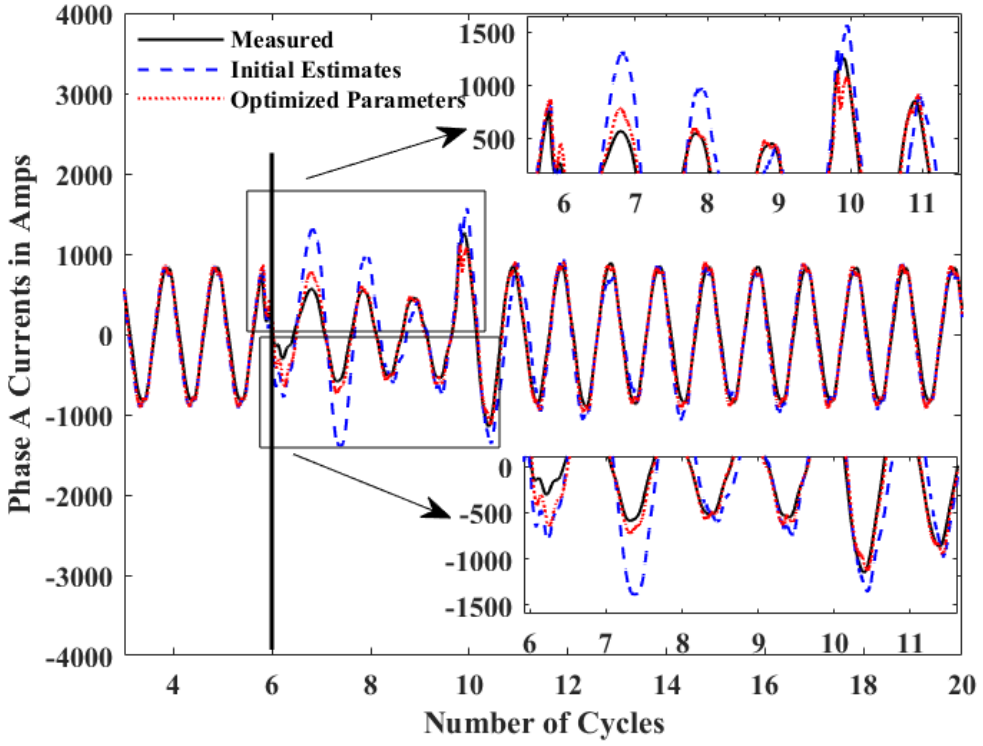

Figure 3.19 Impact of Optimization Approach on Phase A Current of Case 4

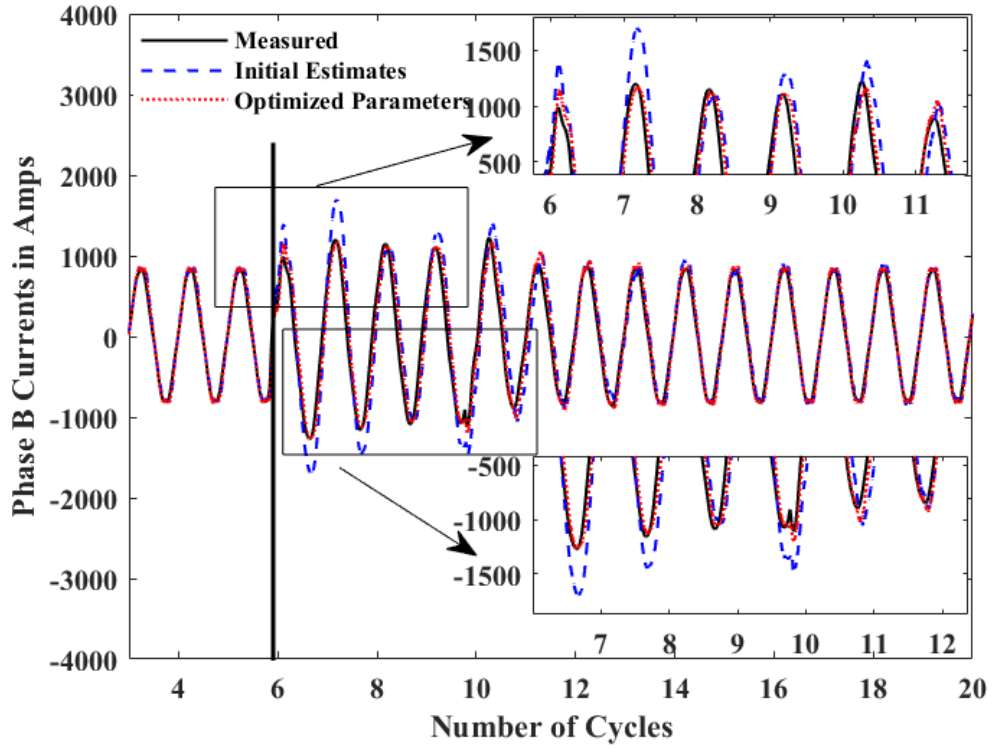

Figure 3.20 Impact of Optimization Approach on Phase B Current of Case 4

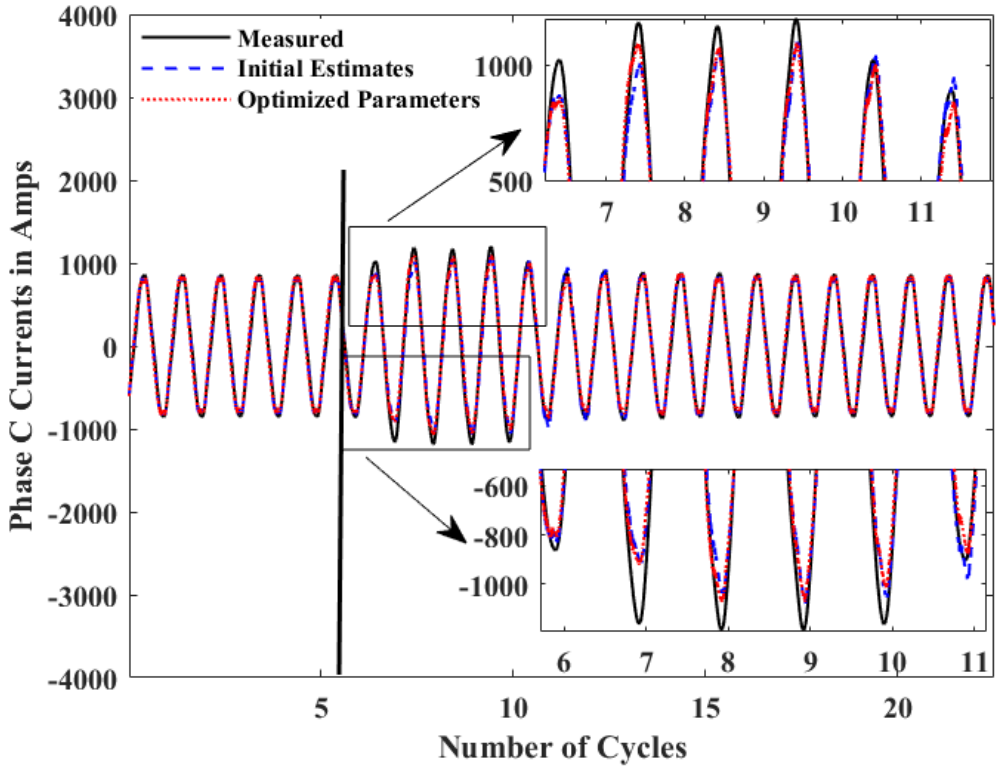

Figure 3.21 Impact of Optimization Approach on Phase C Current of Case 4

From Figure 3.22 – 3.24, it can be clearly observed that the load parameters obtained from Case 4 makes a significant improvement in the simulated current response for the faulted phase (Phase C) and the next most impacted phase (Phase A due to the presence of Delta-Wye 69 kV transformer) in Case 8. This clearly shows that the proposed approach is consistent and has been validated both quantitively (from Table 11) and qualitatively (Figure 3.22 – 3.24).

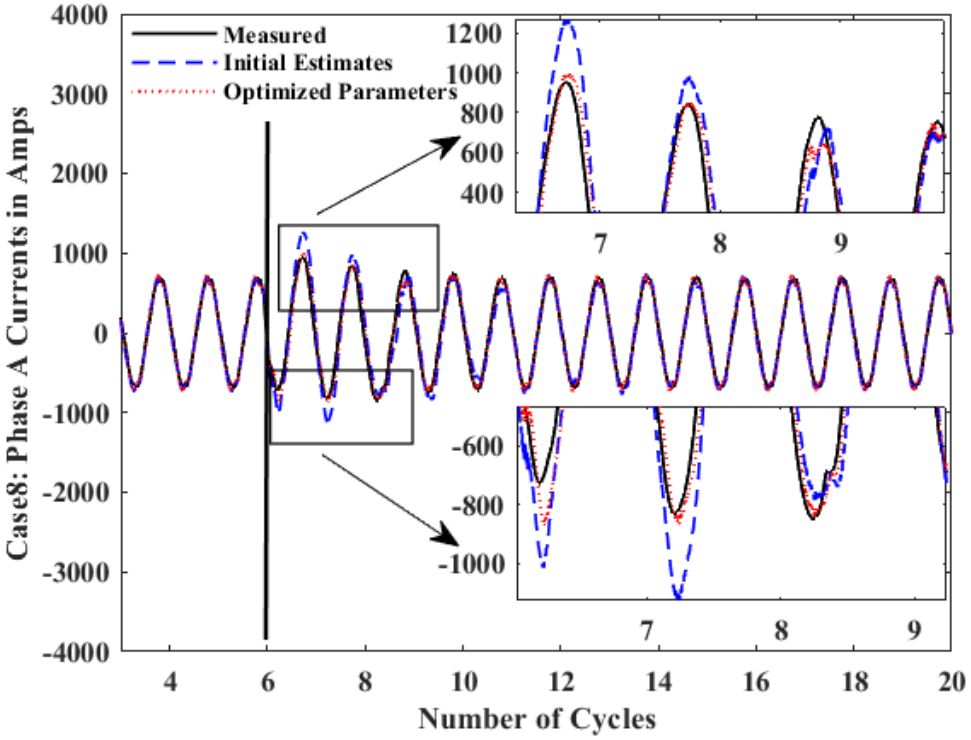

Figure 3.22 Validation of Optimization Approach on Phase A (Most Impacted Non-Faulted Phase) Current of Case 8

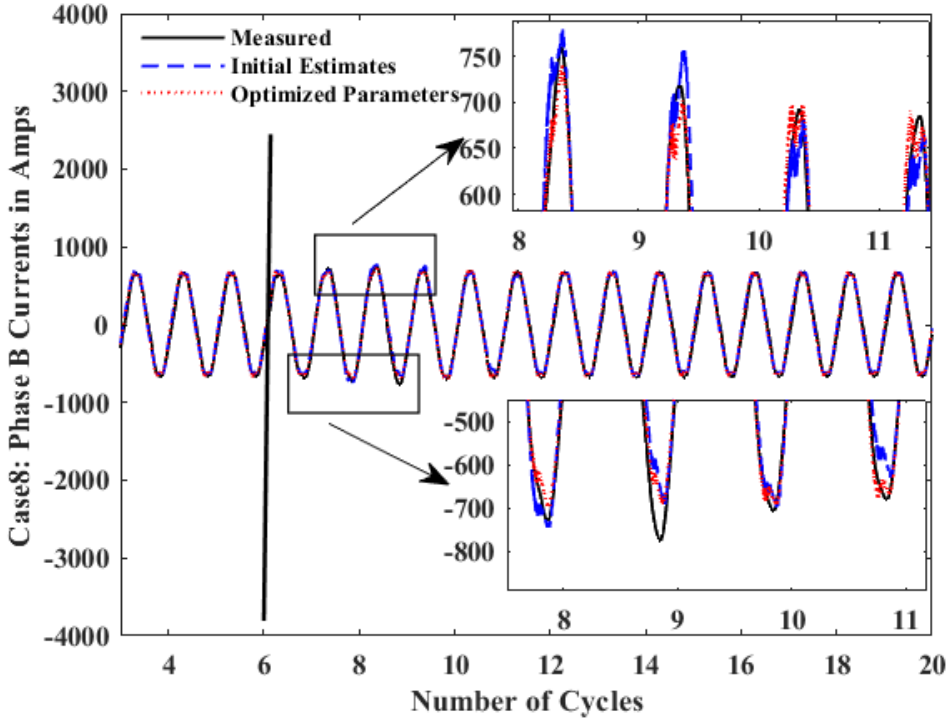

Figure 3.23 Validation of Optimization Approach on Phase B (Least Impacted Phase) Current of Case 8

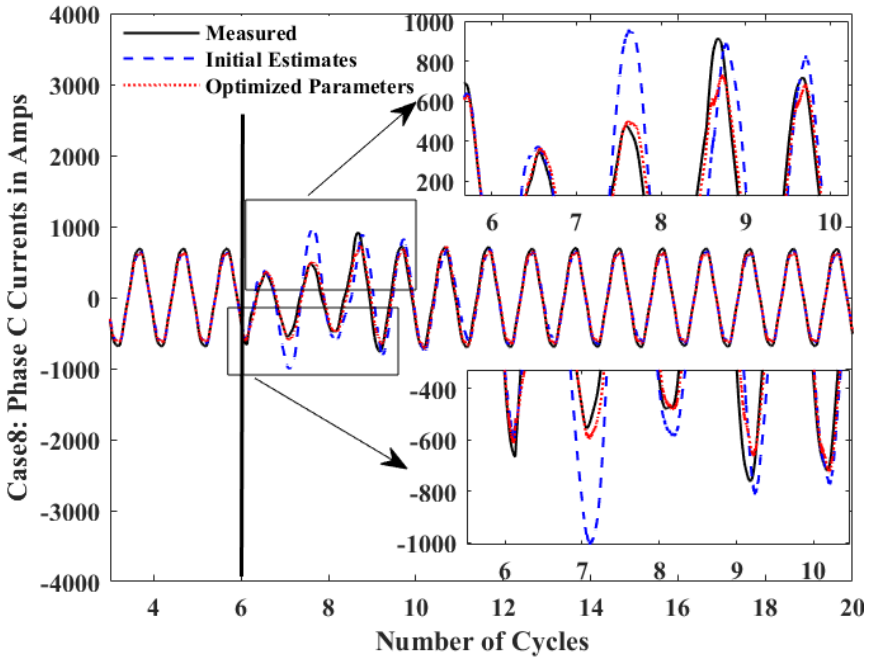

Figure 3.24 Validation of Optimization Approach on Phase C (Faulted Phase) Current of Case 8

The impact of using a different set of initial conditions on the algorithm performance has been presented below using Tables 3.10 – 3.13 where IC1 represents the set of initial values used in Tables 3.13 – 3.11 and IC2 represents a new set of initial conditions chosen randomly between the parameter bounds.

From Table 3.10, it can be observed that the load composition obtained with IC2 conditions is very close to the load composition obtained for IC1 conditions. Similarly, from Tables 3.11 – 3.12, it can be inferred that the load parameters estimated for both the initial conditions are reasonably close to each other for both SPHIMs and 3PHIMs. Additionally, from Table 3.13, it can be clearly seen that the optimization performance has not deteriorated with a change in the initial conditions. It should also be noted that the proposed algorithm took a total of 82 iterations and 75 iterations for all the parameters to converge with IC1 conditions and IC2 conditions respectively which shows that the convergence speed of the algorithm is also similar for different sets of initial conditions

within the considered bounds.

Table 3.10 Estimated Load Composition for Case 4
Using Different Initial Conditions

	SPHIM Load %		**3PHIM Load %**		**Impedance Load %**	
	Init Value	Est Value	Init Value	Est Value	Init Value	Est Value
With IC1 Condition	30%	15%	45%	56%	25%	29%
With IC2 Condition	25%	15%	47.5%	53%	27.5%	32%

Table 3.11 Estimated SPHIM Parameters Comparison for Case 4
Using Different Initial Conditions

Parameter	**IC1 Values**	**Estimated Parameters for IC1 conditions**	**IC2 values**	**Estimated Parameters for IC2 conditions**
Rotor R pu	0.034	0.035	0.038	0.035
Inertia s	0.043	0.055	0.058	0.061
Stator R pu	0.026	0.031	0.03	0.028
Rotor X pu	0.034	0.058	0.043	0.049
Stator X pu	0.043	0.056	0.051	0.053

Table 3.12 Estimated 3PHIM Parameters Comparison for Case 4
Using Different Initial Conditions

Parameter	**IC1 Values**	**Estimated Parameters for IC1 conditions**	**IC2 values**	**Estimated Parameters for IC2 conditions**
Inner Rotor R pu	0.009	0.02	0.011	0.02
Outer Rotor R pu	0.15	0.2	0.13	0.2
Inertia s	0.15	0.35	0.25	0.35
Stator R pu	0.013	0.05	0.026	0.05
Inner Rotor X pu	0.17	0.2	0.125	0.173
Outer Rotor X pu	0.225	0.229	0.15	0.184
Stator X pu	0.067	0.089	0.085	0.087

Table 3.13 Proposed Optimization Approach Performance Comparison for Case 4 Using Different Initial Conditions

Phase	**RMSE per sample in Amps (with initial estimate of parameters)**		**RMSE per sample in Amps, Improvement % (after optimizing parameters)**	
	IC1	IC2	IC1	IC2
A	204.45	113.42	93.56, +54%	87.91, +23%
B	196.38	137	99.74, +49%	107, +22%
C	77	72.02	71.28, +8%	62.83, +13%

3.6 Capturing a Synthetic FIDVR Event Using the Developed Feeder Model

The voltage dip percentages for the faulted phase in Cases 1-8 have been presented in Table 3.1 and Table 3.2. It can be observed from Table 3.1 and Table 3.2 that the voltage drop in all the cases (except Case 1) are significantly lower compared to Case 1 and hence they are not of FIDVR type cases. ***However, it should be noted that the validation provided in this chapter for Case 1(FIDVR event) parameters, by applying them to Case 5 (non-FIDVR event), is still significant as this would show that for the same parameters of the motor models obtained using a FIDVR event, the SPHIMs do not stall during non-FIDVR conditions, in Case 5, which is exactly what we "expect and desire ideally" when there is significantly lower voltage drop in the system when compared to a FIDVR event.*** Although ideally it would be beneficial to check if the motor parameters obtained from Case 1 be validated using another Case measurement which has a FIDVR type of voltage profile. Unfortunately, the local utility which provided the Cases 1-8 measurement data is unable to provide another FIDVR event for the same feeder.

Therefore, some simulations in PSCAD have been conducted to mimic a FIDVR type of event in the 69 kV level in the system as shown below in Figure 3.25, where the

feeder model with the load composition and the motor parameters obtained from Case 1 (using the proposed algorithmic approach) has been used at the head of the feeder bus. The feeder structure used here is the same as that used in Figure 3.13.

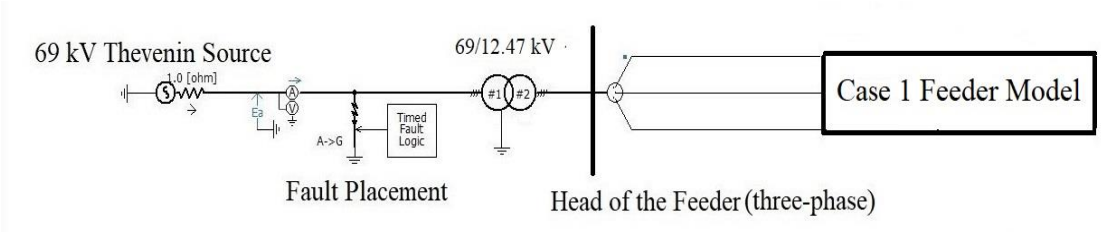

Figure 3.25 Circuit Setup to Synthesize FIDVR Fault Event in PSCAD

In this simulation, a SLG fault has been placed at the 69 kV and the fault duration has been taken to be 0.09 sec (same as Case 1). The fault resistance has been used to vary the sag level of the feeder voltage during the fault. It should also be noted that a 69 kV Thévenin voltage source has been used in this case, whereas in Cases 1-8 (where we know the measured feeder voltages), the 12.47 kV voltages are played-in at the head of the feeder.

In the results shown below, two scenarios have been simulated as follows -

- Scenario 1: A Case with 53% voltage drop at the head of the feeder
- Scenario 2: A Case with 45% voltage drop at the head of the feeder

In Figure 3.26, the faulted feeder head voltage profiles for the two scenarios have been presented. From Figure 3.27, it can be observed that the third segment SPHIMs stall for Scenario 1 (with a high voltage drop such as in Case 1) whereas none of the SPHIMs stall for Scenario 2 (with a lower voltage drop compared to Scenario 1 and Case 1) in Figure 3.28. ***This clearly shows that the load composition and motor load parameters obtained for Case 1 can capture both FIDVR and non-FIDVR type events accurately.***

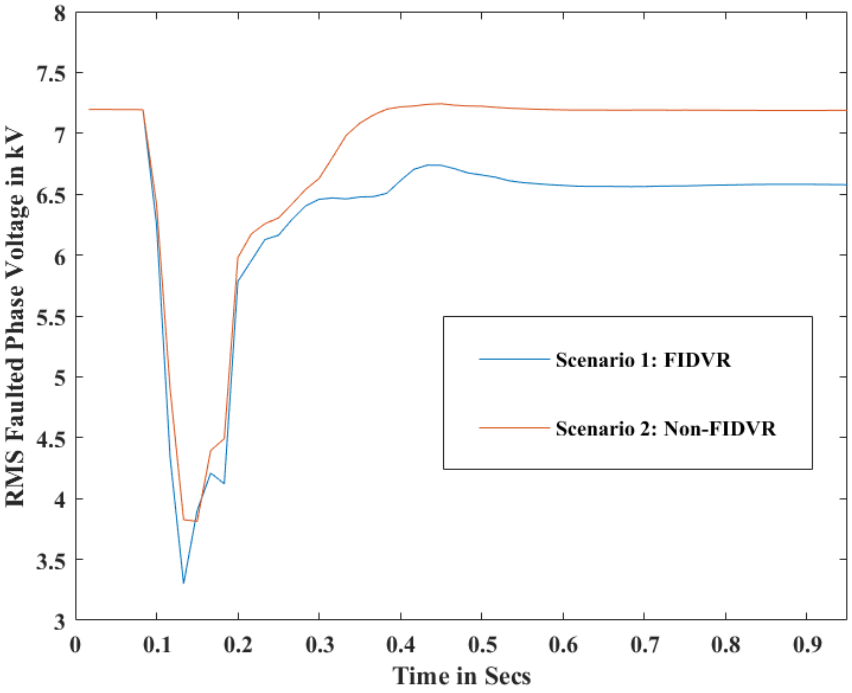

Figure 3.26 Comparison of Voltage Profiles for Scenarios 1 - 2 at the Head of the Feeder.

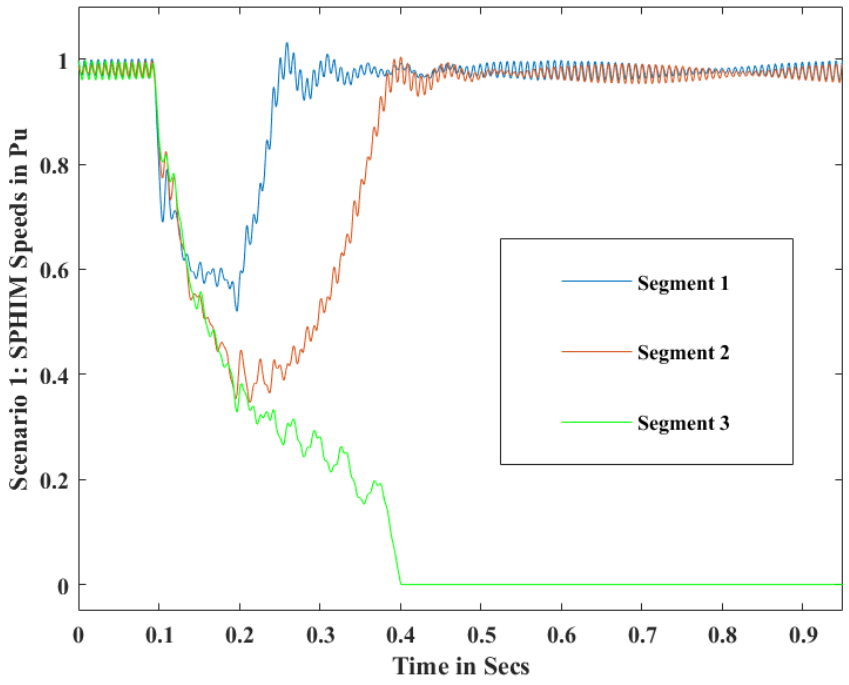

Figure 3.27 Evidence of SPHIM Stalling for Scenario 1 (FIDVR Event)

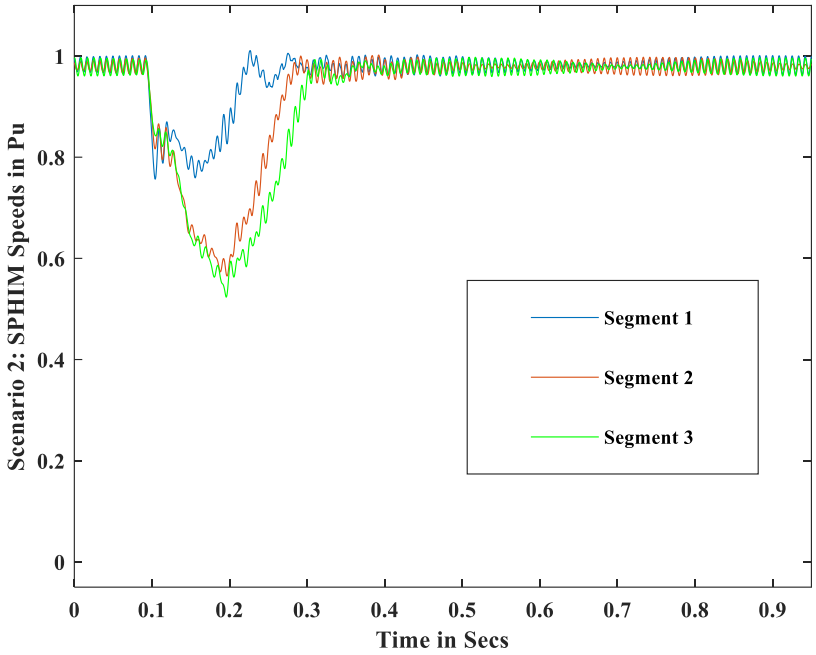

Figure 3.28 Evidence of No SPHIM Stalling for Scenario 2 (Non-FIDVR Event)

CHAPTER 4

EMT CONTACTOR MODEL DEVELOPMENT

4.1 Introduction and Literature Review

An electromagnetic contactor is an important electromechanical device used in industrial power systems to perform various functions such as load protection, motor starter or factory automation controller [42]. The contactors are designed to switch the load or the circuit they control due to the magnetic force, generated in the contactor, which is directly correlated to the voltage excitation provided to its main coil [43]. Contactor modeling is an essential part of the load modeling process [4] and has an increasing importance in the power system dynamic simulations [44]. Contactor protection used for motor loads are typically designed for fast response to severe voltage disturbances in the system.

Many efforts in the literature model the dynamic behavior of the contactors using the finite element method (FEM) [45]. However, FEM analysis is typically used for contactor design purposes and is not practically feasible for power system analysis due to its computational complexity. Some efforts deal with modeling the contactor using a magnetic equivalent circuit (MEC) approach [46]-[47]. In [48], the concept of high-fidelity magnetic equivalent circuit, to factor in the effects of fringe flux in a contactor, has been discussed. However, none of the approaches in the literature provide information about the impact of having the presence of an EMT contactor model in load modeling simulation studies. Therefore, in this work, an analytical model of a 24 V EMT contactor model with a good estimate of the contactor parameters, that captures the performance of typical laboratory tested contactors [49] over a wide range of voltage sags has been presented. For

the detailed three-phase 12.47 kV distribution feeder developed in Chapter 3, the proposed 24 V contactor model has been used to study its impact on the behavior of the SPHIMs [12].

The necessity to improve the contactor models, presently used in the positive sequence simulation packages [28] based on the performance characteristics of the developed 24 V EMT contactor has also been discussed in this Chapter. All the simulations in this Chapter have been conducted in PSCAD/EMTDC [18].

4.2 Contactor Modeling

In the following sub-sections, the procedure to model the contactor and the description of its parameters have been presented:

4.2.1 Analytical Modeling of the Contactor

The geometry of the considered contactor model has been presented in Figure 4.1. It is mainly comprised of the stator (stationary part), armature (moving part), main coil, shading rings, phase springs, and return springs.

It should be noted that, as the contactor geometry is symmetric in structure, the magnetic circuit equivalent corresponding to Figure 4.1 has been simplified and is shown in Figure 4.2.

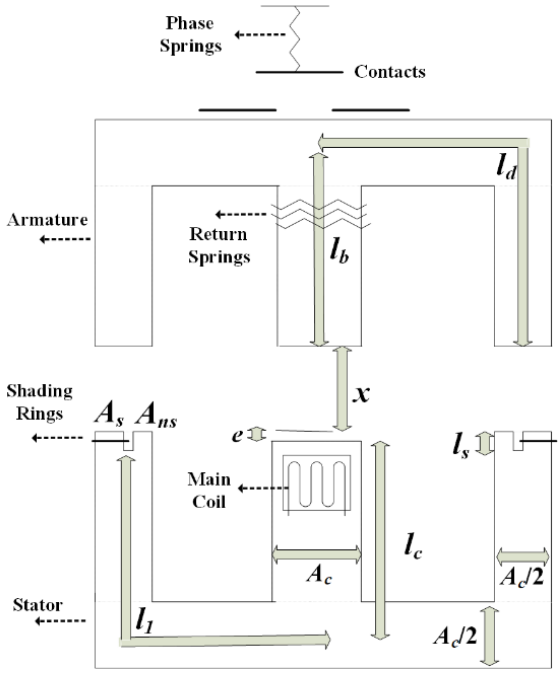

Figure 4.1 Schematic of the Contactor

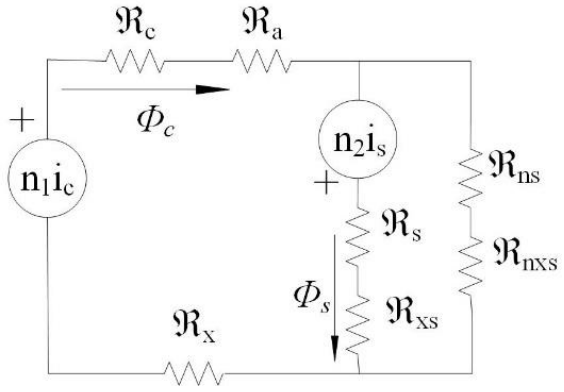

Figure 4.2 Magnetic Circuit of the Contactor

The electrical equations corresponding to the terminal voltage of the main coil and the shading rings (shorted at the ring ends) are as shown in (4.1) and (4.2) respectively. Additionally, the magnetic equations corresponding to Figure 4.2, in terms of magnetomotive forces (MMF) and reluctances, is presented in (4.3) and (4.4).

$$v_c = i_c R_c + n_1 \frac{\partial \phi_c}{\partial t} \tag{4.1}$$

$$0 = i_s R_s + n_2 \frac{\partial \phi_s}{\partial t} \tag{4.2}$$

$$n_1 i_c = (\Re_c + \Re_a + \Re_x)\phi_c + (\Re_{ns} + \Re_{nxs})(\phi_c - \phi_s) \tag{4.3}$$

$$n_1 i_c = (\Re_c + \Re_a + \Re_x)\phi_c + (\Re_{ns} + \Re_{nxs})(\phi_c - \phi_s) \tag{4.4}$$

Where, v_c is the voltage excitation of the coil, i_c and i_s are the coil current and shading current respectively, R_c and R_s are the coil resistance and shading ring resistance respectively, n_1 and n_2 represent the number of turns of the main coil and shading ring respectively. ϕ_c and ϕ_s are the flux linkages passing through the main coil and the shading rings respectively. The reluctances of each part of the magnetic contactor from (4.3) and (4.4) are described in (4.5).

$$\Re_c = \frac{l_c + 2l_1}{\eta A_c},\ \Re_a = \frac{l_b + 2l_d}{\eta A_c},\ \Re_x = \frac{x+e}{\eta A_c}$$

$$\Re_{ns} = \frac{l_s}{\eta(2A_{ns})},\ \Re_{nxs} = \frac{x}{\eta_0(2A_{ns})},\ \Re_s = \frac{l_s}{\eta(2A_s)}$$

$$\Re_{xs} = \frac{x}{\eta_0(2A_s)} \tag{4.5}$$

In (4.5), η_0 is the permeability of the air, η and η_r are the permeability and relative permeability of the contactor core material where $\eta = \eta_0\eta_r$. Also, an equivalent length variable of the armature, l_a, has been defined in this work where - $l_a = l_b + 2l_d$ and $l_d = 2l_b$.

The magnetic energy stored in the flux linkages due to the voltage excitation provided to the contactor terminals and the corresponding magnetic force experienced by the armature is as shown in (4.6) and (4.7) respectively.

$$W_{mag} = \frac{1}{2}\Re_{self\,\phi_c}\phi_c^{\,2} + \frac{1}{2}\Re_{self\,\phi_s}\phi_s^{\,2} + \frac{1}{2}\Re_{mut}\phi_c\phi_s + \frac{1}{2}\Re_{mut}\phi_s\phi_c \tag{4.6}$$

$$F_{mag} = -\frac{\partial W_{mag}}{\partial x} \tag{4.7}$$

Where, $\Re_{self\,\phi_c} = \Re_c + \Re_a + \Re_x + \Re_{ns} + \Re_{nxs}$, $\Re_{self\,\phi_s} = \Re_s + \Re_{xs} + \Re_{ns} + \Re_{nxs}$, $\Re_{mut} = \Re_{ns} + \Re_{nxs}$

The gravitational force exerted on the armature is given by (4.8), where M is the mass of the armature and g is the acceleration due to gravity.

$$F_g = -Mg \tag{4.8}$$

In this work, the spring forces (from both phase springs and return springs) acting on the armature, have been modeled based on [43] and is presented below in (4.9).

$$F_s = \begin{cases} k_1 x + c_1 & if \;\; x < x_c \\ k_2 x + c_2 & if \;\; x \geq x_c \end{cases} \tag{4.9}$$

In (4.9), $k_1 = k_2 + \frac{c_2 - c_1}{x_c}$ and $k_2 = \frac{3 - c_2}{x_{\max}}$. Also, c_1 and c_2 are unknown constants that are to be chosen appropriately to reflect a practical contactor behavior. x_c and $x_{\max}$ represent the contact gap and the maximum distance the armature can move respectively.

Using (4.7), (4.8) and (4.9) and applying the Newton's second law of motion to the armature would yield the following relation:

$$\frac{\partial^2 x}{\partial t^2} = \frac{1}{M}(F_{mag} + F_g + F_s) \tag{4.10}$$

In this work, (4.1) - (4.10) have been discretized and implemented in PSCAD using Norton current sources [18], that are updated each time step using the voltage obtained at the terminals of the contactor model in the current and previous time steps.

4.2.2 Choosing Contactor Parameters

The parameters for the contactor, used in (4.1) - (4.10), are presented in Table 4.1. The parameters in Table 4.2 are chosen to ensure that the performance of the proposed contactor model follows the behavior of the laboratory tested contactors [49], from two different manufacturers and under various voltage sag levels at the contactor terminals. Based on [49], the behavior exhibited by the developed contactor, in this work, is presented in Table 4.2.

In Table 4.2, chattering refers to the phenomenon where the contactor repeatedly trips and reconnects under low voltage conditions which typically occurs during a fault and a contactor trip refers to the contactor electrically switching off the load.

Table 4.1 Contactor Parameters

Parameters		**Corresponding Parameter Values**	
Geometrical	**Electrical, Mechanical and Magnetic**		
l_c	R_c	23 mm	4.5 Ω
l_1	R_s	79 mm	4 mΩ
l_s	n_1	1.62 mm	520
l_a	n_2	104 mm	1
e	c_1	0.04 mm	20
A_c	c_2	240 mm^2	6
A_s	μ_r	60 mm^2	450
A_{ns}	μ_0	20 mm^2	$4\pi*10^{-7}$ N/A^2
x_{max}	M	5.6 mm	0.075 kg
x_c	g	2 mm	9.81 m/s^2

Table 4.2 Developed Contactor Behavior Under Various Voltage Sag Levels

Voltage Sag Level at Contactor Terminals	**Contactor Status**
> 65%	Remain unaffected
50% - 65%	Chatters
< 50%	Trips Completely

4.3 Simulations and Results:

The EMT contactor model developed in Section 4.2 has been simulated in PSCAD [18]. The simulation results pertaining to this model are presented and analyzed in detail below in sub-sections 4.3.1 and 4.3.2:

4.3.1 Individual Contactor Unit

Based on [49], the test circuit as shown in Figure 4.3 is implemented to analyze the behavior of the developed EMT contactor. In [49], the testing on the 230 V laboratory contactors was conducted either under no-load conditions or resistive load using a voltage sag generator. However, the contactor model used in this work is to provide protection to the 230 V SPHIMs [12] and they are typically rated at 24 V after the voltage at the SPHIM terminal is stepped down using a 115 V/24 V transformer. Therefore, to emulate this setup from [49], a phase A, SLG fault has been simulated at the terminals of a 115 V voltage source as shown in Figure 4.3. In Figure 4.3, it should be noted that the signal value (‘0’ indicates the contactor is closed and ‘1’ indicates the contactor is tripped) obtained from the contactor is fed into the breaker in series with the load of interest (resistive load in this case). The value of the signal is obtained dynamically at each time step in the simulation based on the following criterion (4.11), where $signal_t$ and x_t are obtained at the t^{th} time step.

$$signal_t = \begin{cases} 0 & if \ \ x_t < x_c \\ 1 & if \ \ x_t \geq x_c \end{cases} \tag{4.11}$$

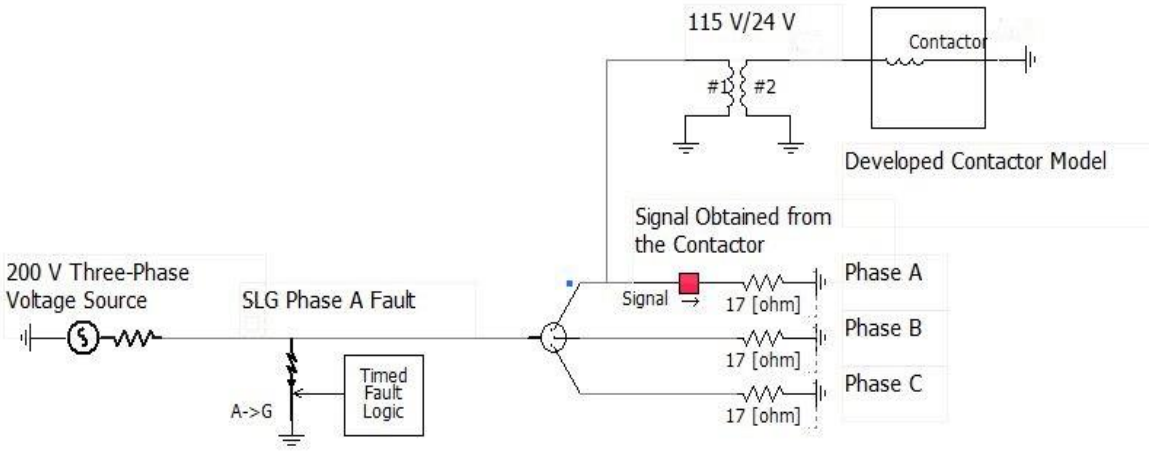

Figure 4.3 Individual Contactor Unit Testing Circuit

From Figure 4.4, it can be observed that when the voltage at the contactor terminals drops down to 40% of the pre-fault voltage, the contactor remains tripped until the fault is cleared after 12 cycles from the moment fault is initiated (indicated by the vertical black line in Figure 4.4).

The forces acting on the armature of the contactor corresponding to Figure 4.4 have been presented in Figure 4.5. Also, it takes 15.6 ms (less than 1 cycle) for the armature to reach the maximum distance (at $x = x_{max}$), as shown in Figure 4.6 using the marked points for the armature position, from its sealed position (at $x = 0$) with the stator after the fault is initiated. In Figure 4.6, it can also be seen the instant at which the power supply to the SPHIMs is interrupted (contactor is tripped) when the armature reaches the contact gap ($x = x_c$).

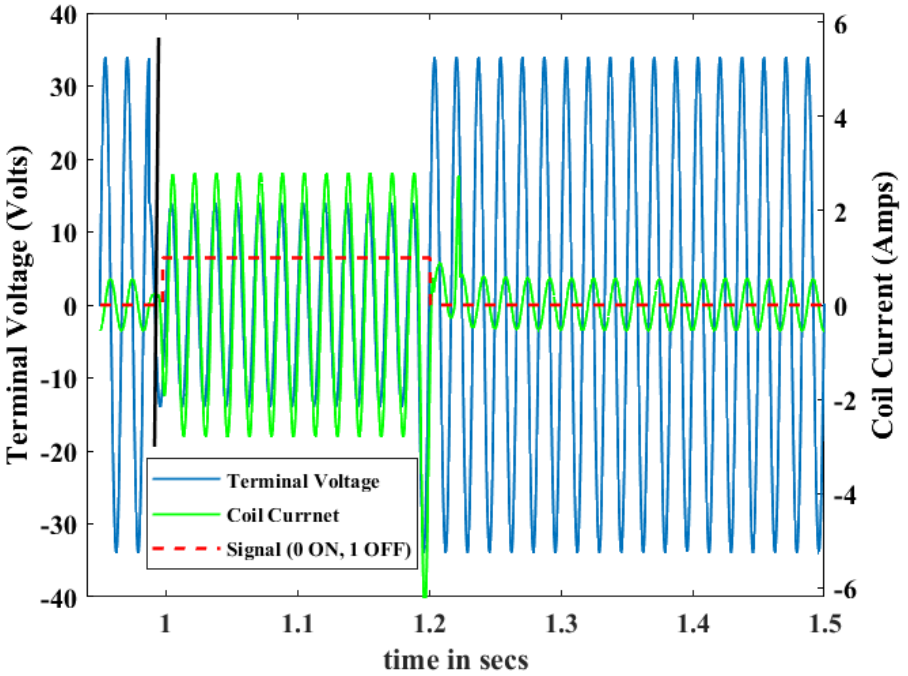

Figure 4.4 Contactor Voltage, Coil Current and the Contactor Signal at 40% Voltage Sag

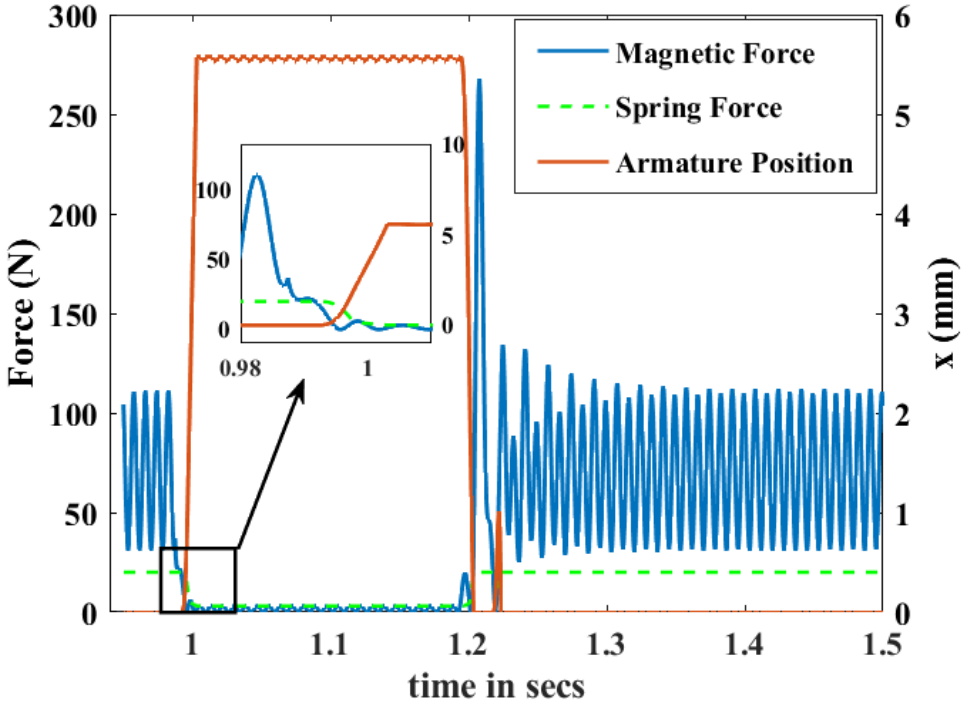

Figure 4.5 Demonstration of Forces Involved in the Contactor Dynamics that Affects the Armature Position at 40% Voltage Sag

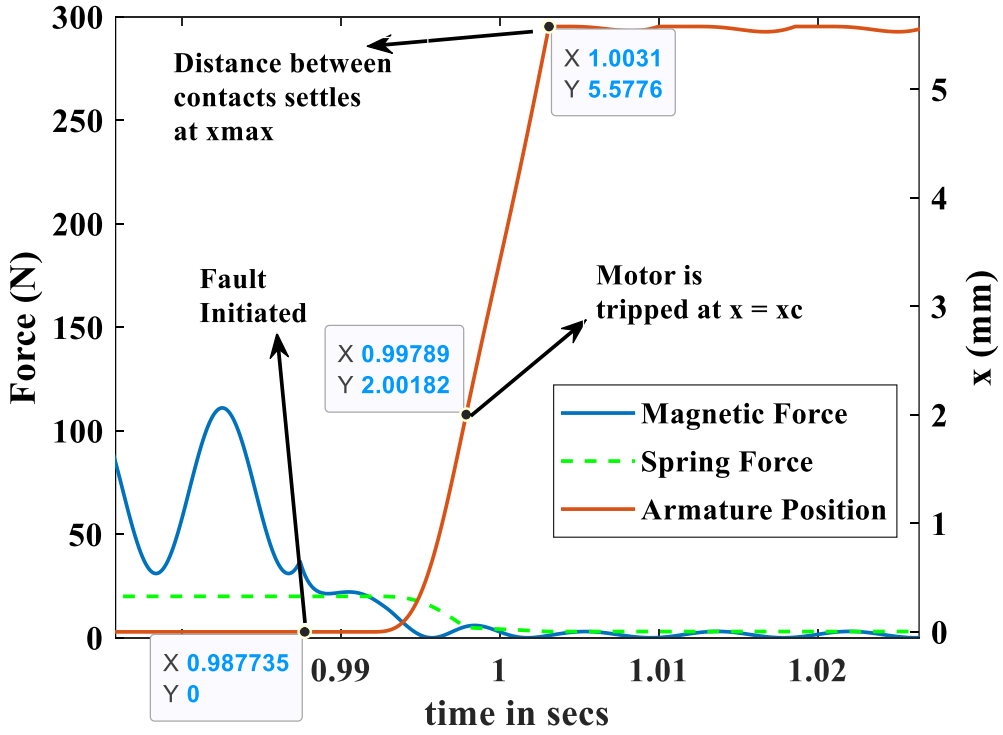

Figure 4.6 Demonstration of Timings at which the Armature Starts to Act (x=0), Reaches x_c and Settles at x_{max} Respectively

4.3.2 Distribution Feeder Analysis

In this sub-section, the impact of having the EMT contactors in the load modeling simulations is discussed in detail. All these simulations have been conducted on the proposed novel three-segment three-phase 12.47 kV feeder model which comprises of 460 V three-phase induction motors, custom built 230 V SPHIM models obtained from [12], resistive load, distribution line segments, distribution transformers and the 24 V EMT contactor developed in this Chapter (which is integrated to the proposed feeder and load model in Chapter 3 using the circuit schematic presented in Figure 4.3). The circuit used in these simulations is presented below in Figure 4.7. It should be noted that the load composition and the load parameters, obtained from Case 1, for a residential feeder during

summer conditions is used in this work for the considered feeder model.

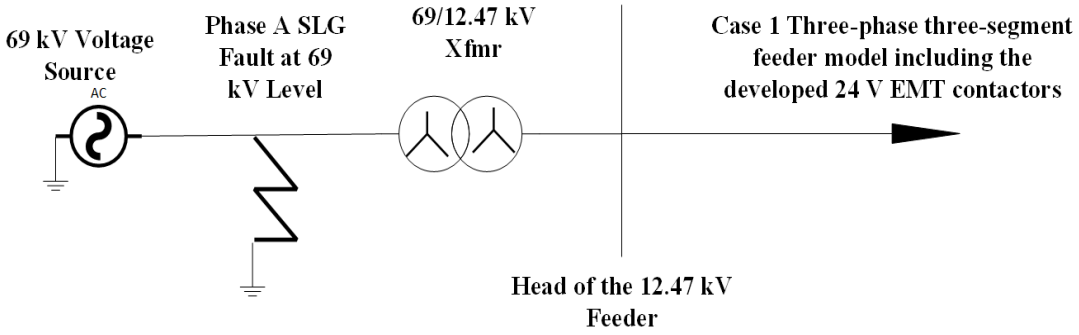

Figure 4.7 Circuit Setup in PSCAD to Analyze the Impact of Contactors on the Proposed 12.47 kV Distribution Feeder Model

Three sets of cases have been analyzed, when a 69 kV phase A SLG fault is applied for 4.5 cycles (7.5 ms), as described below:

- Case A – No Contactors (NC): In this scenario, no contactor model has been used in conjunction with the SPHIMs in the feeder model used in Figure 4.7 without the presence of the 24 V EMT contactors. Due to the low voltage (due to the fault), seen at the terminals of SPHIMs some SPHIMs stalled but none of the SPHIMs are tripped.
- Case B – Electromagnetic Contactor (EMTC): In this scenario, each of the SPHIMs presented on the feeder (3 segments x 3 phases = total of 9 SPHIMs on the feeder) is protected by a separate instance of the 24 V EMT contactor, each acting on the terminals of the individual SPHIMs. It should be noted that the inclusion of this contactor model into the considered feeder model has been implemented using the setup described in Figure 4.3 by replacing the resistive load with the SPHIMs. Here, in the presence of the contactor models, all the SPHIMs were tripped but only some of the SPHIMs had stalled.
- Case C – Contactor Logic (CL): Based on the contactor model used in the composite load model [13] for the protection of 'Motor D' SPHIM model, the SPHIMs in Figure

4.7 are tripped in this scenario using logic statements. When the voltage magnitude (obtained by applying the Fast Fourier Transform on the instantaneous voltage) at the SPHIM terminals falls below a certain threshold ('Vc1off' parameter from [13]) and is reconnected to the feeder when the SPHIM voltage magnitude recovers above a certain threshold voltage ('Vc2on' parameter from [13]) value. In this work, 'Vc1off' and 'Vc2on' have been taken to be 0.5 pu each to mimic the behavior of the developed EMT contactor (tripping behavior under 50% or below voltage sag level from Table 4.2) and they are the default values currently proposed in [13] for the composite load model SPHIM contactors.

It should be noted that in Figures 4.11 - 4.12, the solid black vertical line and dashed black vertical line represents the moments the SLG fault is initiated and cleared in the system respectively. The speed response of the SPHIMs along the three segments for Cases A-C scenarios is presented in Figures 4.8 – 4.10 respectively. It can be observed that for the NC case (Case A), both segment 2 and segment 3 SPHIMs stall and remained in stall condition after the fault is cleared. However, for the CL case (Case C), the speeds of SPHIMs in all three segments go down to zero and remain in stalled condition even after the fault is cleared whereas for the EMTC case (Case B), only segment 3 SPHIMs stall and segment 2 SPHIMs reaccelerate after the fault is cleared. This shows that the behavior of the SPHIMs is significantly different when using the detailed proposed EMT contactor model when compared to the contactor logic approach. This shows that, with the default contactor parameters that are currently being used in positive sequence simulators to represent contactors, it is not sufficient to replicate the behavior of the EMT contactor model in load modeling studies.

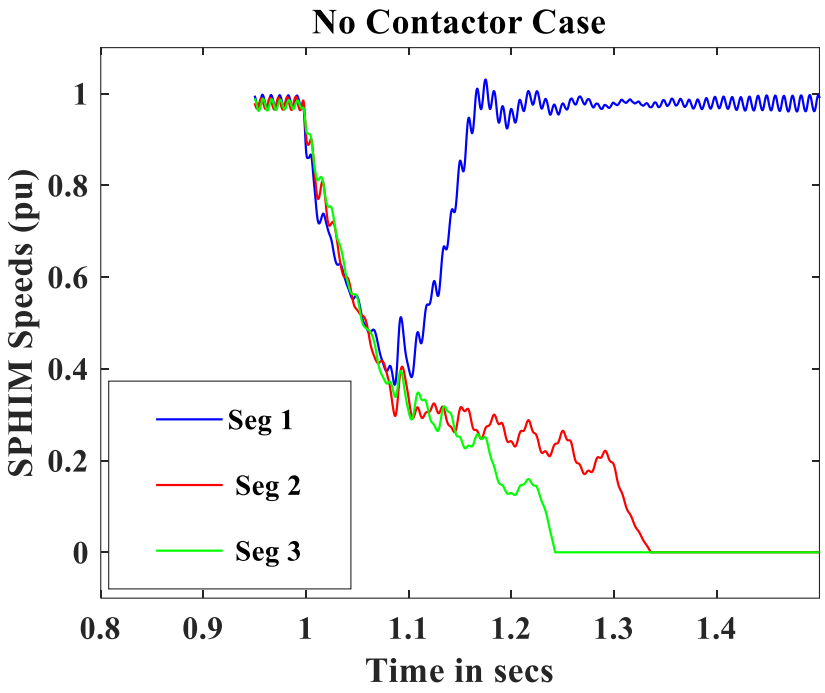

Figure 4.8 SPHIM Speeds Comparison for Case A Scenario (No Contactor Case) for the Faulted Phase

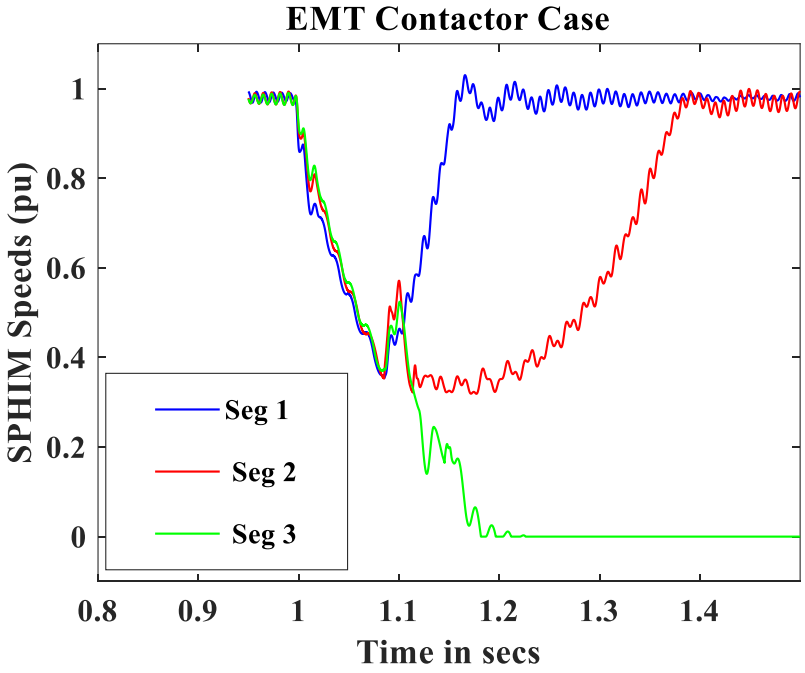

Figure 4.9 SPHIM Speeds Comparison for Case B Scenario (EMTC case) for the Faulted Phase

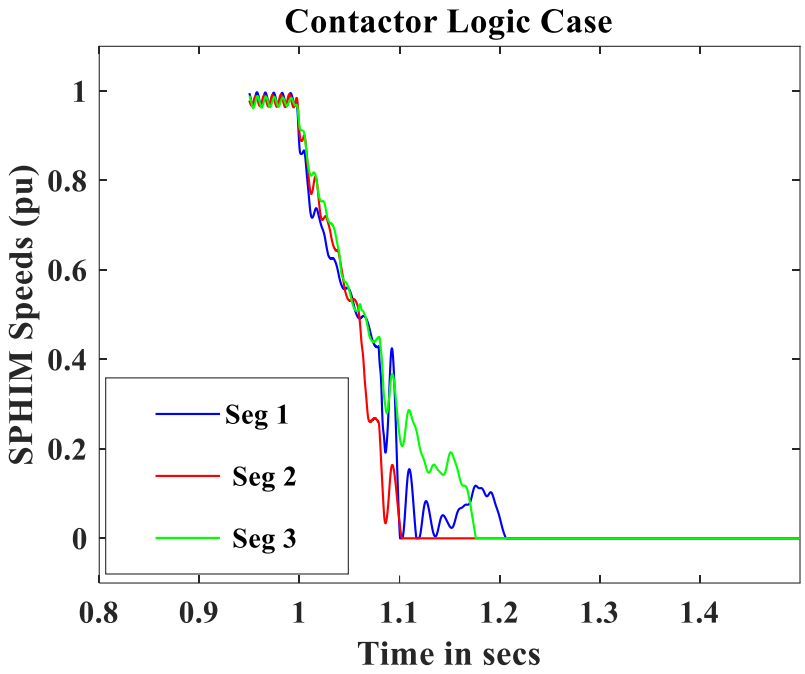

Figure 4.10 SPHIM Speeds Comparison for Case C Scenario (CL case) for the Faulted Phase

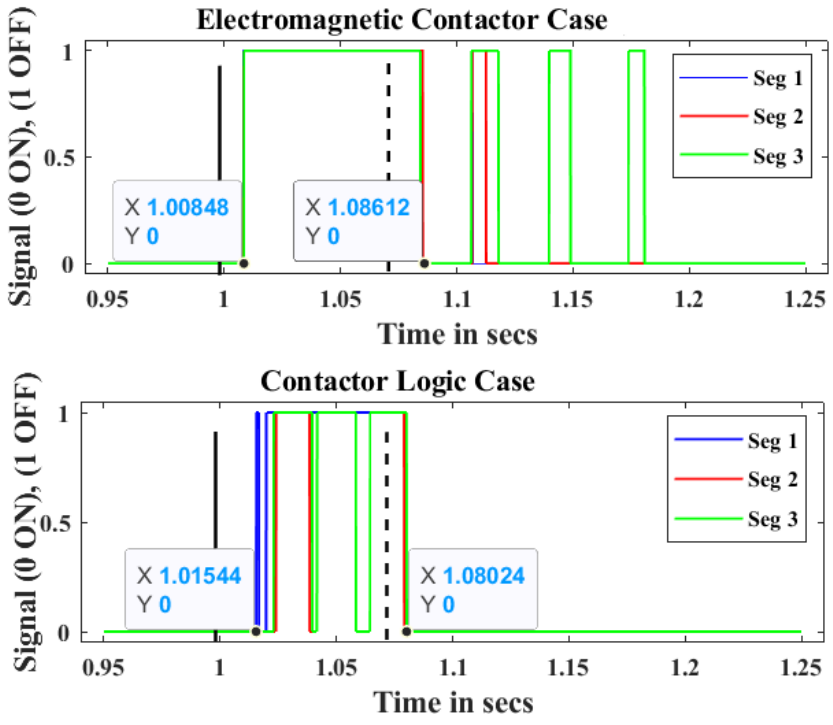

Figure 4.11 Contactor Signals Comparison for Case B and Case C for the Faulted Phase

The contactor signals across the three segments for Case B and Case C have been

presented in Figure 4.11. It can be observed that the EMT contactors tripped almost half a cycle (7 ms) earlier and reconnected 5.88 ms later when compared to their respective Case C CL model responses.

The head of the feeder voltage for Cases A-C are presented in Figure 4.12. It can be clearly seen that the post-fault steady state feeder head voltage for all three cases is less than their pre-fault voltage. This is to be expected because the SPHIMs stalled, in all the cases, due to which they draw large amounts of reactive power in locked rotor condition. It can also be seen that the higher the number of segments of SPHIMs stalled, in a particular case, the smaller its post-fault voltage becomes. Therefore, the Case C CL case has the lowest post-fault voltage due to all three segments of SPHIMs stalling and the Case B EMT contactor case has the highest post-fault voltage with only the SPHIMs in the last segment of the feeder stalling. Additionally, when the fault is present in the system, the feeder head voltage is significantly higher in Case B and Case C compared to Case A (no contactors) because the SPHIMs are disconnected from the feeder in the former cases during this period.

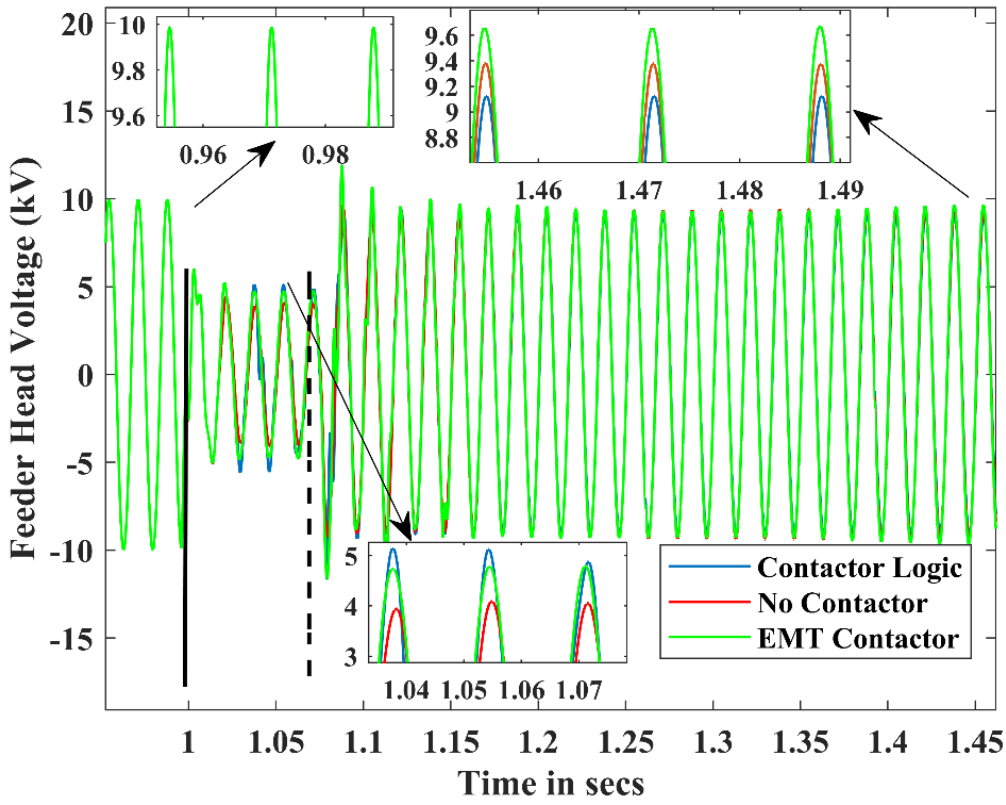

Figure 4.12 Feeder Head Voltage Comparison for Cases A-C Scenarios for the Faulted Phase

CHAPTER 5

POSITIVE SEQUENCE CONTACTOR MODEL DEVELOPMENT

5.1 Introduction

An analytical EMT model of the 24 V contactor, to provide protection for 230 V SPHIMs, has been developed in Chapter 4. It has also been observed that the performance of the proposed EMT contactor is significantly different compared to the contactor logic model (developed based on the existing positive sequence contactor model used in the '*cmpldw*' model for 'Motor D' model). This is because the contactor logic currently being used in the positive sequence contactor models does not capture the detailed dynamics of an EMT contactor model during disturbances in the system. Additionally, the parameters for the positive sequence contactors currently being used in the industry have not yet been validated [4]. Therefore, it is imperative that a methodology needs to be developed to incorporate the EMT contactor behavior characteristics into the currently used positive sequence contactors in the industry. For this reason, in this chapter, the following issues have been tackled in detail:

- ***Issue 1 - Estimating the proposed EMT contactor settings:*** The most important behavioral characteristics of a typical contactor model are – (i) Trip characteristic (the moment at which the contactor trips the load when the voltage at the terminals of the load goes below a given threshold and for a given time for a disturbance in the power system) (ii) Reconnection characteristic (the moment at which the contactor reconnects the tripped load when the voltage at the terminals of the load recovers above a given threshold for a disturbance for a given amount of time in the power system). Therefore,

regression models such as a linear regression model and deep neural network (DNN) models have been developed in this work to estimate these important EMT contactor characteristic settings. Details regarding the developed linear regression model and the DNN models have been presented in the following sub-sections of this chapter.

- ***Issue 2 - Incorporate the estimated EMT contactor settings into the positive sequence load models:*** Currently, there is no contactor model modeled for the 'motorc' model (phasor based single-phase induction motor model) in PSLF [28]. Therefore, a methodology to incorporate the EMT contactor settings, estimated from *'Issue 1'* step to trip and reconnect the 'motorc' model appropriately is also developed in this work and the details of this methodology is presented in this chapter.

Note: Typically, in the literature, the positive sequence contactor models trip settings are based on the positive sequence voltage at the terminals of the load they are supposed to trip. However, the measurement data, for any event across the system, usually available for the planning engineers is at 69 kV (high voltage side of the substation on the sub-transmission side of the system) or at 12.47 kV (low voltage side of the substation on the head of the feeder) level. Therefore, the EMT contactors trip and reconnection settings, across the feeder, obtained from solving 'Issue 1' described above are estimated based on the characteristics of the positive sequence head of the feeder 12.47 kV voltage profile rather than the 230 V voltage at the terminals of SPHIM model considered in the proposed PSCAD feeder and load model in this work. More details about this approach are presented in the later sub-sections of this chapter.

Overall, the detailed procedure, as described in sections 5.2 and 5.3, to incorporate the estimated EMT contactor trip and reconnection settings and the estimated SPHIM

stalling behavior to trip, reconnect and stall the 'motorc' model can be summarized as shown below in five steps and the overall flow process between various models in this methodology in terms of these five steps has been presented in Figure 5.1.

- ***Step 1:*** Choosing features of the contactor (status, trip and reconnection settings)
- ***Step 2:*** Features generation using PSCAD (generate a large number of test cases)
- ***Step 3:*** Development of regression models (linear regression model and deep neural networks) to estimate the contactor features.
- ***Step 4:*** Development of regression models (DNNs) to estimate motor stalling behavior in the presence of the developed contactor model.
- ***Step 5:*** Implementation of the developed contactor model into PSLF environment.

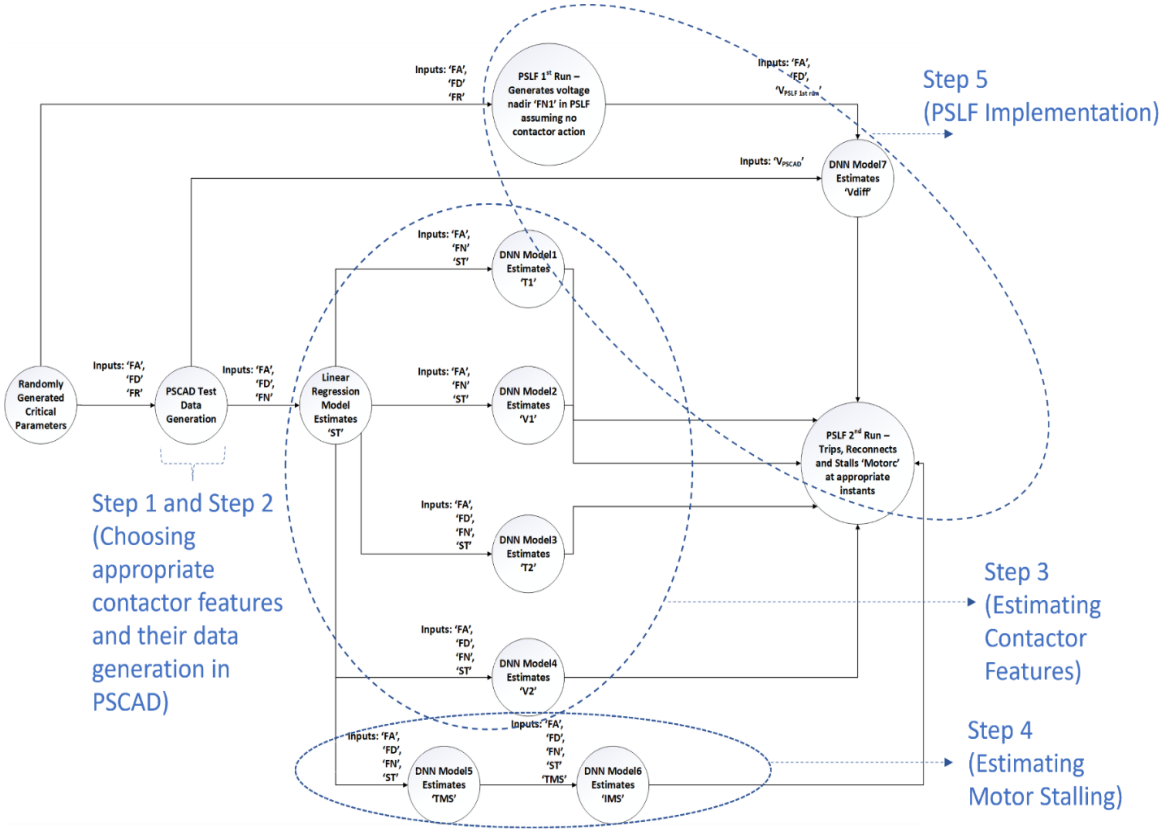

Figure 5.1 Flow Process Between Various Developed Regression and DNN Models Within the Simulation Software Packages (PSCAD and PSLF)

5.2 Estimating the EMT Contactor Trip and Reconnection Settings

The step-by-step procedure to estimate the trip and reconnection settings of the developed 24 V EMT contactor is presented below:

5.2.1 Step 1: Test Cases Generation and Feature Selection

The first step to implement in estimating the EMT contactor settings is to generate a large data set that captures these characteristics of the EMT contactor. The circuit schematic presented in Figure 4.7 (from Chapter 4) has been used in this work to generate a large number of test cases. Using this circuit, a total of 300 phase A SLG fault test cases have been generated by randomly varying the following critical parameters:

- Fault Resistance (*'FR'*): The fault resistance to ground at the 69 kV level at the location of the fault.
- Fault Duration (*'FD'*): The duration in which the fault is present in the system before it is cleared.
- Fault Angle (*'FA'*): The point on the sine wave (on the voltage curve) at the point of fault initiation.

Table 5.1 Bounds for the Considered Critical Parameters to Generate the Test Data

Critical Parameter	**Lower Bound**	**Upper Bound**
Fault Resistance	0 ohms	4 ohms
Fault Duration	4 cycles	6 cycles
Fault Angle	0 radians	1/240 radians

In addition to choosing the critical parameters to vary the impact of the considered

SLG fault, it is important to choose appropriate bounds for these parameters using engineering judgement to ensure the generated test cases are realistic in nature. For this reason, the bounds chosen for the critical parameters are shown in Table 5.1. The following criteria has been used to choose these bounds in this work:

(i) *'FR'* – Based on [49], a wide range of voltage sag levels (between 20% - 80%) has been generated by varying the 'FR' between the chosen bounds from Table 5.1.

(ii) *'FD'* – The faults on the sub-transmission system (69 kV in this work) are typically cleared between 4-6 cycles [50].

(iii) *'FA'* – Due to the symmetric nature of the voltage sinusoidal signal, in the POW EMT simulation, the point of initiation of the fault is varied on the quarter cycle (0^0 to 90^0) of the 69 kV voltage signal.

Note: Based on the test cases generated in PSCAD, it should be noted that for most of the considered test cases, the behavior of the EMT contactors along the considered distribution feeder model has been observed to be the same. For example: For a severe SLG fault case, all the contactors across the three segments of the feeder trip the SPHIMs whereas for a less severe fault the behavior of all the contactors across the feeder are not affected.

The description of the trip and reconnection settings estimated for the proposed EMT contactor are given below –

- *'ST'* – Trip status of the EMT contactor. This variable provides the information if the contactor trips, chatters, or is not affected.
- *'T1'* – Time taken for the EMT contactor to electrically disconnect the load or starts to

chatter (after the fault is applied in the system)

- *'V1'* – Feeder head voltage level (in pu) at which the EMT contactor electrically starts to disconnect or starts to chatter (after the fault is applied) normalized using its pre-fault steady state voltage.
- *'T2'* - Time taken for the EMT contactor to initiate reconnection to the feeder (after the fault is applied in the system)
- *'V2'* - Feeder head voltage level (in pu) at which the EMT contactor electrically starts to reconnect (after the fault is cleared) normalized using it pre-fault steady state voltage.

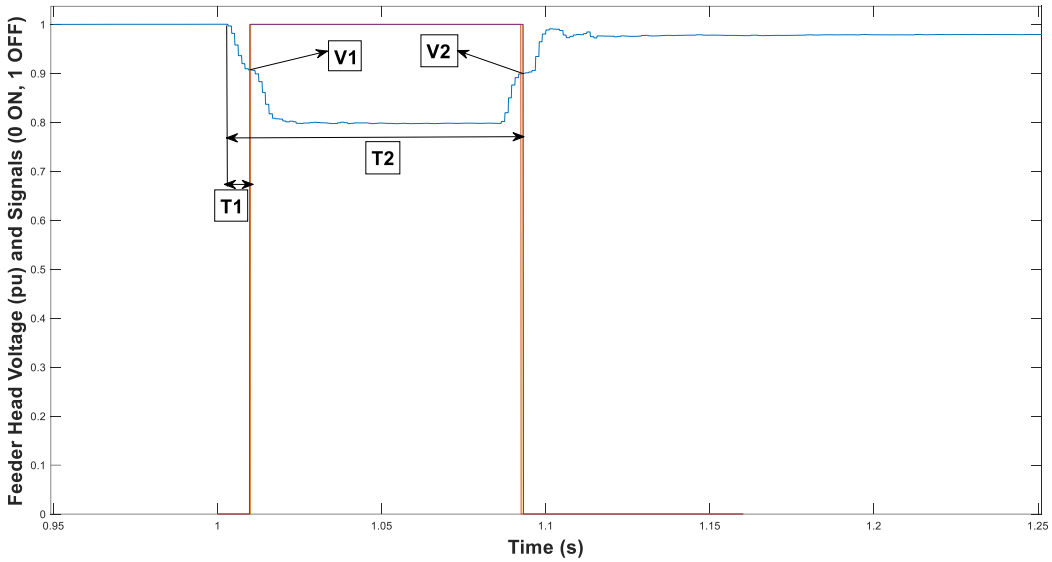

Figure 5.2 Demonstration of Contactor Settings to be Estimated as a Function of the Positive Sequence Feeder Head Voltage

A pictorial description of the above trip and reconnection settings of the proposed contactor model is presented in Figure 5.2 as a function of the feeder head voltage, where all the contactors along the feeder have tripped along the feeder on the faulted phase. In Figure 5.2, it should be noted that only the SPHIMs on phase A (faulted phase) have stalled in all three segments (and all three contactors along phase A tripped completely) and the SPHIMs in the remaining phases are unaffected. This is to be expected because for SLG

faults, only the faulted phase is the most impacted and the other two phases are barely affected (as the 69/12.47 kV transformer being a Y-Y type transformer as shown in Figure 4.7).

5.2.2 Step 2: Linear Regression Model to Estimate *'ST'* Parameter

In this work, the status of the EMT contactor (parameter *'ST'*) is estimated using a ***multi-variable linear regression model***. A multi-variable linear regression model refers to a set of independent input features in linear combination with their corresponding coefficients which is used in estimating a single dependent output variable. Many efforts in the literature use this technique such as for load forecasting [51]-[52] applications. In this technique, the linear regression model is initially trained using test cases from the training data set. The trained regression model is then tested with new test cases from the testing data set to test the efficacy of the trained regression model.

The independent input features used in this work are given below –

- Fault Angle ('*FA*') – The behavior of the contactor model is significantly impacted based on the instant of initiation of the fault on the sinusoidal waveform [50]. For example: If the fault is applied near the voltage zero, the fault event would be very severe in nature Whereas, a fault applied near the voltage peak is a significantly less severe event.
- Fault Duration ('*FD*') – The duration of the fault determines the amount of time the voltage at the terminals of the contactor is depressed in the system.
- Voltage Nadir ('*FN*') – The voltage nadir of the positive sequence voltage at the head of the feeder normalized using its pre-fault steady state voltage for each test case has

been taken to be another input in this work. This nadir value directly correlates to the voltage sag level at the terminals of the contactor. From [49], it is understood that the voltage sag level plays an important role in the behavior of the contactor model when there is a disturbance in the system.

The linear regression expression that has been trained in this work to estimate the status of the contactors is given below –

$$Y_{train} = b_0 + b_1*FA + b_2*FD + b_3*FN \quad (5.1)$$

Where, b_0, b_1, b_2, and b_3 are the estimated coefficients of the linear regression model and Y_{train} is a dependent output variable that is given as an input during the training process whose possible input values are described below:

If the behavior of the three contactors (one each from every segment) along the feeder on the faulted phase for a particular test case are:

(i) **Not affected:** Y_{train} value would be given as 0.

(ii) **Chattering:** Y_{train} value would be given as 1.5.

(iii) **Tripped:** Y_{train} value would be given as 3.

It should be noted that the inputs '*FA*', '*FD*' and '*FN*' in (5.1) are normalized using the following expression –

$$pr' = \frac{pr - \mu_{pr}}{\sigma_{pr}} \quad (5.2)$$

Where pr is the original parameter of interest, pr' is the normalized value of pr, μ_{pr} is the mean of the total samples of the pr population, σ_{pr} is the standard deviation of the total samples of the pr population.

Note: Earlier in sub-section 5.2.1, it was mentioned that a total of 300 cases have

been generated to estimate the EMT contactor settings. ***In these 300 test cases, 225 test cases were used to train the linear regression model and the remaining 75 test cases were used to test the trained regression model.*** *It should also be noted that the normalization of 'FA', 'FD', 'FN' using (5.2) has been done on all the 300 test cases together. In other words, the mean and the standard deviation used in (5.2) is obtained using all 300 test cases. Similarly, the normalization applied on the estimated 'ST' parameter (which is used as an input to the DNN regression models developed later in this Chapter) is implemented on all the 300 cases.*

Note: It should be noted that a time step of 0.5 μs has been used in PSCAD to ensure there is no numerical noise on the voltage signal at the end of the SPHIM terminals due to the contactor action when the system is faulted. This is because at larger time steps such as 5 μs a high frequency numerical noise is observed on the voltage at the SPHIM terminals when there is contactor action.

The regression coefficients obtained from the training process are given below in Table 5.2 –

Table 5.2 Regression Coefficient Values Obtained from Training the Linear Regression Model

Regression Coefficient	**Estimated value from the training process**
b_0 *(bias)*	1.69
b_1 *('FA' coefficient)*	0.0042
b_2 *('FD' coefficient)*	4.87e-06
, b_3 *('FN' coefficient)*	-1.0396

From Table 5.2, it can be clearly seen that the trip status of the contactor is primarily dependent on *'FN'* (significantly higher magnitude for its coefficient) and significantly less correlated to the fault angle *'FA'* and fault duration *'FD'* parameters (comparatively low values of their coefficients).

Therefore, the final regression expression obtained after the training process is as shown below in (5.3) –

$$Y_{test} = 1.69 + 0.0042*FA + 4.87e\text{-}06*FD - 1.0396*FN \quad (5.3)$$

and the testing process for the trained model has been conducted using the criterion described below –

For any particular test case from the testing dataset,

- If estimated $Y_{test} < 1$ then, *'ST'* is taken to be 0 (no tripping)
- If estimated Y_{test} ε (1,2) then, *'ST'* is taken to be 1.5 (chattering)
- If estimated $Y_{test} > 2$ then, *'ST'* is taken to be 3 (tripping)

Therefore, using the above criterion, for each test case in the testing dataset, the estimated value of the *'ST'* has been compared with its corresponding true value obtained from the PSCAD test case. ***Using this testing process, it was observed that an accuracy of 98% has been obtained for the developed linear regression model to estimate the trip status of the proposed EMT contactor model.***

In Table 5.3, the efficacy of the developed regression model has been demonstrated for a few test cases from the testing data set. It is observed that the developed regression model estimates the *'ST'* parameter for the EMT contactor model with a good accuracy. It

should also be noted that the R^2 [53] value of the developed regression model is approximately 0.81. This clearly shows that there is a strong linear correlation between the considered input features and the output variable from which it can be inferred that the proposed linear regression approach, to estimate the contactors status, also makes sense from a statistical point of view.

Table 5.3 Demonstration of Accuracy of the Developed Regression Model to Estimate the Contactors Status

Test Case	***'FA'* (radians)**	***'FD'* (secs)**	***'FN'* (pu)**	**True *'ST'***	**Estimated *'Y_{test}'***	**Estimated *'ST'* (Status of the contactors)**
1	0.00082	0.077	0.918845	0	0.318	0 (No trip)
2	0.00154	0.076	0.912943	0	0.417	0 (No trip)
3	0.001211	0.08651	0.874816	1.5	1.039	1.5 (Chattering)
4	0.000369	0.069995	0.871156	1.5	1.096	1.5 (Chattering)
5	0.002642	0.081263	0.777809	3	2.628	3 (Trips)
6	0.003965	0.098349	0.760356	3	2.917	3 (Trips)

5.2.3 Step 3: DNN Model Development to Estimate the Contactor Trip and Reconnection Settings

After obtaining the status of the contactor model using the developed linear regression model, it is important to estimate the trip and reconnection settings of the proposed contactor model. For this reason, the developed linear regression model has been used to estimate the *'T1', 'V1', 'T2'* and *'V2'* parameters. From testing this approach, it was observed that the values of these parameters are estimated with very poor accuracy

compared to their corresponding true values obtained from the corresponding PSCAD test cases. Additionally, it was observed that the R^2 [53] value for the linear regression models developed for these trip and reconnection parameters for the contactor is 0.48. This clearly shows that for the considered input features, there is not much linear correlation present with their corresponding output variables. Therefore, it can be concluded that the linear regression approach to estimate the contactor trip and reconnection settings would not be appropriate. ***Hence, the approach of deep neural networks (DNNs) has been adopted in this work to capture the complex non-linearity relationship [54] between the considered input features and the estimated contactor trip and reconnection settings.***

The approach of DNNs is more robust compared to the traditional linear and non-linear regression techniques used in the literature to learn the functional relationship between any given set of inputs and the outputs (if there exists a relationship between the inputs and the outputs). This is because DNNs are a computation model (comprising of neurons in layers) similar to a human brain learning from its experiences (where connections are formed in the brain's biological nervous system). In the literature, DNNs have already been utilized in several applications. For example, DNNs have been employed to design advanced control schemes for improving power system stability [55]. Some of the applications of DNNs have been explored, in [56], [57], by tackling key power system topics such as load forecasting, fault diagnosis, transient stability and economic dispatch.

In Figure 5.3, a general structure of a DNN with its components (different types of layers) is presented. Each layer in a DNN comprises of a set of nodes (neurons). Typically, a DNN contains the following types of layers:

- Input Layer: This layer contains the input neurons (each input neuron corresponds to

an input feature given to the DNN model)

- Hidden Layers: The number of hidden layers and the number of neurons each layer comprise of are classified as some of the hyperparameters (parameters that are typically tuned in a DNN framework to obtain the best results) in the DNN model. More details about these hyperparameters are presented later in this sub-section.
- Output Layer: The layer which contains the number of neurons equal to the number parameters to be estimated using the DNN model.

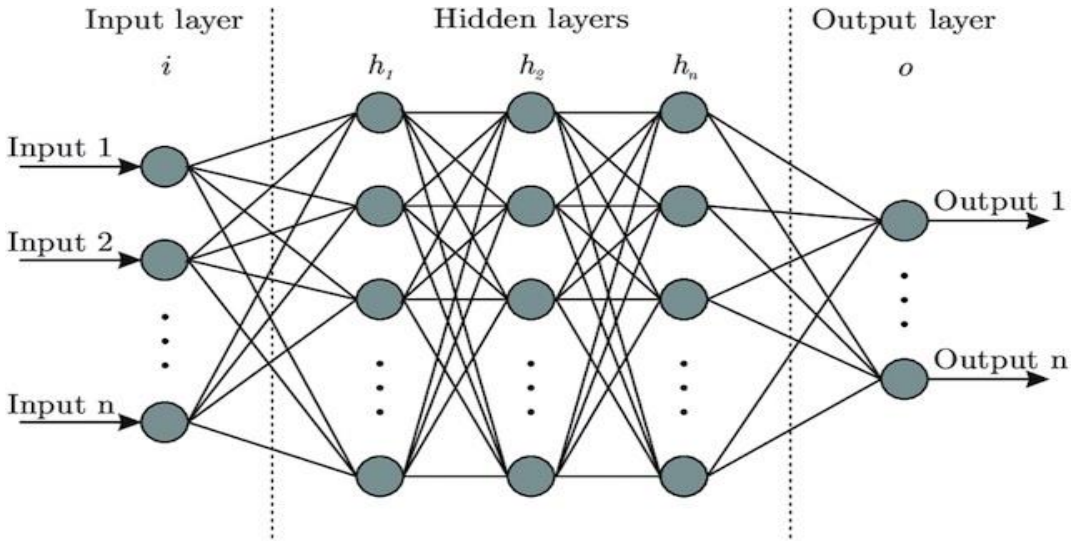

Figure 5.3 The Structure of a Generic DNN which Comprises of Input Layers, Hidden Layers, and Output Layers

In the DNN model, each neuron is populated with a value using the following expression –

$$NV_{i,j} = f\left(W^t X + b_{i,j}\right) \tag{5.4}$$

Where, $NV_{i,j}$ is the value of the i^{th} neuron in the j^{th} layer, $W^t = [w_{1,j-1}, w_{2,j-1}, \ldots\ldots, w_{n,j-1}]$, $X = [x_{1,j-1}, x_{2,j-1}, \ldots\ldots, x_{n,j-1}]^t$, $b_{i,j}$ is the bias for the i^{th} neuron in the j^{th} layer, $w_{i,j-1}$ is the weight from the i^{th} neuron in the $(j-1)^{th}$ layer to the neuron

of interest, $x_{i,j-1}$ is the value of the i^{th} neuron in the $(j-1)^{th}$ layer, and f is the activation function (also known as transfer function).

There are many activation functions available, in the literature, such as ReLU, linear and Sigmoid [58]-[59]. In this work, ReLU function has been employed as the activation function which is described as shown below in (5.5) –

$$f(x) = \begin{cases} 0, & x < 0 \\ x, & x \geq 0 \end{cases} \tag{5.5}$$

This is because, in the literature, recently ReLU became the most popular choice of activation function as it is resilient against the vanishing gradient issue [58] that occur in a DNN problem.

Also, in the training process of a DNN model, the back-propagation algorithm is typically used. In this algorithm, the mean square error (MSE) between the target output variable and the calculated output variable would be back propagated to the previous layers by adjusting the neuron weights and biases in each iteration to reduce the MSE. In this work, the Adam optimizer [60], in open-source python (Google Colab) [61] has been used as the platform to accomplish this. Typically, the Adam optimizer algorithm's working principle is based on the stochastic gradient descent algorithm in addition to computing the individual adaptive learning rates for the weights and the biases parameters using the estimates from the first and second order gradients [60].

Regarding the choice of appropriate input features for the proposed DNN models, the following criterion has been used, assuming the *'ST'* parameter obtained from the linear regression model is known (whose estimation accuracy of 98% is good enough to be considered as one of the known parameters) –

(i) For estimating *'T1', 'V1'* parameters, phenomena which occur before the fault is cleared in the system (therefore *'FD'* has not been used as an input), the following input features (after applying normalization using (5.2)) are used:

- *'FA'*
- *'FN'*
- *'ST'*

(ii) For estimating *'T2', 'V2'* parameters, phenomena which occur after the fault is cleared in the system (therefore *'FD'* has been used as an input), the following input features (after applying normalization using (5.2)) are used:

- *'FA'*
- *'FN'*
- *'ST'*
- *'FD'*

Note: It should be noted that four different DNN models (one for each estimated contactor setting) have been developed in this work to estimate the contactors trip ('T1', 'V1') and reconnection ('T2', 'V2') settings. Also, as mentioned earlier in the previous sub-section, a total of 300 test cases had to be generated to estimate the contactor trip and reconnection settings using DNNs with good accuracy. It should also be noted that in these 300 test cases only 230 cases have been used to develop the DNN models. This is because in 70 test cases, there is no contactors action (tripping or chattering) when the fault event is not severe enough. Therefore, those test cases are not useful to be used to estimate the contactors trip and reconnection settings. Also, in the considered 230 test cases, 173 test cases (75% of the total test cases) are used for the training dataset and 57 test cases (25%

of the total test cases) are used for the testing data set to develop the DNN models.

In order to obtain a good accuracy of the estimated outputs using the developed DNN models, it is important to tune the hyperparameters such as choosing the number of hidden layers and the number of neurons in each layer, identifying the number of iterations necessary to train the DNN. The final tuned (chosen) hyperparameters, for each developed DNN model in this work, are presented in Table 5.4.

Table 5.4 Final Chosen Hyperparameters for the Developed DNN Models in this Work

Model Number	**Estimated Output Parameter**	**Number of Hidden Layers**	**Number of neurons for each hidden layer respectively**	**Number of iterations before the training process is terminated**
DNN Model 1	*'T1'*	5	10, 4, 10, 5 and 2	2800
DNN Model 2	*'V1'*	4	6, 6, 5 and 3	2100
DNN Model 3	*'T2'*	4	13, 7, 13 and 7	900
DNN Model 4	*V2'*	4	13, 7, 16 and 8	1200

It should also be noted that, as mentioned earlier in this sub-section, 3 neurons (3 input features) for the input layer have been used for DNN model 1 and DNN model 2 whereas 4 neurons (4 input features) have been used for the input layer of DNN model 3 and DNN model 4. Also, as only one output parameter is estimated for each DNN model, the output layer in each DNN model contains only one neuron.

Using the procedure, described in this sub-section, to develop the proposed four DNN models, the performance (on both the training and testing data sets) of these four

DNN models have been presented below in Table 5.5.

Table 5.5 Demonstration of the Overall Performance of the Developed DNN Models

Model	**Average Training RMS Error**	**Average Testing RMS Error**
'T1' DNN model	1.53 ms	2.52 ms
'V1' DNN model	0.0083 pu (0.83 % pu)	0.0095 pu (0.95 % pu)
'T2' DNN model	3.60 ms	4.77 ms
'V2' DNN model	0.013 pu (1.3 % pu)	0.021 pu (2.1% pu)

From Table 5.5, it can be observed that the developed DNN models estimate the contactor trip and reconnection settings with a good accuracy because:

(i) For *'T1'* and *'T2'* models: Both the training and testing cases average RMS error is significantly less than 1 time step in PSLF (typically, a quarter cycle or 4.16 ms is used as a time step in planning studies) in the case of '*T1'* model and approximately 1 time step average RMS error in PSLF for the *'T2'* model. This shows that the instant at which the contactor is estimated to be tripped or reconnected in PSLF is within an error of ± 1 time step (timeframe in which the system behavior would not change drastically) in PSLF studies.

(ii) For *'V1'* and *'V2'* models: Both the training and testing cases average RMS error for these models are observed to be within the acceptable 5% error bandwidth in the voltages.

In Table 5.6 – 5.9, the demonstration of the accuracy of the developed DNN models

for a few specific test cases (from the overall 57 testing samples used for the development of DNNs) are presented. From these tables, it can be clearly seen that the developed DNN models estimate the desired contactor trip and reconnection parameters with a good accuracy.

Table 5.6 Demonstration of Accuracy of *'T1'* DNN Model for Some Test Cases

True V1 (pu)	True Va1(pu)	True T1 (ms)	Estimated T1 (ms)
0.912	0.662	14.6	15.07
0.88	0.642	11.67	11.74
0.882	0.649	36.81	35.80
0.921	0.676	8.63	11.55
0.889	0.668	17.62	18.13

Table 5.7 Demonstration of Accuracy of *'V1'* DNN Model for Some Test Cases

True T1(ms)	True Va1(pu)	True V1(pu)	Estimated V1 (pu)
11.69	0.662	0.887	0.889
15.35	0.683	0.911	0.906
11.68	0.557	0.849	0.853
14.60	0.626	0.912	0.887
15.73	0.663	0.903	0.904

Table 5.8 Demonstration of Accuracy of *'T2'* DNN Model for Some Test Cases

True T1 (ms)	True V1 (pu)	True Va1 (pu)	True T2 (ms)	Estimated T2 (ms)
14.60	0.912	0.626	103.76	107.41
11.68	0.849	0.557	111.88	111.82
11.95	0.91	0.672	88.51	91.91
35.03	0.878	0.635	81.59	80.38
35.03	0.874	0.628	96.59	89.18

Table 5.9 Demonstration of Accuracy of *'V2'* DNN Model for Some Test Cases

True T1 (ms)	True V1 (pu)	True Va1 (pu)	True Va2 (pu)	True V2 (ms)	Estimated V2 (ms)
14.60	0.912	0.626	0.749	0.905	0.924
11.68	0.849	0.557	0.535	0.841	0.849
11.22	0.888	0.668	0.605	0.863	0.866
31.39	0.884	0.631	0.725	0.919	0.915
12.51	0.848	0.548	0.52	0.837	0.863

The description of the various voltages used in Tables 5.6 - 5.9 is given below –

- True V1 – Measured Positive Sequence Feeder Head Voltage (at the point electrical disconnection of contactors) normalized using its pre-fault steady state voltage obtained from PSCAD.
- True Va1 – Measured Faulted Phase A Feeder Head Voltage (at the point of electrical disconnection of contactors) normalized using its pre-fault steady state voltage obtained from PSCAD.
- True V2 – Measured Positive Sequence Feeder Head Voltage (at the point of electrical

reconnection of contactors) normalized using its pre-fault steady state voltage obtained from PSCAD.

- True Va2 – Measured Faulted Phase A Feeder Head Voltage (at the point of electrical reconnection of contactors) normalized using its pre-fault steady state voltage obtained from PSCAD.

Note: It should be noted that, in Tables 5.6 - 5.9, typically V1, V2 quantities are observed to be much higher compared to their respective Va1 and Va2 values. This is to be expected because, in V1 and V2 quantities, the drop in the feeder head positive sequence voltage is offset by the two non-faulted phases. Also, in Tables 5.6 – 5.9, the Blue quantities represent additional information and the Red Quantities represent the comparison information between the true value and its corresponding estimated value of the parameter of interest.

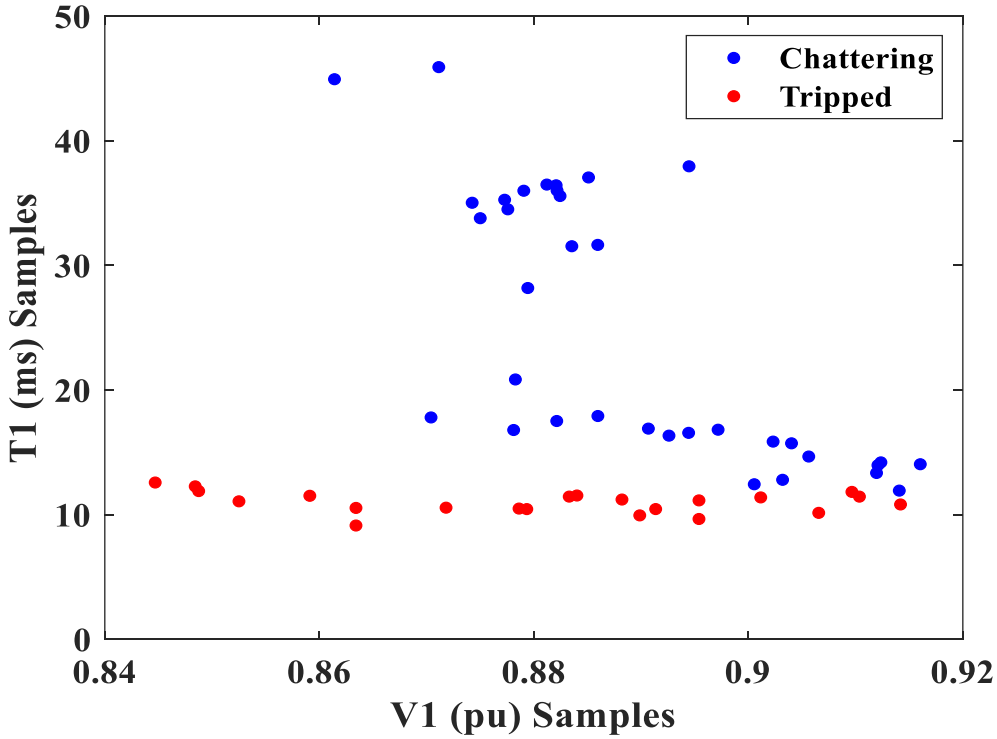

Figure 5.4 Comparison Between the *'T1'* and *'V1'* Values for All the 57 Testing Dataset Samples

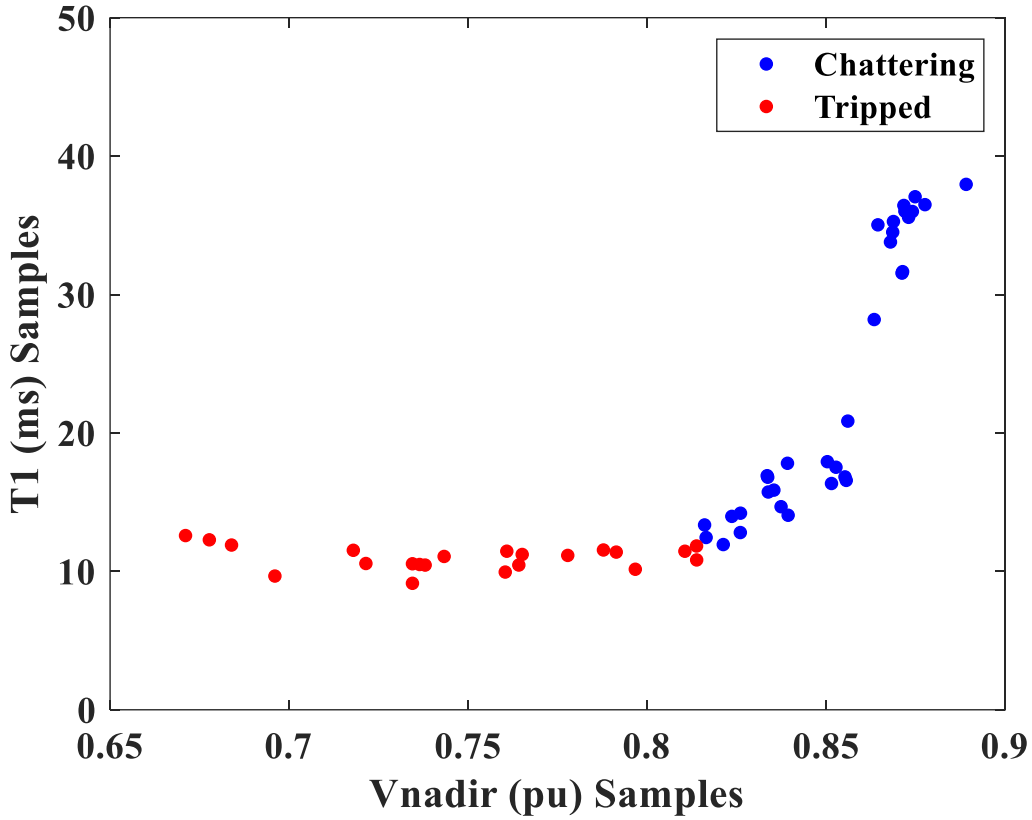

Figure 5.5 Comparison Between the *'T1'* and *'FN'* for All the 57 Testing Dataset Samples

Interesting Observations from Figure 5.4 and Figure 5.5:

1. In Figure 5.4, the comparison between the true T1 values and their corresponding true V1 values for all the 57 testing cases is presented. ***Here, it can be observed that in most of the samples the typical value of 'T1' parameter (time taken for the contactors to trip after the fault is applied) is between 10 ms and 15 ms for the cases when the contactors are completely.*** However, for samples where the contactors chatters, it was observed that when ***'V1' parameter is between 0.87 pu – 0.89 pu, in some cases the 'T1' values are within the range 15ms – 20ms and in the remaining cases within this 'V1' range the 'T1' values are within the range 30ms – 40ms.***

2. From Figure 5.5, it can be clearly seen that if the feeder head positive sequence voltage nadir *'FN'* value, for any test case, falls **below 0.85pu** then the contactors start to act (**either chatters or completely trips**) between **10ms -20ms** after the fault is applied on the system. However, for the cases where the *'FN'* value is **above 0.85pu** value, the contactors are observed to start to act (**chatters)** after significantly longer duration between **30ms – 40ms.**

5.2.4 Step 4: DNN Model Development to Estimate the SPHIM Stalling Behavior

In addition to estimating the contactor critical features, it is also important to estimate the SPHIM stalling behavior (whether the SPHIMs stall or reaccelerates) accurately for a given SLG scenario to capture FIDVR phenomenon accurately. Similar to estimating the contactor trip and reconnection settings, the DNN regression models have been employed in this work to estimate the stalling phenomenon of the SPHIMs along the feeder. Therefore, two DNN regression models have been developed to accomplish this and the details for each DNN model has been discussed below –

- **'*TMS*' DNN Model:** This DNN model is developed to estimate the total number of segments in which SPHIMs stalled. For estimating the *'TMS'* parameter, phenomena which occur typically after the fault is cleared in the system or at the end of the fault duration, the following input features (after applying normalization using (5.2) and obtained from PSCAD) are used:
  - *'FA'*
  - *'FD'*
  - *'FN'*

- *'ST'*

- **'*IMS*' DNN Model:** This DNN model is developed to estimate the individual segments in which SPHIMs stalled in which the estimated *'TMS'* parameter has been used as another input and since this phenomenon which occurs typically after the fault is cleared in the system or at the end of the fault duration, the following input features (after applying normalization using (5.2) and obtained from PSCAD and *'TMS'* model) are used:
  - *'FA'*
  - *'FD'*
  - *'FN'*
  - *'ST'*
  - *'TMS'*

The possible values for the *'TMS'* parameter are either 0,1, 2, or 3 (as there are three segments along the feeder). Also, the possible values for the 'IMS' parameter are {0,1}, {0,1} and {0,1} for the three segments respectively where *'IMS'* value being 0 or 1 in a particular segment corresponds to SPHIMs not being stalled or being stalled in that segment respectively. After developing the *'TMS'* and '*IMS'* DNN models using 300 test cases (75% training cases and 25% testing cases), an accuracy of 95% (71 test cases passed out of 75) and 96% (72 test cases passed out of 75) for the DNN models have been achieved. The DNN details for these two models are presented below in Tables 5.10 – 5.11.

Table 5.10 Final Chosen Hyperparameters for the Developed SPHIM Stalling DNN Models in this Work

Model Number	**Estimated Output Parameter**	**Number of Hidden Layers**	**Number of neurons for each hidden layer respectively**	**Number of iterations before the training process is terminated**
DNN Model 5	*'TMS'*	5	16, 10, 8, 6 and 4	1654
DNN Model 6	*'IMS'*	4	35, 30, 30 and 20	1500

Table 5.11 Demonstration of Failed Test Cases for *'IMS'* DNN Model

	Segment 1 *'IMS'* True Value	Segment 2 *'IMS'* True Value	Segment 3 *'IMS'* True Value	Segment 1 *'IMS'* Estimated Value	Segment 2 *'IMS'* Estimated Value	Segment 1 *'IMS'* Estimated Value	*'FN'*
Case 1	0	0	0	0.999	8.38e-07	2.15e-08	0.853
Case 2	0	0	1	3.81e-09	0.9986	0.0045	0.87
Case 3	1	1	0	0.001	0.9999	0.982	0.839

In Table 5.11, it should be noted that the estimated *'IMS'* value is categorized as follows in (5.6) –

$$IMS_{est} = \begin{cases} 0, \text{if } 'IMS' < 0.5 \\ 1, \text{ if } 'IMS' \geq 0.5 \end{cases} \tag{5.6}$$

From Table 5.11, it was also observed that in all the failed test cases, the contactors are chattering, and the positive sequence feeder head voltage nadir *'FN'* is observed to be between 0.84-0.87.

5.3 Incorporating the Estimated EMT Contactor Trip and Reconnection Settings into Positive Sequence Simulation Framework

The final objective of this work is to utilize the estimated EMT contactor trip and reconnection settings, using the developed linear regression model and the DNN models to trip the positive sequence single-phase induction motor models. This is achieved by implementing the following steps –

- Step 1: Circuit Setup in PSLF
- Step 2: PSLF 1st dynamic run and PSLF voltage nadir estimation
- Step 3: PSLF 2nd dynamic run and incorporation of estimated EMT contactor settings and SPHIMs stalled behavior to trip, reconnect and stall the 'motorc' model [62] at appropriate instants.

5.3.1 Step 1: Circuit Setup in PSLF

To implement the above-mentioned objective to incorporate the estimated EMT contactor settings and SPHIM stalling behavior, PSLF [28] is chosen as the software package to conduct the positive sequence simulations in this work. Therefore, a distribution circuit model similar to the proposed feeder and load model and the test setup in PSCAD (Figure 4.3) is considered in PSLF and its schematic is shown in Figure 5.6 below. For this feeder model in PSLF, the following points have been considered –

- A 69 kV Thévenin voltage source has been considered in this model with the same Thévenin resistance assumed in the PSCAD feeder model.
- A Y-Y 69/12.47 transformer has also been utilized in this model with the same leakage impedance (6%) assumed in the PSCAD 69/12.47 Y-Y transformer model.

- The 69 kV SLG fault, in the PSLF simulations, is placed at Bus2 in Figure 5.5.
- The PSLF feeder model (on the 12.47 kV side) is distributed into three segments with a 3.8% voltage drop across the feeder (same as in the PSCAD feeder model).
- The 'motor1' model, available in the PSLF library [7], is assumed to represent the 3PHIM load in the PSCAD feeder model.
- The 'Blwscc' model, available in the PSLF library [7], is used to represent the resistive load in the PSCAD feeder model.
- A custom built 'motorc' model (developed based on the analytical formulation given in [62]) is used in this PSLF circuit to represent the EMT SPHIM model that is present in the PSCAD feeder model. It should be noted that 'motorc' model is a phasor based SPHIM model whose working principle is based on a dual rotating field theory (backward emf and forward emf) [62]. To represent this model (unbalanced single-phase behavior) in a positive sequence environment such as PSLF [28], the 'motorc' model is represented as a three-phase balanced SPHIM model. It should also be noted that in the PSLF simulations conducted in this work, the final objective is to trip, reconnect and stall the considered 'motorc' model at appropriate instants based on the estimated EMT contactor trip and reconnection characteristics and the estimated SPHIMs stalled behavior from PSCAD. This is because there is no contactor model currently modeled into the 'motorc' model and it was observed that the 'motorc' model does not stall for SLG faults in PSLF. This is to be expected because as the 'motorc' model is a three-phase balanced SPHIM model (2 non-faulted phases support the faulted phase of the motor) and as the PSLF does not have the capability to capture the

POW phenomenon which is crucial to capturing the 'motorc' stalling behavior.

- The load composition for the PSLF feeder model is assumed to be the same as the load composition taken in the PSCAD feeder model (Case 1 residential feeder model under summer loading conditions). Therefore, the load composition in the PSLF feeder model is partitioned into - 51% 'motorc' model, 16% 'motor1' model, 33% 'blwscc' model.

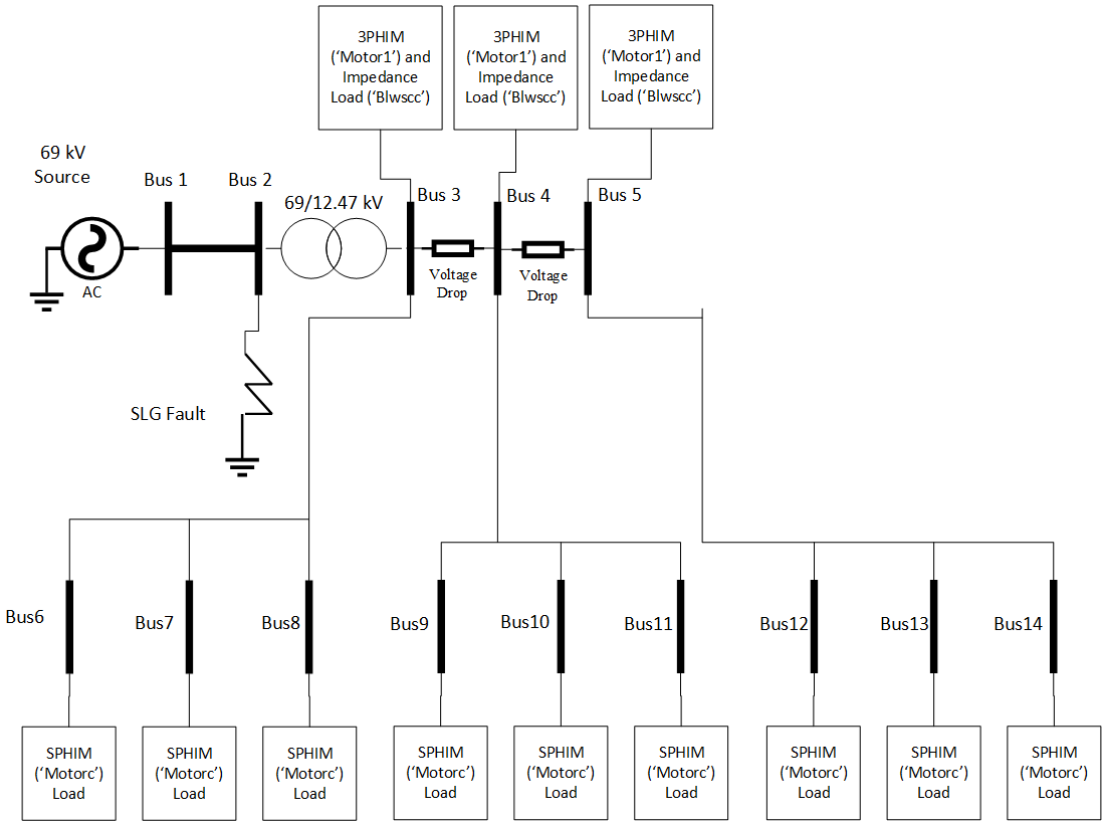

Figure 5.6 Circuit Schematic Used in PSLF

Note: It should be noted that in Figure 5.6, nine dummy buses (Bus6-Bus14) are used to place the SPHIM load where these 3 buses each are connected to Bus3, Bus4 and Bus5 respectively with zero impedance lines. This setup is used because the SPHIM load can be tripped by switching off the status of the line, in the middle of a dynamic run, connecting the dummy bus to its corresponding original load bus. Additionally, for each

original load bus three dummy buses are chosen to make it convenient to stall the required number of 'motorc' motors depending on the number of stalled SPHIM segments in the corresponding run in PSCAD. For example: In the third test case presented in this sub-section, the SPHIMs in only segment 3 of the faulted phase have stalled in the PSCAD simulation. Therefore, only 'motorc' models at buses Bus11 and Bus14 are forced to stall in PSLF based on the estimated SPHIM stall behavior using DNN model 5 and model 6. More details about the comparisons made between the PSCAD simulation and the PSLF simulations have been presented in detail in the later parts of this sub-section.

5.3.2 Step 2: PSLF 1st Dynamic Run and PSLF Voltage Nadir Estimation

It should be noted that, in this work, it is not possible to utilize the estimated EMT contactor tripping and reconnection settings and estimated SPHIM stall behavior to trip, reconnect and stall the 'motorc' model in one single PSLF dynamic simulation run. This is because, for any test case, the positive sequence feeder head voltage nadir is one of the important inputs to the developed DNN models. However, currently, there is no contactor model being used in the PSLF simulation runs and the motor load models used in PSLF circuit is not the same as the models being used in PSCAD. Therefore, it is not expected to obtain an accurate positive sequence feeder head voltage nadir value (same as the corresponding voltage nadir value obtained from the PSCAD simulation run for the same test case) in a single PSLF dynamic simulation run because there is no contactor action on the 'motorc' model in the 1st dynamic simulation run. Therefore, initially, the following steps are implemented in order, to obtain the right estimate of the value of the nadir of the positive sequence feeder head voltage in the 1st dynamic simulation run in PSLF:

(i) For the circuit as shown in Figure 5.6, a SLG fault short circuit analysis is conducted in PSLF using appropriate sequence data (provided in the appendix of this report) for the voltage source, lines, transformer, and the loads.

(ii) The Z_2+Z_0 equivalent impedance is obtained from the short circuit analysis conducted in (i).

(iii) Thereafter, during the dynamic simulation run, a three-phase fault has been placed at Bus 2 and an equivalent fault impedance $Z = Z_2+Z_0+3Z_f$ is used where Z_f is the fault impedance to ground used in the corresponding PSCAD simulation (*'FR'*).

In the 1st dynamic simulation run conducted in PSLF (by following the above three steps), it was observed that, for test cases with no contactor tripping or chattering, the positive sequence voltage nadir observed for the feeder head voltage is the ***same*** (accurate to second decimal) as the positive sequence voltage nadir observed from its corresponding PSCAD case run (with same fault parameters such as fault duration *'FD'* and fault resistance *'FR'*). However, for cases where the contactor either chatters or trips, it was observed that the voltage nadir obtained in PSLF varied from its corresponding PSCAD voltage nadir with an error between 0.001 – 0.025 pu. This is to be expected because the contactor trip, reconnection settings and SPHIM stalled behavior have not yet been modeled into the PSLF 'motorc' model. Also, it was observed that the outputs for the developed DNN models are sensitive to small perturbations made in the value of voltage nadir input feature. This clearly means that for any test case considered in PSLF, to utilize the developed DNNs to trip, reconnect and stall the 'motorc' model, the positive sequence feeder head voltage nadir needs to be estimated as accurately as possible.

Therefore, another DNN model (with four hidden layers with 8, 15, 8 and 5

neurons respectively) is developed in this work using the same algorithm that was used to develop the other DNNs in this work, using the earlier generated 300 test cases (225 training and 75 testing cases respectively) to estimate the positive sequence feeder head voltage nadir difference between a the voltage nadir value obtained from the PSCAD simulation run and its corresponding PSLF simulation run using the following input features (after normalization using (5.2)):

- Input 1 – Fault Resistance *'FR'*
- Input 2 – Fault Duration *'FD'*

Therefore, for both the training test cases and the testing test cases, the output variable (V_{diff}) for this DNN model is the difference between the positive sequence voltage nadir obtained from the PSLF 1st run normalized using its pre-fault steady state voltage ($V_{PSLF\ 1st\ run}$) and its corresponding PSCAD run (V_{PSCAD}). In other words, V_{diff} can be expressed mathematically as shown below –

$$V_{diff} = V_{PSCAD} - V_{PSLF\ 1st\ run} \tag{5.7}$$

Note: It should be noted that V_{PSCAD} obtained for each test case is equal to the 'FN' input feature obtained from the corresponding test case.

Based on the testing process conducted on the developed DNN to estimate V_{diff}, it was observed that V_{diff} is estimated with very good accuracy (average RMS error of around 0.003 pu).

5.3.3 Step 3: PSLF 2nd Dynamic Simulation Run and Incorporation of Estimated EMT Contactor Settings to Trip 'motorc' Model

For any test case, based on the estimated V_{diff} value obtained using the procedure described in the previous step, the actual positive sequence feeder head voltage nadir normalized using its pre-fault steady state voltage ($V_{PSLF\ 2nd\ run}$) calculated (using (5.7)) can be used as an input to the DNNs developed to estimate the contactor trip and the reconnection settings in the 2nd PSLF run. As the DNN models to estimate these trip and reconnection settings are already developed in an open-source python (Google Colab) script [61], the weights and biases for these neural network models are extracted and fed into the EPCL script used to conduct the 2nd dynamic simulation run in PSLF. Appropriate input features (such as $V_{PSLF\ 2nd\ run}$, *'FD'*, *'FA'*, *'ST' and 'TMS'*) are given depending on the developed DNN model as described in the earlier sub-sections of this Chapter.

Based on the trip settings obtained in PSLF (using the developed DNN models at the start of the 2nd PSLF dynamic simulation run), the 'motorc' models are tripped (when estimated *'ST'* = 3), reconnected and stalled (if necessary) in PSLF (during the 2nd dynamic simulation run at appropriate moments) using the following criterion –

- The 'motorc' models in the three segments of the feeder (Bus8, Bus11 and Bus14) are tripped when the head of the feeder voltage goes below *'V1'* for *'T1'* secs after the fault is initiated.
- The tripped 'motorc' models are reconnected to the feeder after the fault is cleared when the positive sequence head of the feeder voltage recovers above *'V2'* and after *'T2'* secs from the moment fault is initiated.

- The ‘motorc’ models are tripped by switching off the status of the lines connecting their dummy buses to their corresponding original load buses to zero and setting the terminal voltage and terminal current of the ‘motorc’ models to be zero when the line status is off.
- The ‘motorc’ models, on buses Bus8, Bus11 and Bus14, are forced to stall at appropriate segments, if necessary, based on the estimated *‘TMS’* and *‘IMS’* values for the considered various fault cases. The procedure to forcefully stall the ‘motorc’ models by implementing various scenarios which have been discussed below in detail -

➢ **‘Contactor Step Stall’**: In this case, the ‘motorc’ models at the buses of interest are forced to stall in PSLF after they are reconnected. This is accomplished by adding a large load torque (75 pu) as a step response when the motors are reconnected back to the feeder.

➢ **‘Contactor Ramp Stall’**: In this scenario, the ‘motorc’ models at the buses of interest are forced to stall in PSLF after they are reconnected. This is accomplished by adding large load torques (1.1 pu) incrementally at each time step when the tripped motors are reconnected back to the feeder.

5.4 Developed Methodology Implementation in PSLF and its Results

In this sub-section, the efficacy of the proposed methodology is demonstrated using three new test cases has been discussed below –

➢ **Case 1: Fully Tripped Contactors and Fully Stalled SPHIMs**

The fault parameter inputs considered in this case are –

- *‘FA’* – 0.000435 radians

- *'FD'* – 0.0706 secs
- *'FR'* – 0.29 ohms

In this case, all the contactors are observed to be fully tripped and the SPHIMs in all the segments of the feeder to be stalled in PSCAD. From Figure 5.7, it should be noted that the post-fault steady state voltage is significantly different in the PSCAD case compared to its corresponding PSLF case ('No contactor' case) because the SPHIMs in all the segments of the PSCAD feeder model stalled when the contactors got reconnected after the SLG fault is cleared in the system. Whereas, in PSLF, the 'motorc' for the model in all three segments reaccelerated to its nominal speed, for the 'No contactor case', after the contactors are reconnected. This is to be expected because we are unable to replicate the POW impact on the SPHIM stalling phenomenon in PSLF (which uses only RMS signals and cannot capture the POW phenomenon) using the considered 'motorc' model. However, in Figure 5.7, it can be observed that for the 'Contactor Step Stall' case and 'Contactor Ramp Stall' case response of the positive sequence feeder head voltage in PSLF is very similar to the PSCAD case immediately after the motors are reconnected (especially the post-fault settling time with the contactor case in PSLF is much closer to the PSCAD case compared to the case without any contactor action in PSLF). This clearly shows that the inclusion of the developed linear regression and DNN models into PSLF helps capture the benefits of an EMT software, such as PSCAD, to capture the critical POW information that is crucial to identifying FIDVR phenomena without compromising on the computational time (huge drawback of an EMT software). In Figure 5.7, it should also be noted that only one part of 'motorc' model at buses 8, 11 and 14 each are stalled to correspond to the stalled

SPHIMs in PSCAD in only the faulted phase.

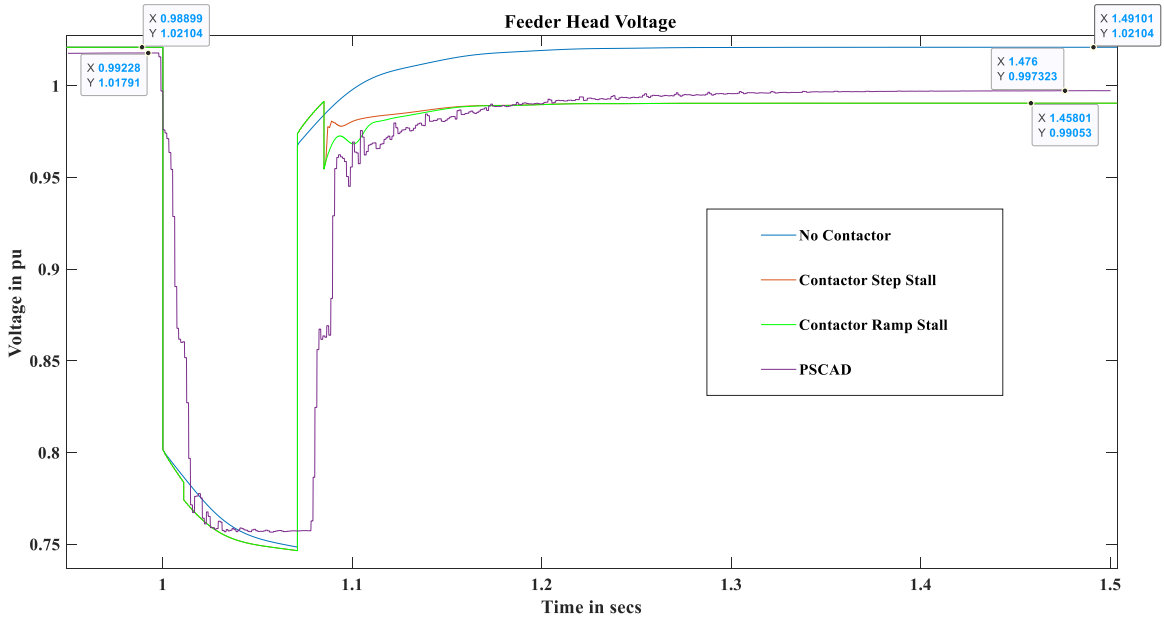

Figure 5.7 Positive Sequence Feeder Head Voltage (at Bus3) Comparison in PSLF (No Contactor and Contactor Cases to Trip, Reconnect and Stall 'motorc') and its Corresponding PSCAD Plot Generated with Same Input Feature Values for Case 1

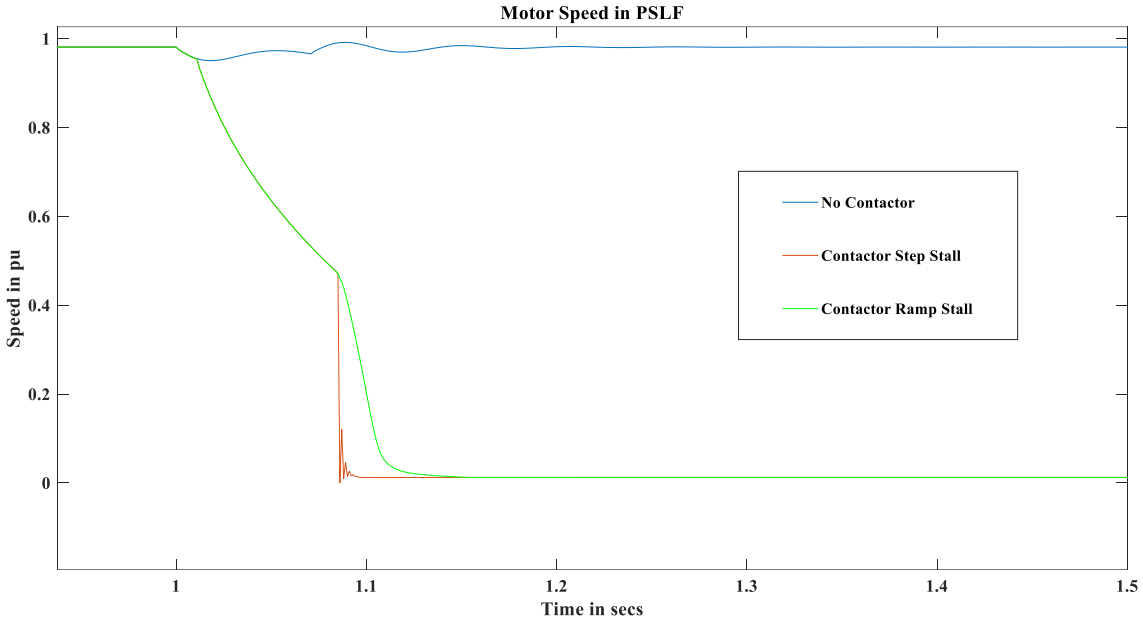

Figure 5.8 'motorc' (at Bus14) Speed Comparison in PSLF

In Figure 5.8, it can be observed that the speed response of the 'motorc' model, at Bus14, is significantly different between the cases, when there is no contactor to trip 'motorc' model and cases when there is a contactor present in the system to trip 'motorc'. Additionally, it can also be seen that for 'Contactor Step Stall' case and 'Contactor Ramp Stall' case, the 'motorc' model is forcefully stalled after it is reconnected to the feeder when the fault is cleared because of the estimated stalling information available at the start of the run due to the developed *'TMS'* and *'IMS'* regression DNN models. In this figure, it can also be observed that the slope of deceleration of the 'motorc' model speed is different when the 'motorc' model is tripped compared to the period when the 'motorc' model is forced to stall (either by Step Stall method or Ramp Stall method) after the contactor of the 'motorc' model is reconnected to the feeder.

In Figure 5.9 and Figure 5.10, the plots for the 'motorc' terminal voltage and terminal current are presented. In these plots, the instances when the 'motorc' model terminal voltage and current has been forcefully set to zero (when 'motorc' model is tripped based on the estimated *'T1'* and *'V1'* values) and reset to the feeder network voltage (when 'motorc' model is reconnected based on the estimated *'T2'* and *'V2'* values) and its corresponding inrush current drawn by the motor can be observed clearly.

The SPHIM speeds in all three-segments in the corresponding PDCAD simulation is presented in Figure 5.11. It can be clearly seen from the figure that all the SPHIMs stall and do not reaccelerate back to their nominal speeds after the fault is cleared.

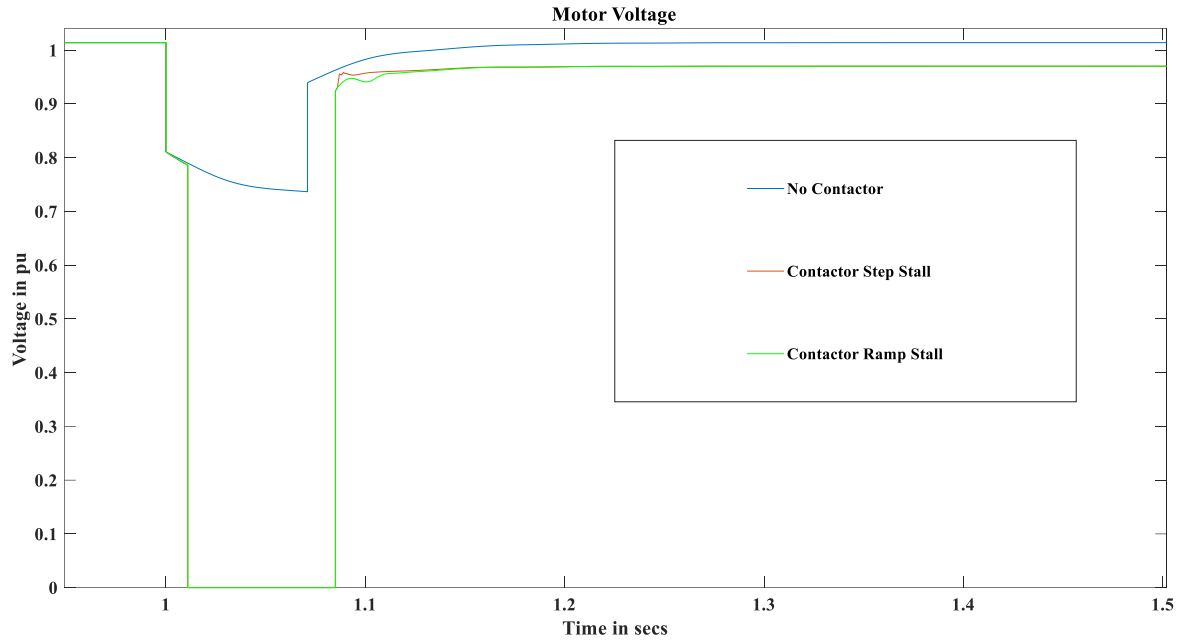

Figure 5.9 ‘motorc’ Terminal Voltage Comparison in PSLF

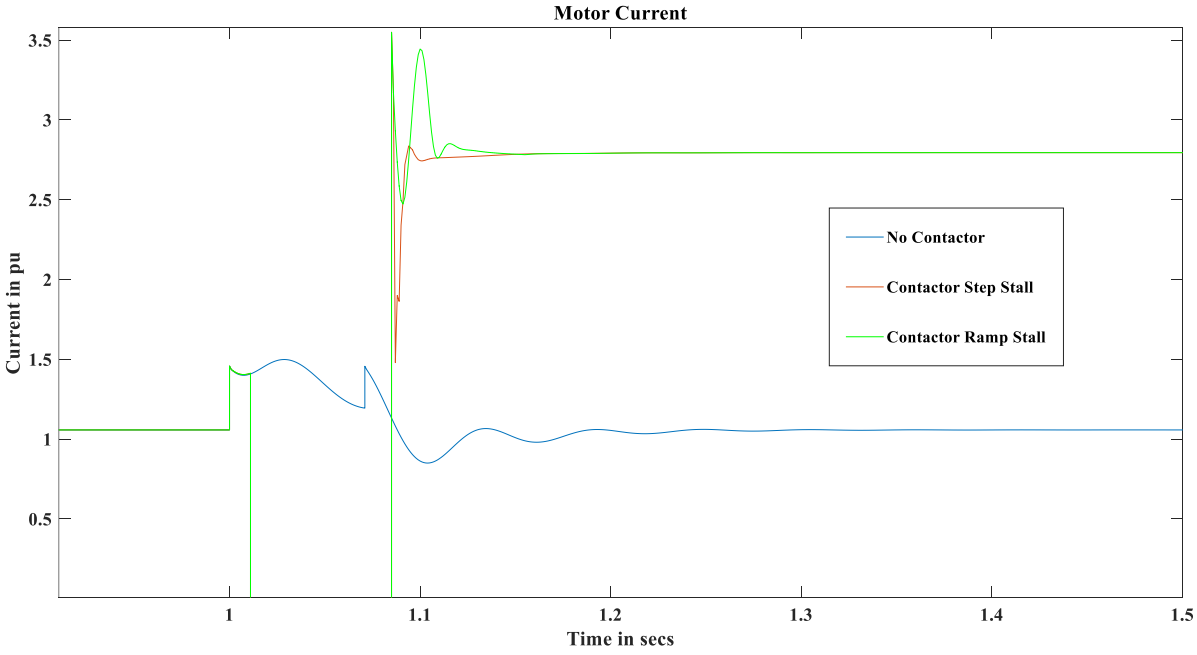

Figure 5.10 ‘motorc’ Terminal Current Comparison in PSLF

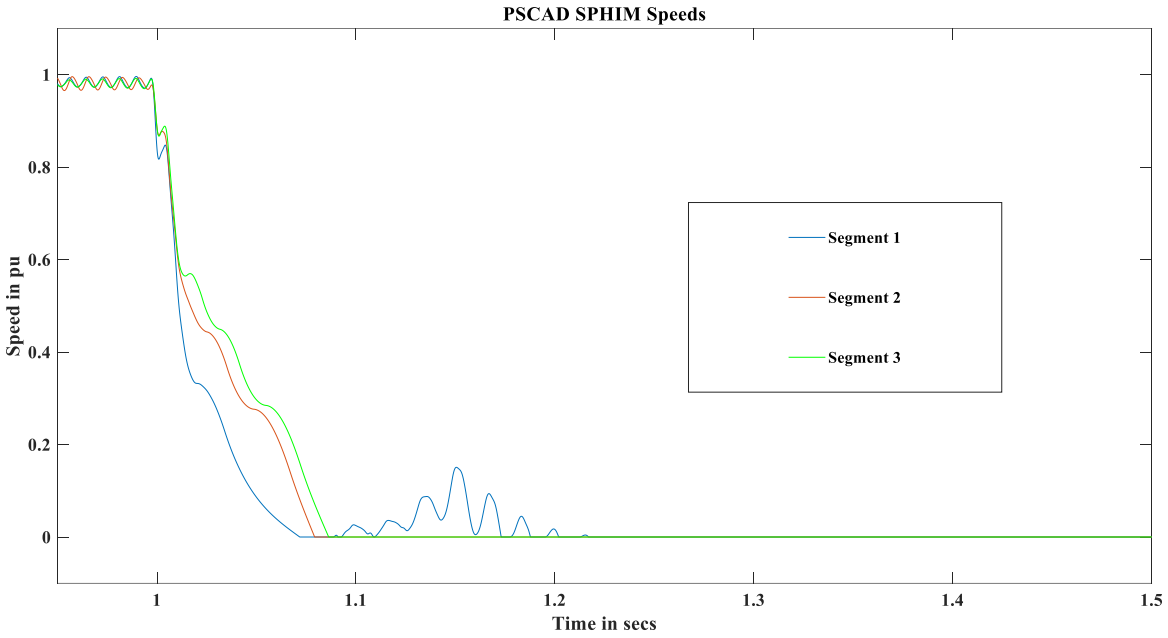

Figure 5.11 Evidence of SPHIMs Stalling in All Three Segments in the PSCAD simulation for Case 1

- **Case 2: No Contactor Tripping and No SPHIM Stalling**

The fault parameter inputs considered in this case are –

- *'FA'* – 0.000865 radians
- *'FD'* – 0.0773 secs
- *'FR'* – 3.23 ohms

A less severe fault scenario is considered in this case. It should be noted that no contactor action has been observed and no SPHIMs stalled in PSCAD for the considered inputs. From Figure 5.12, it can be clearly seen that the PS feeder head voltage response observed in PSLF (where there is no impact on the feeder response due to the developed regression models due to the low severe fault considered) is very close to the PS feeder head voltage observed in the corresponding PSCAD simulation. This clearly shows that

there is necessity to include the developed regression models as the severity of the fault increases in the system and is not necessarily important for low severe fault events.

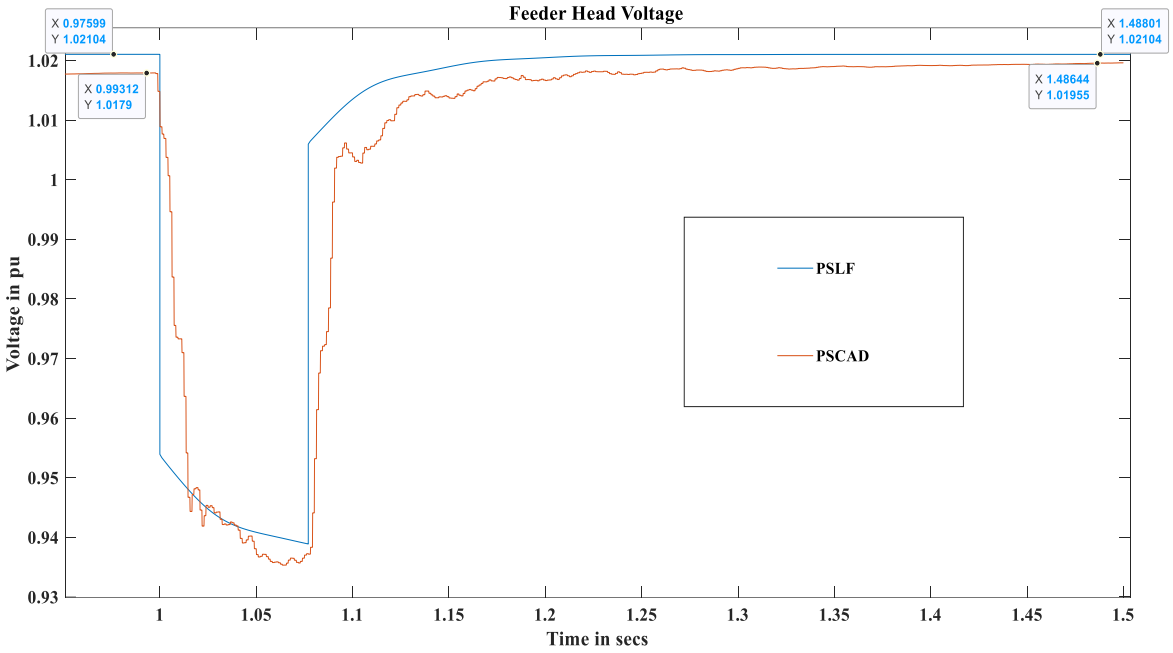

Figure 5.12 Positive Sequence Feeder Head Voltage (at Bus3) Comparison in PSLF and its Corresponding PSCAD Plot Generated with Same Input Feature Values for Case 2

- **<u>Case 3: Contactor Chattering and Partial SPHIM Stalling</u>**

The fault parameter inputs considered in this case are –

- *'FA'* – 0.0022 radians
- *'FD'* – 0.071 secs
- *'FR'* – 1.95 ohms

In this case, the contactors are observed to be chattering in all three segments and SPHIMs stalled in only the third segment and the SPHIMs in other segments reaccelerated after they are reconnected in PSCAD for the considered inputs and this phenomenon has also been captured by the developed DNN models. The PS feeder head voltage comparison between the PSCAD and its corresponding PSLF responses for this case is presented in

Figure 5.13.

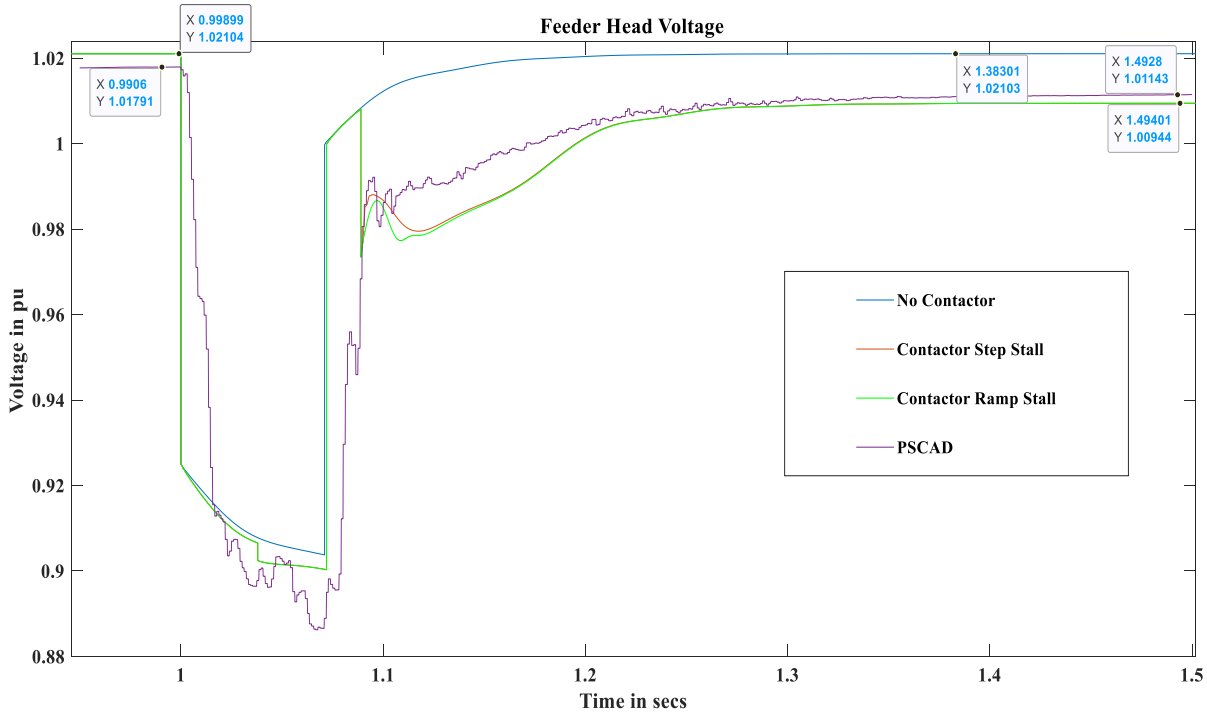

Figure 5.13 Positive Sequence Feeder Head Voltage (at Bus3) Comparison in PSLF (No Contactor and Contactor Cases to Trip, Reconnect and Stall 'motorc') and its Corresponding PSCAD Plot Generated with Same Input Feature Values for Case 3

From Figure 5.13, it can be clearly seen that the PSLF responses (which has the regression models to capture both the contactor behavior and the SPHIM stalling behavior) has the closest resemblance to the corresponding PSCAD response (especially after the 'motorc' models are reconnected to the feeder). It should also be noted that for this case of contactor chattering, the 'motorc' models are tripped completely to account for the worst-case impact that could be caused by the contactor chattering on the feeder response.

It can be observed from Figure 5.14 that for the considered fault scenario, only the third segment SPHIMs in PSCAD stall and the other segments SPHIMs reaccelerate back to their nominal speeds. Also, from Figure 5.15, it can be clearly seen that for the

considered fault scenario there is very minimal impact on the speed responses of the SPHIMs in PSLF in the absence of the developed regression models. However, in the presence of the developed regression models to capture the contactor chattering and the SPHIMs stalling behavior in PSLF the SPHIMs speed responses, as shown in Figure 5.16, is very close to the response in the corresponding PSCAD simulation (from Figure 5.14).

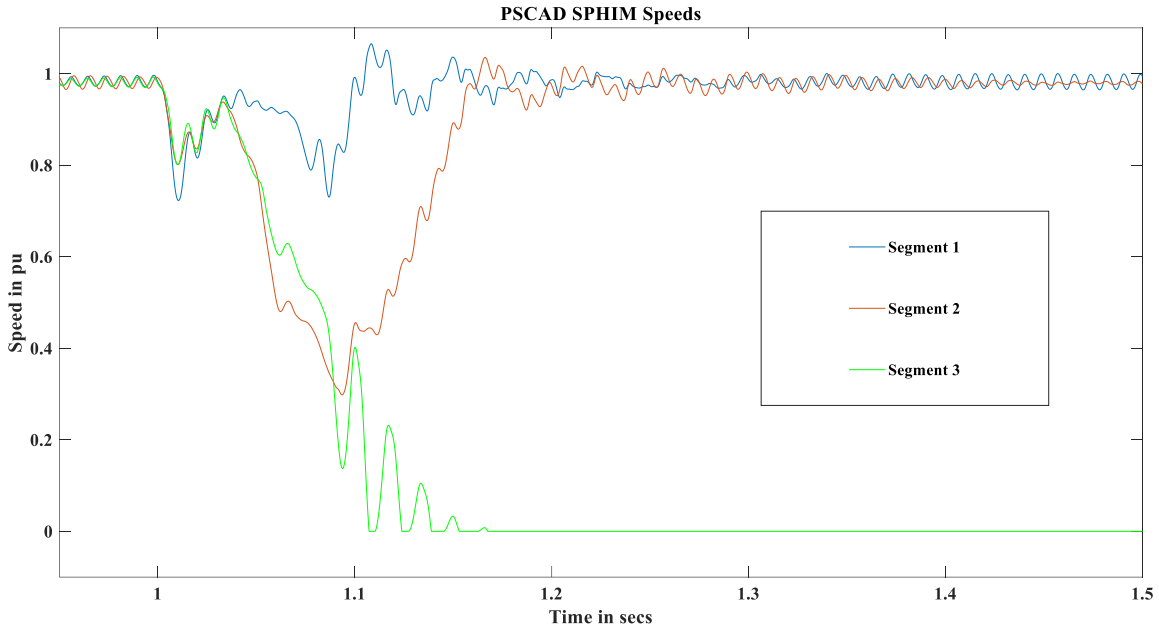

Figure 5.14 Evidence of SPHIMs Stalling in Only the Third Segment and SPHIMs Re-Acceleration in Segment 1 and Segment 2 of the Proposed Feeder Model in the PSCAD Simulation for Case 3

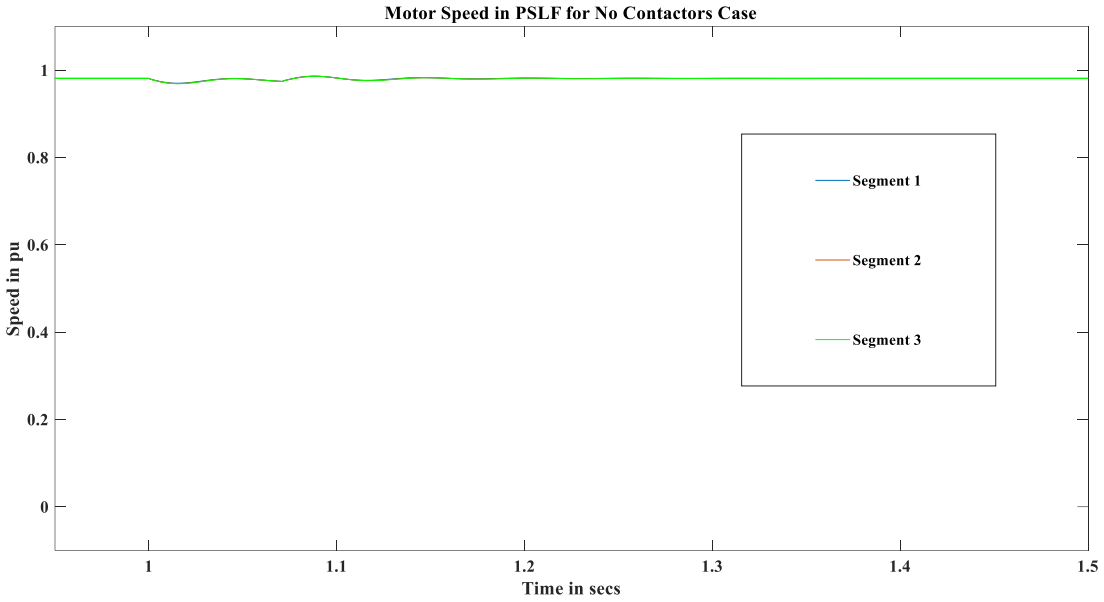

Figure 5.15 Evidence of Minimal Impact on the SPHIMs Responses in PSLF for Case 3 Without the Utilization of the Developed Linear and DNN Regression Models

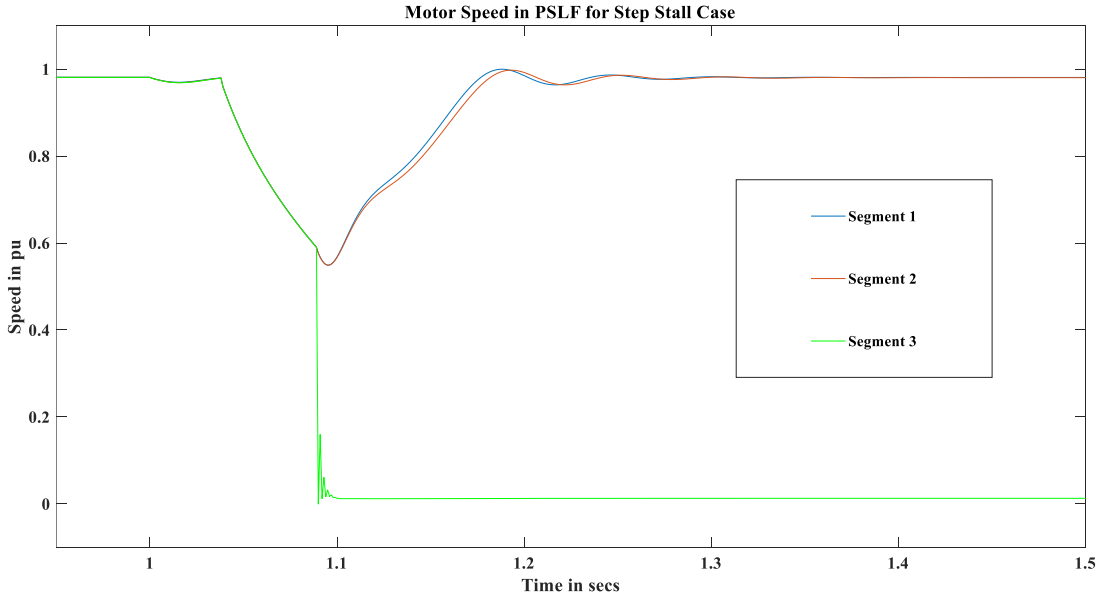

Figure 5.16 Very Accurate SPHIMs Responses in PSLF for Case 3 with the Utilization of the Developed Linear and DNN Regression Models

CHAPTER 6

VALIDATION OF THE SLG FAULTS ALGORITHM TO ESTIMATE CONTACTOR SETTINGS AND ON A PRACTICAL UTILITY FEEDER

6.1 Analyzing the Local Utility Feeder Data

In addition to applying the proposed algorithm to estimate the contactor trip and reconnection settings and the motor stalling behavior on the proposed three-segment three-phase feeder model (in Chapter 3), it is important to validate this methodology on a feeder and load model using the topological details and the loading conditions obtained from a practical feeder. Therefore, from the same local utility (from which the voltage and currents measurement data were obtained in Chapter 3), the practical feeder information for Substation A has been utilized in this work. It was observed that there are four three-phase 12.47 kV feeders on the low voltage side of the Substation A as shown below in Table 6.1

_

Table 6.1 Demonstration of Accuracy of *'V2'* DNN Model for Some Test Cases

Substation A Feeder Name	**Feeder Head Voltage (kV)**	**Total P consumed (MW)**	**Total Q consumed (MVAR)**
FD 122	12.47	3.63	0.13
FD 123	12.47	5.36	0.23
FD 124	12.47	3.47	0.18
FD 125	12.47	4.26	0.12

As mentioned earlier, the main objective of this chapter is to obtain the topological data and the loading conditions of the Substation A practical feeders and apply it on the

proposed three-phase three-segment aggregated feeder model (whose load parameters and load composition has been obtained for Substation A by estimating them using Case 1 in Chapter 3) to validate the contactors and motor stalling critical features data obtained (generated in PSCAD) in Chapter 5. Therefore, the following information is obtained from the local utility data –

(i) ***Total Feeder Head MVA:*** It is important to know the total MVA drawn by all the distribution feeders originating from Substation A. The aggregated MVA would then be used in the PSCAD proposed three-phase three-segment model for pre-fault conditions. The total MVA drawn by feeders FD 122, FD 123, FD 124 and FD 125 (as shown in Table 6.1) is used to obtain the aggregated MVA of the Substation A feeder model in PSCAD.

(ii) ***Three-Section Segmentation:*** To mimic the proposed three-phase three-segment model in this work, the loads across the feeders need to be segmented into three sections appropriately based on their distribution concentrations across the feeders.

(iii) ***Voltage Drop Data:*** Based on the three-part segmentation of the practical feeder, the voltage drops across the three sections from the Substation A needs to be obtained.

For the sake of simplification of the analysis, the above-mentioned information ('Three-Section Segmentation' and 'Voltage Drop Data') from the local utility data was obtained for only feeder FD 122 and the steps required to do that are presented below –

- **Step 1: Nodes, Sectional Data**

In the data provided by the local utility, all the sections and their corresponding nodes (buses) along the feeder (each section has a 'From node' and a 'To node' which represents the direction of power flow respectively) were provided for FD 122 feeder.

Although, in total, there are 485 sections and correspondingly 478 different nodes in FD 122 feeder, only 90 sections (180 nodes) have loads present on them. However, to get a good understanding of the areas with loads and the distribution of the load along the feeder and its general topology it is important to have a good visualization of the provided data.

- **Step 2: Python Implementation to Generate Graph**

To visualize the FD 122 feeder pictorially using node data, all the node data, for FD 122 feeder, were converted into a sparse symmetrical matrix form (478x478 dimensions) where all the columns and rows spanning the matrix correspond to 'From Nodes' and 'To Nodes' respectively. Where, the matrix elements m_{ab} are populated using (6.1).

$$m_{ab} = \begin{cases} 1, if\ n_{ab}\ do\ exists \\ 0,\ n_{ab}\ doesn't\ exist \end{cases} \quad (6.1)$$

Where, n_{ab} is the section between nodes a and b.

The populated sparse matrix is then read through a python script which uses directed graphs methodology to generate the FD 122 feeder topology pictorially. 'Kamada-Kawai' [63] force-directed layout library function was used in this work to generate the graph. The final graph obtained using this methodology is presented in Figure 6.1. The color coding of the nodes in this graph are given as described below –

- 'Cyan' colored nodes: They represent the nodes which are part of the sections of the feeder in which no loads are present.
- 'Red' colored nodes: They represent the nodes which are part of the sections of the feeder in which phase A power supplied loads are present.
- 'Green' colored nodes: They represent the nodes which are part of the sections of the

feeder in which phase B power supplied loads are present.

- ‘Yellow’ colored nodes: They represent the nodes which are part of the sections of the feeder in which phase C power supplied loads are present.
- ‘Blue’ colored nodes: They represent the nodes which are part of the sections of the feeder in which three-phase power supplied loads are present.

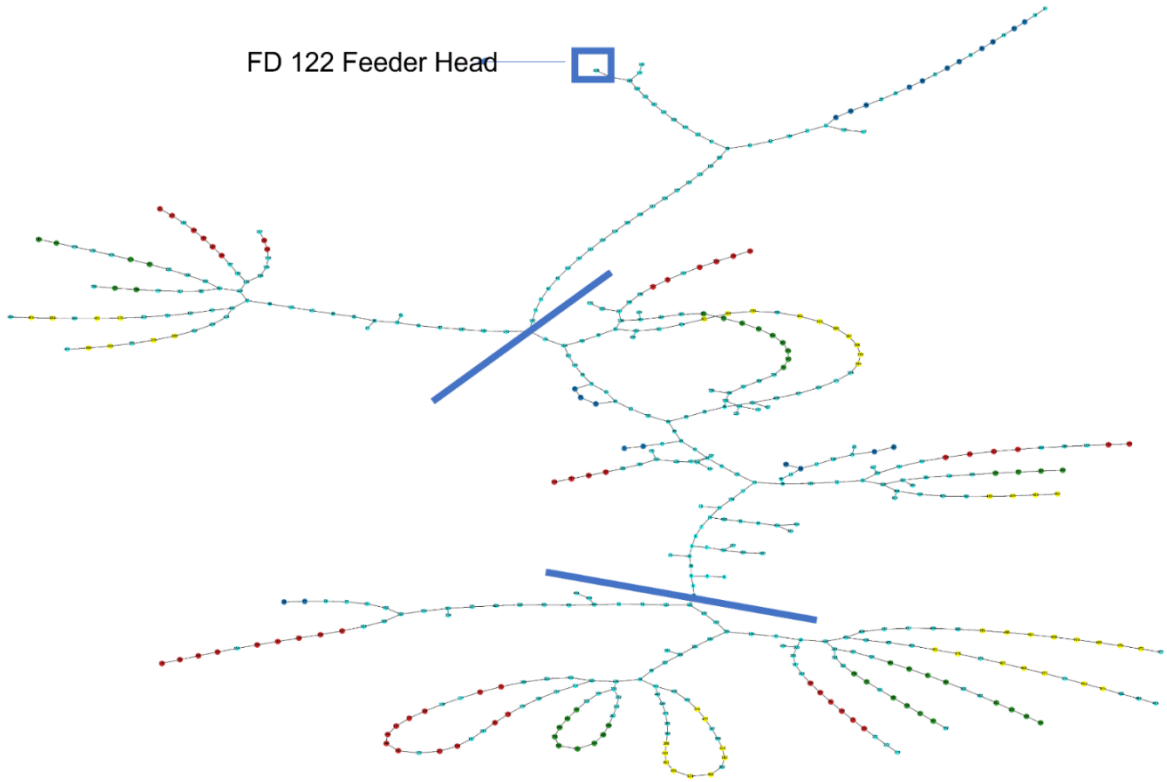

Figure 6.1 FD 122 Feeder Overall Layout Consisting of All the Node Data

From Figure 6.1, it should also be noted that the head of the feeder node for FD 122 has been marked with a rectangle at the top of the graph and based on the overall load distribution across the feeder the loading zones have been divided into three parts using two solid blue lines.

- **Step 3: Sectional Impedance Data**

There are five types of conductors (impedance between two nodes) present in the feeder whose sequence impedance data (in ohms/mile) are given below in Table 6.2. It should also be noted that the length of each line (in feet) between two nodes were provided by the local utility.

Table 6.2 Sequence Impedance Data for the Conductors Along the Feeder

Conductor Type	**R1c (ohms/mile)**	**X1c (ohms/mile)**	**R0c (ohms/mile)**	**X0c (ohms/mile)**
UG 2A	1.91	0.37	3.27	0.82
UG 4/0 A	0.63	0.38	1.87	0.69
UG 500A	0.25	0.21	2.095	2.09
UG 750A	0.23	0.31	0.665	0.36
Busbar	0	0	0	0

- **Step 4: Voltage Drop Calculations**

The final step in this analysis is to obtain the voltage drop calculations across the feeder based on the available topological and impedance data obtained from Step 2 and Step 3 respectively. The following steps are taken to obtain the voltage drop values across the feeder –

- A feeder head voltage of 1.02 pu was assumed in this work.
- Using simple KCL and KVL laws, along the feeder sections, and considering total MVA at the head of the feeder to be 3.63 MVA (from Table 6.1), the current flows and the voltage drops along the feeder were calculated using only positive sequence impedance data (from Table 6.2) and the active/reactive powers calculated along the

paths based on the provided loading values for the sections in which loads are present.

- The equivalent impedance across the feeder for radial paths (a combination of no-load nodes and load present nodes) has been calculated using (6.2)

$$z_{eq} = \sum_{nl=0}^{h1} z_{nl} + \frac{\sum_{lo=0}^{h2} z_{lo}}{h2} \quad (6.2)$$

Where, z_{eq} is the equivalent impedance of the total radial path, z_{nl} is the impedance in ohms in the nl^{th} no load section, z_{lo} is the impedance in the lo^{th} section in which load is present, $h1$ and $h2$ are the number of no-load nodes and loaded nodes along the radial line respectively. It should be noted that the equivalent impedance for any parallel path in this topology is calculated as the mean of the equivalent impedances obtained from two or more radial paths that is part of the considered parallel path.

The final three-segment feeder model obtained using the above steps is presented in Figure 6.2. It should be noted that the 'Segment *k* Loads' correspond to the loads present in the k^{th} segment of the feeder and the same load types (SPHIM load, 3PHIM load, resistive load and the necessary distribution transformers to step down the voltage from the 12.47 kV level to its respective load voltage level) that are used in the proposed three-segment three-phase feeder model as presented in Figure 3.13. As mentioned earlier, the voltage drops across the modified three-segment feeder model has been obtained using Steps 1-4.

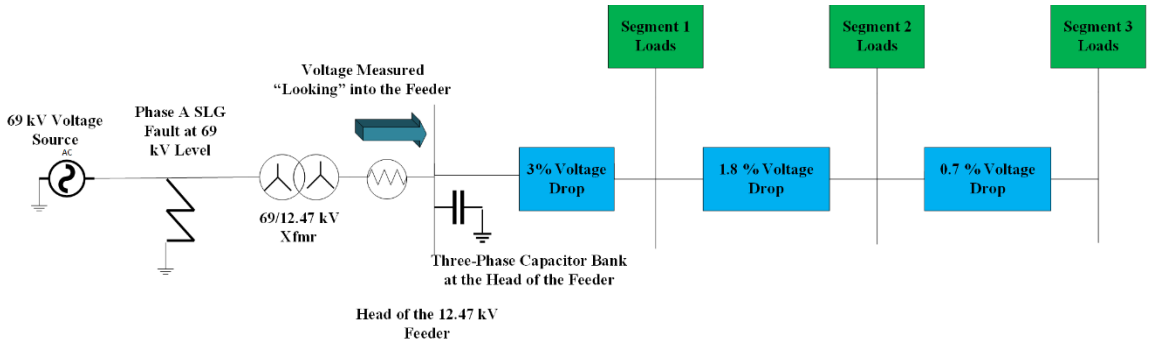

Figure 6.2 Modified Three-Segment Feeder Model Based on the SRP Topological and Loading Data

Additionally, the load composition in Figure 6.2 is observed to be distributed as follows –

- Segment 1 (19%)
- Segment 2 (35%)
- Segment 3 (46%)

It should also be noted that the load composition distributed across the three segments in the original proposed three-segment feeder model (Figure 3.13) was Segment 1 (30%), Segment 2 (35%) and Segment 3 (35%). Therefore, in addition to increasing the pre-fault total feeder head MVA consumption from 11.5 MVA (original proposed feeder model in Chapter 5) to 16.7 MVA in the modified feeder model presented in Figure 6.2, the load distribution in Segment 1 and Segment 3 has been adjusted in the original proposed three-segment feeder model to match with the local utility load composition data for the given feeder.

6.2 Validating the Proposed Three-Segment Feeder Model with the Modified Three-Segment Feeder Model

Once the complete modified three-phase three-segment feeder model has been

obtained it is important to check the validity of the critical parameters for the contactor behavior and the SPHIM staling behavior such as '*ST*', '*T1*', '*T2*', '*V1*' and '*V2*', '*TMS*' and '*IMS*' for the modified feeder model with their corresponding original proposed feeder model contactor and SPHIM stalling features. Therefore, the modified feeder model, as shown in Figure 6.2, is simulated in PSCAD for three SLG fault scenarios (no-trip contactor case, contactor chattering case and fully tripped contactor case) and its features comparison with the original feeder model for the same fault parameters ('*FA*', '*FD*', '*FR*') is presented below in Table 6.3.

Table 6.3 Comparison of Contactor Tripping and Reconnection Characteristics and SPHIM Stalling Behavior for the Both Feeders in the Faulted Phase

Feeder Type	**Case Type**	***ST***	***T1* (ms)**	***V1* (pu)**	***T2* (ms)**	***V2* (pu)**	***TMS***	***IMS***
Original	Fully Tripped	3	11.6	0.894	79.8	0.896	3	(1,1,1)
Original	Chattering	1.5	16.35	0.892	70.3	0.871	3	(1,1,1)
Original	No-Trip	0	-	-	-	-	0	(0,0,0)
Modified	Fully Tripped	3	12.1	0.899	79.5	0.893	3	(1,1,1)
Modified	Chattering	1.5	34.98	0.865	89.75	0.932	3	(1,1,1)
Modified	No-Trip	0	-	-	-	-	0	(0,0,0)

Table 6.4 Comparison of the PS Feeder Head Voltage Contactor Tripping and Reconnection Characteristics for the Both Feeders and their Respective Faulted Phase Contactors Terminal Voltages

Feeder Type	**Case Type**	***V1* (pu)**	***VaV1 Seg1 (pu)***	***VaV1 Seg2 (pu)***	***VaV1 Seg3 (pu)***	***V2* (pu)**	***VaV2 Seg1 (pu)***	***VaV2 Seg2 (pu)***	***VaV2 Seg3 (pu)***
Original	Fully Tripped	0.894	0.699	0.735	0.751	0.896	0.697	0.706	0.71
Original	Chattering	0.892	0.684	0.712	0.723	0.871	0.622	0.643	0.653
Original	No-Trip	-	-	-	-	-	-	-	-
Modified	Fully Tripped	0.899	0.756	0.792	0.809	0.893	0.719	0.735	0.744
Modified	Chattering	0.865	0.591	0.59	0.599	0.932	0.779	0.804	0.811
Modified	No-Trip	-	-	-	-	-	-	-	-

From Table 6.3, it can be observed that the contactor features and the motor stalling behavior is either same or very close for both the feeders for both fully tripped and No-tripped cases. However, for the contactor chattering case, there is a significant difference between the observed trip and reconnection characteristics of the contactors between the feeders. This is to be expected because the voltage drops seen at the load terminals and the contactor terminals in each respective segment is different due to the different topology of the two feeders and the varied voltage drops along both the feeders. This clearly shows that the regression models developed in Chapter 5 for the original three-segment feeder model needs to be re-trained as a user-specific three-segment feeder model based on the considered practical feeder information.

The description of the various voltages shown in Tables 6.4 are given below –

- *VaV1 Segz* – Measured terminal voltage (at the '*T1*' time instant after the fault is initiated) of the z^{th} segment contactor in the faulted phase (phase A) normalized using

its pre-fault steady state voltage obtained from PSCAD.

- *VaV2 Segz* – Measured terminal voltage (at the '*T2*' time instant after the fault is initiated) of the z^{th} segment contactor in the faulted phase (phase A) normalized using its pre-fault steady state voltage obtained from PSCAD.

From Table 6.4, it can be clearly seen that the PS feeder head voltage at which the contactors along the faulted phase start to trip and reconnect is significantly higher compared to their respective faulted phase terminal voltages of the three contactors along the feeder on the faulted phase. This is to be expected because of the presence of non-faulted phases having a mitigating impact on the positive sequence feeder head voltage.

CHAPTER 7

A DISCUSSION ON THREE-PHASE FAULT ANALYSIS FOR ESTIMATING CONTACTOR FEATURES AND MOTOR STALLING BEHAVIOR

7.1 Necessity of a New Algorithm Development for Three-Phase Faults

In Chapter 5 and Chapter 6, the developed algorithm to estimate the contactor trip and reconnection characteristics and the SPHIM stalling behavior was implemented only for asymmetrical faults (SLG faults). In this chapter, the proposed algorithm is modified to deal with symmetrical faults (three-phase faults). One of the major difference that can be observed in the SPHIMs and its contactor behavior between the SLG faults and three-phase faults is that for the former case only the faulted phase SPHIMs (along the three-segments) and their associated contactors are affected due to the fault but in the latter case the SPHIMs and their associated contactors in all the three-phases and across all three segments are affected when a three-phase fault is applied to the system. This has huge implications on the proposed SLG faults algorithm in Chapter 5 because the regressions models are trained based on the data where only Phase A SPHIMs and their associated contactors are affected and therefore, the proposed methodology to estimate the contactor characteristics and the SPHIM stalling behavior needs to be appropriately modified to accommodate the impact that the three-phase faults would have on all three-phases. For example – when a three-phase fault is initiated, the point on the wave at which the fault is seen is different in all three-phases. As mentioned earlier in this report, the point on the wave at which the fault is initiated has a huge impact on determining if the motors stall on a particular phase or not.

To demonstrate the need for new regression models for three-phase fault analysis, the following test case (where, a three-phase fault is applied on the same feeder model considered in Chapter 5 at the 69 kV level of the system) is demonstrated below using Figures 7.1-7.7.

From Figure 7.1, it can be observed that when a three-phase fault is placed in the system (indicated by the dashed black vertical line), the point on wave is different on all three-sinusoidal voltages (due to 120^0 phase difference between each phase).

From Figures 7.2 – 7.4, ***it can be clearly seen that the impact of having a three-phase fault results in different points on wave for each phase and results in a varied SPHIMs stalled behavior across the three-phases.*** For the case displayed, in Phase A and Phase B, all the three-segment SPHIMs stalled but in Phase C only the SPHIMs in segment 1 have stalled and the SPHIMs in the other segments reaccelerated back to their nominal speed. This is to be expected because the point of wave at the fault on the phase C voltage sine wave (at the moment of initiation of fault) is near the peak whereas in the other phases the fault is initiated close to their zeros.

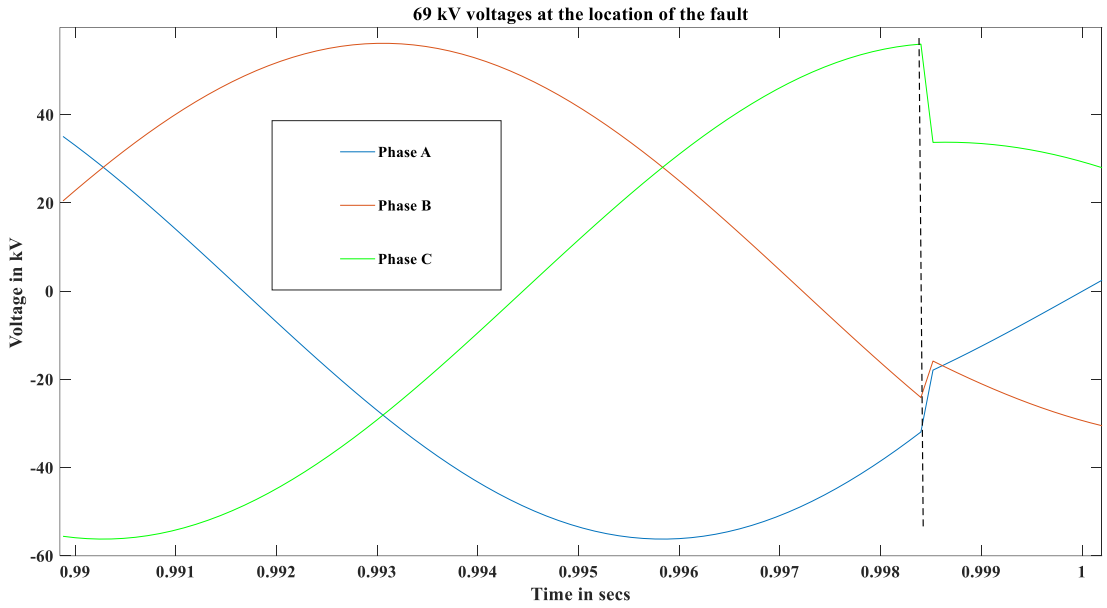

Figure 7.1 Three-Phase Fault Point of Impact on All Three-Phase Voltage Sinusoidal Waves

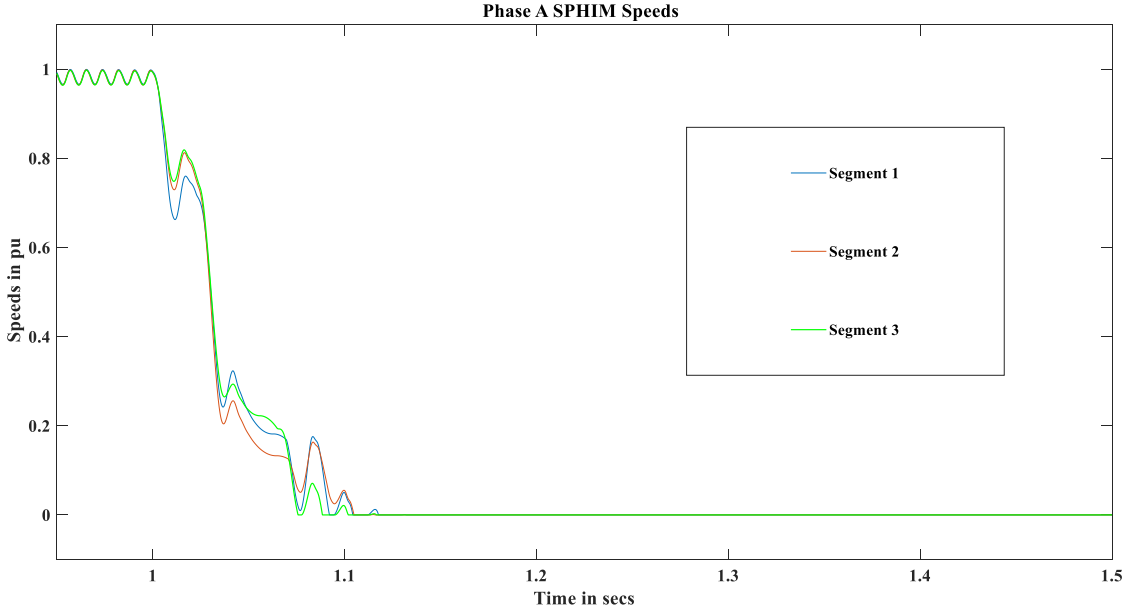

Figure 7.2 SPHIMs in All Three Segments Stalling in Phase A

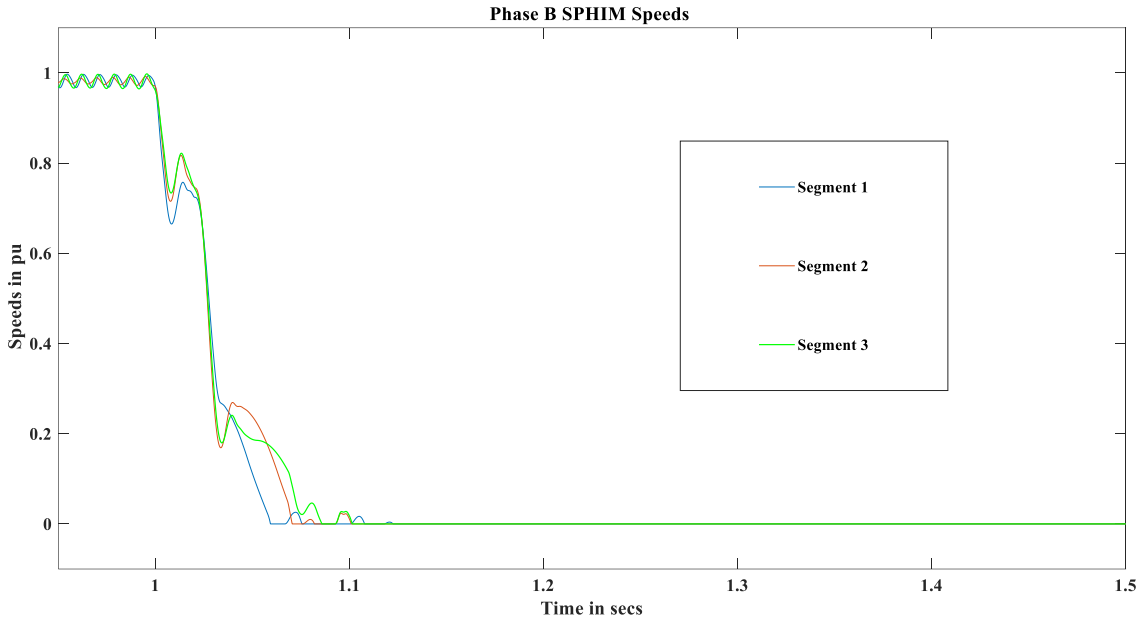

Figure 7.3 SPHIMs in all Three Segments Stalling in Phase B

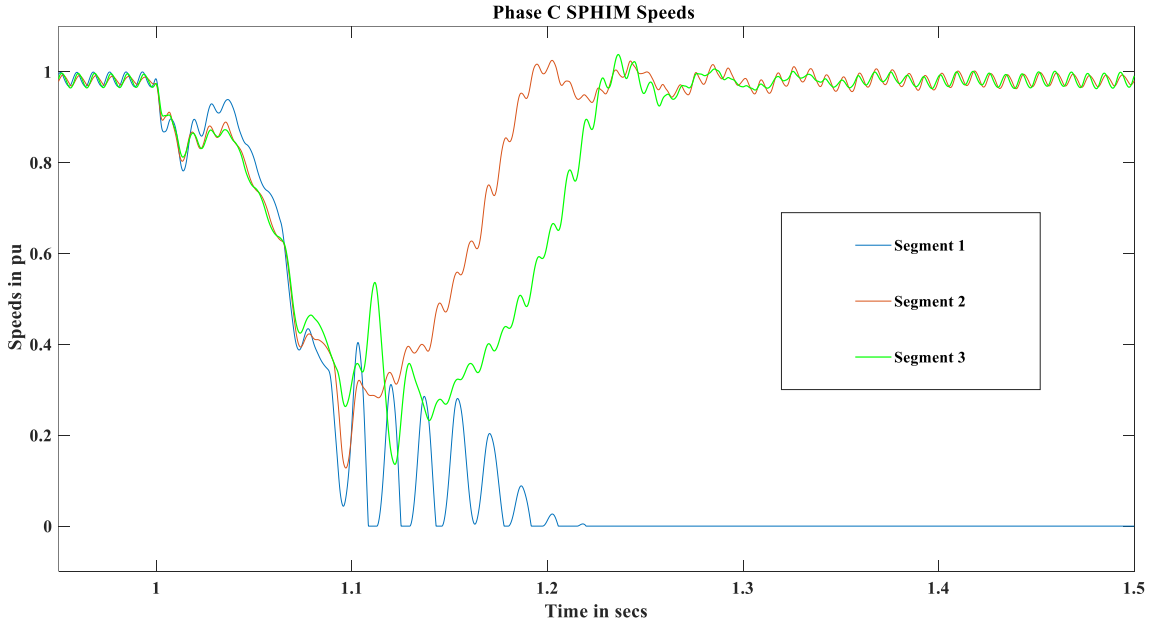

Figure 7.4 SPHIMs Only in Segment 1 Stalled in Phase C

From Figures 7.5 – 7.7, ***it can be inferred that although the general behavior of the contactors across different phases in all the segments is the same (all the contactors are chattering in this case), the timings at which the contactors start to trip and the***

timings at which the contactors completely reconnected back to the feeder is significantly different across the three-phases. It should be noted that the dashed vertical line and the solid vertical black line in Figures 7.5 – 7.7 correspond to the instants the fault is initiated and cleared respectively.

Using Figures 7.1 – 7.7, it can be concluded that it is important to develop new regression models for a given feeder for three-phase faults. Additionally, these plots provide the evidence that the current assumption (the behavior of loads in all three-phases is the same for a three-phase fault) being taken in the planning studies being done in the industry is not accurate and hence it is essential that this varied behavior of loads and the contactors across the three-phases need to be considered during load modeling studies in positive sequence simulators.

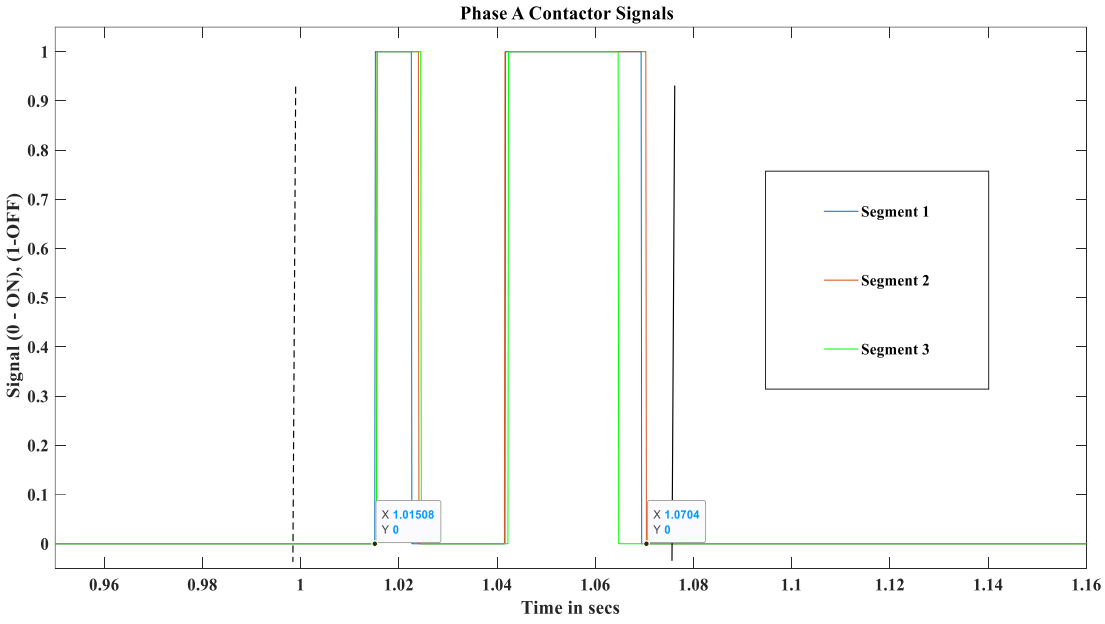

Figure 7.5 Contactors Chatter in All Three-Segments of Phase A

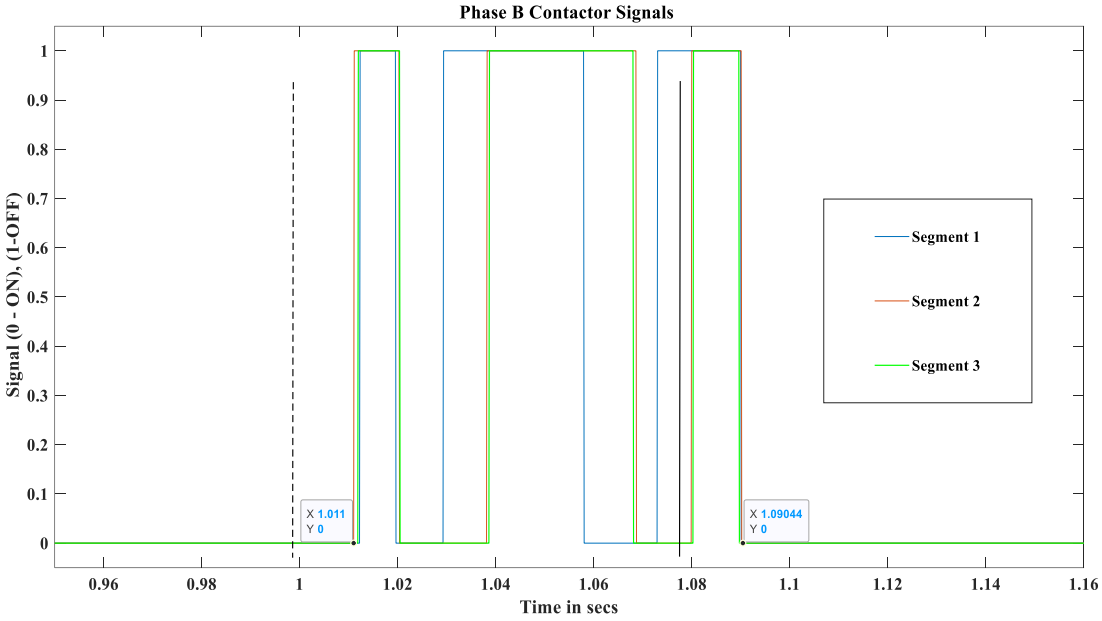

Figure 7.6 Contactors Chatter in All Three-Segments of Phase B

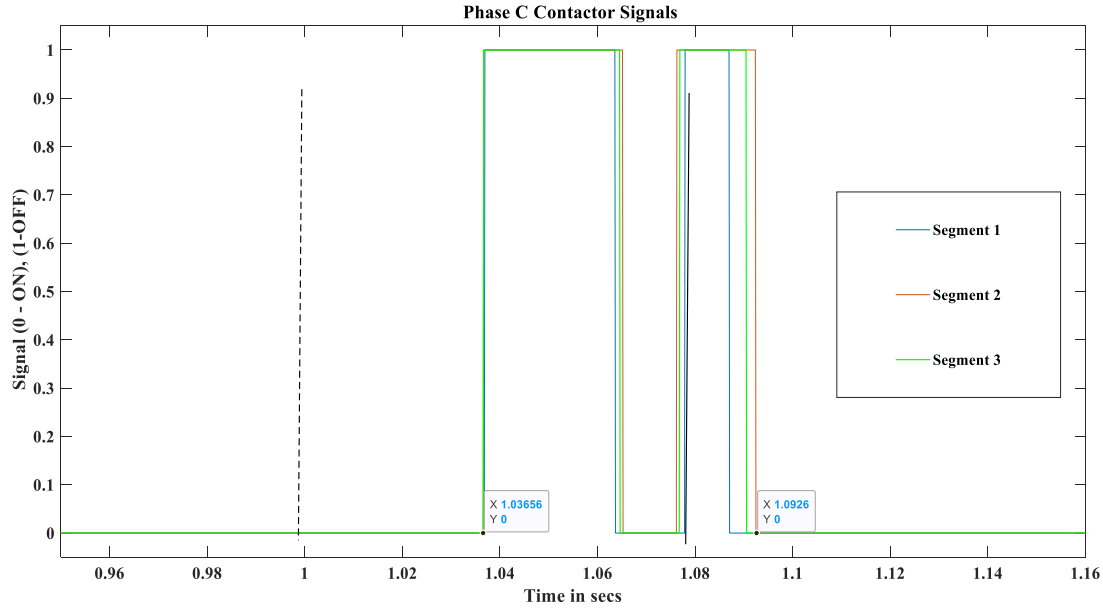

Figure 7.7 Contactors Chatter in all Three-Segments of Phase C

7.2 Analysis and Results of the New Algorithm Development for Three-Phase Faults

Overall, the same general idea of the algorithm that is used to estimate the contactor

trip and reconnection features and the SPHIM stalling behavior, in Chapter 5, is used for the analysis of three-phase faults in this Chapter on the same three-phase, three-segment feeder model (Figure 3.13) with the following modifications –

- **Fault Angle *'FA'*** – As there are three-phases involved in three-phase fault analysis (as opposed to a single-phase in SLG faults), the bounds for the parameter *'FA'* have been considered to be from 0^0 to 120^0. This is because considering only 0^0 to 90^0 bounds would not cover the symmetrical quarter cycle nature of the fault angles for all three-phases.
- ***'T1'* and *'T2'*** – From Figures 7.5 – 7.7, it is observed that the timings at which the contactors start to trip and reconnect completely is different in all three-phases. Therefore, the *'T1'* and *'T2'* for a particular test case is calculated based on the earliest instant at which any of the 9 contactors in the feeder starts to trip and the last instant at which any of the 9 contactors along the feeder reconnects back respectively.

Therefore, considering the above modifications, initially, 300 new test cases are generated (*'FR'* and *'FD'* parameters are the same from the 300 SLG test cases generated in the earlier Chapters), and the following results are obtained.

➢ **Contactor Modeling Results:**

The behavior of the contactors in all the segments and in all the phases for almost all the cases are observed to be of the same status. Using linear regression, the contactor status has been estimated with an accuracy of 96%. The final linear regression expression obtained for three-phase fault analysis is as given below in (7.1).

$$ST_{3ph} = 1.72 + 0.0037*FA_{3ph} + 0.0029*FD_{3ph} - 1.044*FN_{3ph} \quad (7.1)$$

Where, ST_{3ph} is the estimated status of the contactor (0 – no-tripping, 1.5 – chattering and 3 for tripping), FA_{3ph}, FD_{3ph} and FN_{3ph} are the fault angle, fault duration and the PS feeder head voltage nadir normalized using its pre-fault steady state voltage input parameter used in three-phase fault analysis respectively.

Using the same methodology (by tuning the hyperparameters of DNN regression models using Google Colab python scripts and using the same inputs) that has been used to estimate the contactor trip and reconnection settings for SLG faults, the contactor features are estimated in this Chapter for three-phase faults with good accuracy. The DNN details (hyperparameters) and the accuracy of the developed regression models has been presented below in Table 7.1 and Table 7.2 respectively.

Table 7.1 Final Chosen Hyperparameters for the Developed DNN Models in this Work for Three-Phase Faults Analysis

Model Number	**Estimated Output Parameter**	**Number of Hidden Layers**	**Number of neurons for each hidden layer respectively**	**Number of iterations before the training process is terminated**
DNN Model 8	*'$T1_{3ph}$'*	4	20, 10, 5 and 5	400
DNN Model 9	*'$V1_{3ph}$'*	5	20, 7, 10, 5 and 5	1500
DNN Model 10	*'$T2_{3ph}$'*	4	13, 7, 13 and 7	900
DNN Model 11	*'$V2_{3ph}$'*	5	10, 8, 6, 4 and 3	4000

From Table 7.2, it can be clearly seen that the estimated contactor parameters are validated because both the *'$T1_{3ph}$'* and *'$T2_{3ph}$'* parameters are estimated within ± 1 PSLF time step accuracy error (quarter cycle) and both the *'$V1_{3ph}$'* and *'$V2_{3ph}$'* parameters are

estimated within the desired 5% voltage error bandwidth.

Table 7.2 Demonstration of the Overall Performance of the Developed DNN Models for Three-Phase Faults Analysis

Model	**Average Training RMS Error**	**Average Testing RMS Error**
'$T1_{3ph}$' DNN model	2.43 ms	2.75 ms
'$V1_{3ph}$' DNN model	0.011 pu (1.1 % pu)	0.021 pu (2.1 % pu)
'$T2_{3ph}$' DNN model	3.19 ms	2.9 ms
'$V2_{3ph}$' DNN model	0.027 pu (2.7 % pu)	0.049 pu (4.9% pu)

- **<u>SPHIM Stalling Results and Discussion:</u>**

The same methodology (by developing *'TMS'* and *'IMS'* DNN models) that has been used in SLG faults analysis is employed here to estimate the number of SPHIMs that stalled across the three-segments and across the three-phases for any given test case. However, the key difference between the SLG faults (the 'TMS' and 'IMS' DNN models are developed for only the faulted phase as the SPHIMs in the non-faulted phases are unaffected) to this analysis lies in developing the *'TMS'* and *'IMS'* models for all three-phases separately (as the SPHIMs in all three-phases could stall for three-phase faults). Using this procedure, it was observed for the given 300 test cases, the maximum accuracy of the *'TMS'* models (in all three-phases) is observed to be around 77%. Therefore, the number of test cases has been increased to 900 (using 720 training and 180 testing cases partition) which helped increase maximum accuracy to climb up to 83%. This clearly shows that for the given analysis to be successful a lot more (thousands!) test cases need

to be generated to achieve a desirable accuracy of more than 95% for all three- phases *'TMS'* and *'IMS'* models. This is to be expected because, as shown in Figures 7.2- 7.4, for similar kind of inputs from SLG fault analysis, there are 9 different possible outputs (9 SPHIMs across the feeder) for any test case rather than 3 possible outputs (for SLG faults only phase A SPHIMs are affected) which increases the complexity between the inputs and the outputs relationship for the *'TMS'* and *'IMS'* DNN models. To capture this complex non-linear relationship, it is recommended to increase the number of hyperparameters (number of hidden layers and the number of neurons in each hidden layers) in the DNN models for which more test cases need to be generated to estimate the increased number of weights and biases in the DNN models with a good accuracy.

CHAPTER 8

CONCLUSIONS AND FUTURE WORK

8.1 Conclusions

Overall, it can be concluded that, in this work, efforts were directed successfully to improve the feeder and load models currently being used in the EMT and the positive sequence power system studies. Specifically, this improvement is done in two stages as shown below:

- **Stage 1:** *Synthesizing the feeder and load model for EMT studies*

A distribution feeder representation and load models are developed in this stage of the work. An algorithmic approach is used to estimate both load composition and the load parameters using POW measurements made at the feeder substation. The algorithmic approach is applied to feeders supplying both residential and industrial/commercial areas during different seasons (summer and winter) where the loading levels are very different. The parameters and load composition obtained for the considered feeder models at the same locations are found to be consistent and validated for both summer and winter conditions using four new test cases that represent different faults occurring at different times during the year.

The proposed approach only requires limited amount of data for events such as transmission faults observed at the head of the feeder. The proposed algorithm effectively obtains both the load composition and load parameters and is able to capture FIDVR type events that cause severe voltage stability issues in the system. It was also observed that the loading conditions (summer or winter conditions) do not significantly impact the

parameters obtained for the motor loads for a particular feeder.

Local utilities can also use the proposed methodology to obtain an accurate estimation of the load composition for the feeders of interest, according to their loading conditions, in their systems as the current practice for them is to use a pre-determined fixed load composition in their power system simulation studies.

- **Stage 2:** *Improving the proposed feeder and load model obtained from Stage 1 further by integrating the contactor model for the protection of SPHIM load.*

In this stage, the analytical formulation of a 24 V EMT contactor model is developed in this work. The parameters of the proposed contactor model are chosen to mimic the behavior of the two laboratory tested contactors [49] under various voltage sag levels. It was observed that it takes less than 1 cycle for the contacts to separate electrically when the contactor trips under low voltage conditions.

The developed 24 V EMT contactor is tested, on the three-segment three-phase distribution feeder model obtained from Stage 1 in this work, to analyze the behavior of the SPHIMs in the feeder model. It was observed that the system response is significantly different when the proposed contactor model is employed for the protection of SPHIMs when compared to the system response obtained with no contactors present along the feeder. It was also observed that the system response is significantly different, for a scenario where a contactor logic, based on [13], is utilized to trip the SPHIMs under low voltage conditions when compared to the scenario using the proposed EMT contactors. This is to be expected because the tripping logic currently being used in the positive sequence simulators does not capture the detailed dynamics of the EMT contactor.

Therefore, efforts were directed to represent the key performance characteristics of

the developed EMT contactor to trip the 'motorc' SPHIM model in positive sequence PSLF simulations. This was accomplished by developing regression models, such as deep neural networks and multivariable linear regression models, to estimate the critical tripping (*'T1'*, *'V1'*) and reconnection settings (*'T2'*, *'V2'*) of the proposed EMT contactor model with good accuracy. It was also observed that the time taken for the contactors to start to act (either chattering or tripping) is significantly different when the value of the positive sequence feeder head voltage nadir falls just below or stays above the 0.85 pu threshold. In addition to this, two other DNN models have been developed (*'TMS'* and *'IMS'* DNN models) to estimate the SPHIM stalling behavior with more than 95% accuracy.

Using the estimated trip and reconnection settings of the EMT contactor and the SPHIM stalling behavior, the 'motorc' model (in a circuit structure set up similar to the developed PSCAD feeder and load model) was tripped, reconnected back to the feeder and stalled at appropriate moments successfully. It was observed that the system response is significantly different between the cases with no contactor and with contactor/motor stalling action (whose trip, reconnection and stalling parameters are obtained from the developed linear regression model and the DNN models) in the 'motorc' model. It was also observed that by including the developed regression models into the PSLF framework, the PSLF system response (voltage response at the head of the feeder) is very close to the response observed from its corresponding PSCAD simulation immediately after the 'motorc' is reconnected and stalled (if necessary). This clearly shows that the proposed methodology to trip, reconnect and stall the 'motorc' SPHIM models in PSLF (positive sequence simulations) has significantly improved the accuracy of the system response. It was also observed that for less severe faults (which do not lead to contactors acting during

the fault), the PSLF system response is close to the PSCAD system response as the utility of the developed regression models becomes unnecessary in this scenario.

Using the local utility feeder topological and loading data, a modified three-phase segment feeder model was successfully developed. It was observed that the contactor features and the motor stalling behavior is either the same or very close, for both the proposed original three-phase three-segment feeder model and the modified feeder model, for both the no-tripping and fully tripped test cases. However, for the contactor chattering test case, the contactor features obtained for both the feeders (using the same fault parameters as inputs) is significantly different and it can be concluded that the proposed feeder model in this work needs to be modified based on the available local utility topological and loading data to make the proposed methodology more realistic in nature.

For three-phase faults, it was observed that the contactors features and the SPHIM stalling behavior is significantly different for all the three-phases due to the impact of the difference in the moment of fault initiation in all three sinusoidal voltage waveforms across the three-phases. Therefore, the methodology to estimate the contactor features and the SPHIMs stalling behavior for SLG faults, has been modified slightly to develop new regression models (both linear regression model and DNN models) that estimates the contactor status trip and reconnection characteristics with a good accuracy. Additionally, a discussion is provided to obtain the desired accuracy to estimate SPHIM stalled behavior using new DNN regression models by generating thousands of test cases.

8.2 Future Work

The proposed methodology is developed and implemented to trip the 'motorc' model in PSLF for a particular loading condition of the system. Additionally, a single set of load parameters were used in the considered feeder models while developing the proposed DNN methodology to estimate the contactor and motor stalling features. Therefore, it is important to develop this methodology further to become more robust and generic in nature by training the proposed feeder model at different loading conditions (high load level, moderate load level, low load level in both summer and winter conditions) and using a different sets of load parameters (within realistic bounds) such that the contactor and motor stalling features can be estimated as a function of load composition and the load parameters using DNN regression models to capture this complex relationship. This is very important because as, as discussed in this report, the developed regression models in this work need to be re-trained with a new data set when there are significant changes in the proposed feeder model and hence this would be impractical in planning studies for the engineers where every feeder in the grid would have a different load composition and has a different set of load parameters.

The proposed methodology, to trip, reconnect and stall the 'motorc' model needs to be tested more rigorously using large grid networks such as in a 15000-bus WECC system to study the impact (due to the inclusion of the developed regression models in the distribution system) on the high voltage levels parts of the transmission system using positive sequence simulators.

From the results presented in Chapter 7, it can be clearly seen that there is a growing

need to direct the efforts towards bridging the gap between the utilization of the benefits (ability to capture the POW characteristics) of an EMT simulator into PS simulators without compromising on the computational burden issue (requiring thousands of test cases to be trained for three-phase fault analysis for estimating motor stalling behavior which would take weeks to generate the data!) it is associated with.

REFERENCES

[1] Vittal, Vijay, James D. McCalley, Paul M. Anderson, and A. A. Fouad, *Power system control and stability*, Third Edit. John Wiley & Sons, 2019.

[2] P. Kundur, *Power System Stability and Control* (The EPRI Power System Engineering Series). New York, NY, USA: McGraw-Hill, 1994.

[3] A. Arif, Z. Wang, J. Wang, B. Mather, H. Bashualdo and D. Zhao, "Load Modeling—A Review," in IEEE Transactions on Smart Grid, vol. 9, no. 6, pp. 5986-5999, Nov. 2018, doi: 10.1109/TSG.2017.2700436.

[4] S. Nekkalapu, V. Vittal, J. Undrill, B. Keel, B. Gong and K. Brown, "Synthesis of Load and Feeder Models Using Point on Wave Measurement Data," in IEEE Open Access Journal of Power and Energy, vol. 8, pp. 198-210, 2021, doi: 10.1109/OAJPE.2021.3079724.

[5] Q. Zhang et al., "Transmission Expansion Planning Coordinated with Distribution Networks Considering High Renewable Energy Penetration," 2020 IEEE Sustainable Power and Energy Conference (iSPEC), 2020, pp. 415-422, doi: 10.1109/iSPEC50848.2020.9351027.

[6] S. Nekkalapu, "Standard Feeder and Load Model Synthesis using Voltage and Current Measurements", " M.S. Thesis, School of ECEE, Arizona State University, 2018.

[7] GE-PSLF 18.01 user manual, General Electric Intl. Ltd, Schenectady, USA, 2021.

[8] B. Choi and H. Chiang, "Multiple Solutions and Plateau Phenomenon in Measurement-Based Load Model Development: Issues and Suggestions," in IEEE Transactions on Power Systems, vol. 24, no. 2, pp. 824-831, May 2009.

[9] Siming Guo and T. J. Overbye, "Parameter estimation of a complex load model using phasor measurements," 2012 IEEE Power and Energy Conference at Illinois, Champaign, IL, 2012, pp. 1-6.

[10] D. Kosterev et al., "Load modeling in power system studies: WECC progress update," 2008 IEEE Power and Energy Society General Meeting - Conversion and Delivery of Electrical Energy in the 21st Century, 2008, pp. 1-8, doi: 10.1109/PES.2008.4596557.

[11] Bradley Williams, Wayne Schmus, Douglas Dawson, "Transmission Voltage Recovery Delayed by Stalled Air Conditioner Compressors," IEEE Transactions on Power Systems, vol.7, no.3, pp.1173-1181, August 1992.

[12] Y. Liu, V. Vittal, J. Undrill and J. H. Eto, "Transient Model of Air-Conditioner Compressor Single Phase Induction Motor," in IEEE Transactions on Power Systems, vol. 28, no. 4, pp. 4528-4536, Nov. 2013.

[13] Technical Reference Document: Dynamic Load Modeling, North American Reliability Corporation (NERC), Dec 2016.

[14] "Load representation for dynamic performance analysis (of power systems)," in IEEE Transactions on Power Systems, vol. 8, no. 2, pp. 472-482, May 1993, doi: 10.1109/59.260837.

[15] L. Wang, J. Jatskevich, C. Wang and P. Li, "A Voltage-Behind-Reactance Induction Machine Model for the EMTP-Type Solution," in IEEE Transactions on Power Systems, vol. 23, no. 3, pp. 1226-1238, Aug. 2008.

[16] D. Wang, K. Turitsyn and M. Chertkov, "DistFlow ODE: Modeling, analyzing and controlling long distribution feeder," 2012 IEEE 51st IEEE Conference on Decision and Control (CDC), Maui, HI, USA, 2012, pp. 5613-5618, doi: 10.1109/CDC.2012.6426054.

[17] J. M. Undrill and R. E. Clayton, "Distribution line performance with imperfect grounding," IEEE Transactions on Industry Applications, vol. 24, no. 5, pp. 805-811, Sep/Oct 1988.

[18] PSCAD/EMTDC user manual, Manitoba HVDC, 2016.

[19] M. Yao D. K. Molzahn and J. L. Mathieu "The impact of load models in an algorithm for improving voltage stability via demand response" Proc. IEEE Annu. Allerton Conf. Commun. Control Comput. pp. 149-156 Jan. 2017.

[20] S. Son S.H. Lee D. Choi K. Song J. Park Y. Kwon et al. "Improvement of Composite Load Modeling Based on Parameter Sensitivity and Dependency Analyses" IEEE Trans. on Power Systems vol. 29 no. 1 pp. 242-250 2014.

[21] P. Etingov. (2019). Load Model Data Tool (LMDT). [Online]. Available: https://svn.pnl.gov/LoadTool.

[22] A. Gaikwad, P. Markham and P. Pourbeik, "Implementation of the WECC Composite Load Model for utilities using the component-based modeling approach," 2016 IEEE/PES Transmission and Distribution Conference and Exposition (T&D), Dallas, TX, 2016, pp. 1-5.

[23] J. V. Milanovic, et. al, "International Industry Practice on Power System Load Modeling," in IEEE Transactions on Power Systems, vol. 28, no. 3, pp. 3038-3046, Aug. 2013.

[24] K. P. Schneider, J. C. Fuller, and D. P. Chassin, “Multi-state load models for distribution system analysis,” IEEE Trans. Power Syst., vol. 26, no. 4, pp. 2425–2433, Nov. 2011.

[25] S. Pandey et al., “Online estimation of steady-state load models considering data anomalies,” IEEE Trans. Industry Appl., vol. 54, no. 1, pp. 712– 721, Jan. 2018.

[26] X. Wang, Y. Wang, D. Shi, J. Wang and Z. Wang, "Two-Stage WECC Composite Load Modeling: A Double Deep Q-Learning Networks Approach," in IEEE Transactions on Smart Grid, vol. 11, no. 5, pp. 4331-4344, Sept. 2020.

[27] K. Yamashita, M. Asada and K. Yoshimura, "A development of dynamic load model parameter derivation method," 2009 IEEE Power & Energy Society General Meeting, Calgary, AB, 2009, pp. 1-8.

[28] Positive Sequence Load Flow software (PSLF), General Electric, 2021.

[29] Y. Liu, et. al, Open-Source High Fidelity Aggregate Composite Load Models of Emerging Load Behaviors for Large-Scale Analysis. PNNL, Richland, WA:2020.

[30] B. Park and M. Olama, "Mitigation of Motor Stalling and FIDVR via Energy Storage Systems with Temporal Logic Specifications," in IEEE Transactions on Power Systems, doi: 10.1109/TPWRS.2020.3012625.

[31] Q. Huang and V. Vittal, "Application of Electromagnetic Transient-Transient Stability Hybrid Simulation to FIDVR Study," in IEEE Transactions on Power Systems, vol. 31, no. 4, pp. 2634-2646, July 2016.

[32] R. Bravo, et. al, Final Project Report Load Modeling Transmission Research, Lawrence Berkeley National Laboratory (LBNL), Mar.2010.

[33] Badrzadeh, B, Electromagnetic Transient Simulation Models for Large-Scale System Impact Studies in Power Systems Having a High Penetration of Inverter-Based Resources; Technical Report; Energy Systems Integration Group: Reston, VA, USA, 2019.

[34] Badrzadeh, B., Emin, Z., Hillberg, E., Jacobson, D., Kocewiak, L. H., Lietz, G., Silva, F. M. F. D., & val Escudero, M. (2020). The Need for Enhanced Power System Modelling Techniques and Simulation Tools. CIGRE Science & Engineering, 17(February), 30-46.

[35] A. Shahsavari, M. Farajollahi and H. Mohsenian-Rad, "Individual Load Model Parameter Estimation in Distribution Systems Using Load Switching Events," in IEEE Transactions on Power Systems, vol. 34, no. 6, pp. 4652-4664, Nov. 2019.

[36] J. Nocedal and S. J. Wright, Numerical Optimization. NewYork,NY, USA: Springer-Verlag, 2006.

[37] D. Kosterev and A. Meklin, "Load Modeling in WECC," 2006 IEEE PES Power Systems Conference and Exposition, Atlanta, GA, USA, 2006, pp. 576-581, doi: 10.1109/PSCE.2006.296381.

[38] E. A. Yahaya. (2015). Advantage of Double Cage Rotor over Single Cage Rotor Induction Motor. IISTE Journals. [Online]. Vol.6, No.12. Available: https://pdfs.semanticscholar.org/993e/57857a1d146e3107277e85220a96c5760e35.pdf

[39] Advanced Load Modeling, EPRI, Palo Alto, CA, and Public Service Company of New Mexico, Albuquerque, NM: 2002. 1007318.

[40] Measurement-Based Load Modeling. EPRI, Palo Alto, CA: 2006. 1014402.

[41] A. Faris, et. al, Load Composition Analysis in Support of the NERC Load Modeling Task Force 2019-2020 Field Test of the Composite Load Model, Lawrence Berkeley National Laboratory (LBNL), Jun.2020.

[42] W. Kanokbannakorn, T. Saengsuwan and S. Sirisukprasert, "The modeling of AC magnetic contactor for immunity studies and voltage sag assessment," The 8th Electrical Engineering/ Electronics, Computer, Telecommunications and Information Technology (ECTI) Association of Thailand - Conference 2011, 2011, pp. 621-624, doi: 10.1109/ECTICON.2011.5947916.

[43] Saengsuwan, Trin. (2018), “An improved AC electromagnetic contactor model based on EMTP” IEEJ Transactions on Electrical and Electronic Engineering. 13. 10.1002/tee.22497.

[44] Y. Liu et al., "Impact of Building-Level Motor Protection on Power System Transient Behaviors," 2018 IEEE Power & Energy Society General Meeting (PESGM), 2018, pp. 1-5, doi: 10.1109/PESGM.2018.8586530.

[45] S. Fang, H. Lin and S. L. Ho, "Magnetic Field Analysis and Dynamic Characteristic Prediction of AC Permanent-Magnet Contactor," in IEEE Transactions on Magnetics, vol. 45, no. 7, pp. 2990-2995, July 2009, doi: 10.1109/TMAG.2009.2015053.

[46] J. Pedra, F. Corcoles and L. Sainz, "Study of AC contactors during voltage sags," 10th International Conference on Harmonics and Quality of Power. Proceedings (Cat. No.02EX630), 2002, pp. 565-570 vol.2, doi: 10.1109/ICHQP.2002.1221497

[47] S. W. Jeong, G. J. Lee and J. H. Gim, "The study on the characteristics of operating limits of AC contactor during voltage sag," 2009 Transmission & Distribution Conference & Exposition: Asia and Pacific, 2009, pp. 1-4, doi: 10.1109/TD-ASIA.2009.5356981.

[48] J. Cale, S. D. Sudhoff and Li-Quan Tan, "Accurately modeling EI core inductors using a high-fidelity magnetic equivalent circuit approach," in IEEE Transactions on Magnetics, vol. 42, no. 1, pp. 40-46, Jan. 2006, doi: 10.1109/TMAG.2005.859439.

[49] Karady, George G., Saurabh Saksena, Baozhuang Shi, and Nilanjan Senroy. "Effects of voltage sags on loads in a distribution system." Power System Engineering Research Centre (2005).

[50] Vittal, Vijay, Le Xie, Sameer Nekkalapu, Xinbo Geng, and Athindra Venkatraman. " Improved Dynamic Load Modeling Using Power System Measurements for Enhanced Transmission and Distribution System Operation and Planning." Power System Engineering Research Centre (2021).

[51] I. Keka and B. Çiço, "Pattern detection of load profiles based on regression model with multiple variables," 2018 7th Mediterranean Conference on Embedded Computing (MECO), 2018, pp. 1-4, doi: 10.1109/MECO.2018.8406001.

[52] M. V. Selvi and S. Mishra, "Investigation of Performance of Electric Load Power Forecasting in Multiple Time Horizons With New Architecture Realized in Multivariate Linear Regression and Feed-Forward Neural Network Techniques," in IEEE Transactions on Industry Applications, vol. 56, no. 5, pp. 5603-5612, Sept.-Oct. 2020, doi: 10.1109/TIA.2020.3009313.

[53] Kramer, Matthew. "R2 statistics for mixed models." Proceedings of the conference on applied statistics in agriculture. Vol. 17. 2005.

[54] W. Li, L. Xing, K. Huang, Q. Ai and L. Wang, "Generalized Load Modeling Method Based on Clustering and Neural Network," 2020 International Conference on Artificial Intelligence in Information and Communication (ICAIIC), 2020, pp. 619-622, doi: 10.1109/ICAIIC48513.2020.9065202.

[55] P. Gupta, "Coordinated Wide-Area Control of Multiple Controllers in a Modern Power System", " P.h.D. Thesis, School of ECEE, Arizona State University, 2021.

[56] Siddhartha Khaitan. A Survey Of Techniques for using Neural Networks in Power Systems. 2017.

[57] Haque, Mehrdad Tarafdar and Atabak Mashhadi Kashtiban. “Application of Neural Networks in Power Systems; A Review.” *International Journal of Energy and Power Engineering* 1 (2007): 897-901.

[58] M. Bernico, Deep Learning Quick Reference: Useful Hacks for Training and Optimizing Deep Neural Networks with TensorFlow and Keras. Packt Publishing Ltd, 2018.

[59] J. Heaton, “T81-558: Applications of deep neural networks: module 3 and module 4.”

[60] Z. Zhang, "Improved Adam Optimizer for Deep Neural Networks," 2018 IEEE/ACM 26th International Symposium on Quality of Service (IWQoS), 2018, pp. 1-2, doi: 10.1109/IWQoS.2018.8624183.

[61] https://www.tensorflow.org/api_docs/python/tf/keras

[62] B. Lesieutre, D. Kosterev and J. Undrill, "Phasor modeling approach for single phase A/C motors," 2008 IEEE Power and Energy Society General Meeting - Conversion and Delivery of Electrical Energy in the 21st Century, 2008, pp. 1-7, doi: 10.1109/PES.2008.4596554.

[63] Kamada, Tomihisa, and Satoru Kawai. "An algorithm for drawing general undirected graphs." Information processing letters 31.1 (1989): 7-15.

APPENDIX A

SEQUENCE DATA AND DYNAMIC DATA USED TO CONDUCT THE SHORT-CIRCUIT STUDY (TO ESTIMATE THE EQUIVALENT FAULT IMPEDANCE FOR A SLG FAULT) AND DYNAMIC RUN IN PSLF RESPECTIVELY

#Start of Sequence Data

bus 1 ! 69 ! : 1 0 1 1

bus 2 ! 69 ! : 1 0 1 1

bus 3 ! 12.47 ! : 1 0 1 1

bus 4 ! 12.47 ! : 1 0 1 1

bus 5 ! 12.47 ! : 1 0 1 1

gen 1 ! ! ! : 1 10 0.0021 0.0000001 0.0021 0.0000001 0.0021 0.0000001

line 1 ! ! ! 2 ! ! "1" 1 : 1 1 0 0.00005 0 0 0.00015 0 0 0 0 0 0 0 0 0

line 3 ! ! ! 4 ! ! "1" 1 : 1 1 0.095 0.205 0 0.2572 0.655 0 0 0 0 0 0 0 0 0

line 4 ! ! ! 5 ! ! "1" 1 : 1 1 0.095 0.205 0 0.2572 0.655 0 0 0 0 0 0 0 0 0

tran 2 ! ! ! 3 ! ! ! : 1 1 1 1 10 0 0.06 0 0 0 0 0 0.06 0 0 0 0

gen 3 ! ! "1" : 1 2.05 0 -5.55 0 -5.55 0 -5.55

gen 3 ! ! "2" : 1 1.64 0 -8.33 0 -8.33 0 -8.33

gen 4 ! ! "1" : 1 2.88 0 -5.55 0 -5.55 0 -5.55

gen 4 ! ! "2" : 1 1.64 0 -8.33 0 -8.33 0 -8.33

gen 5 ! ! "1" : 1 2.88 0 -5.55 0 -5.55 0 -5.55

gen 5 ! ! "2" : 1 1.64 0 -8.33 0 -8.33 0 -8.33

#Start of Dynamic Data
blwscc 3 "bus3" 12.47 "BL" : #9 0 1 1 0 0 0 0 0 0 0 0

blwscc 4 "bus4" 12.47 "BL" : #9 0 1 1 0 0 0 0 0 0 0 0

blwscc 5 "bus5" 12.47 "BL" : #9 0 1 1 0 0 0 0 0 0 0 0

gthev 1 "bus1" 69 "1 " : #9 mva=10 0.0021 0.000001 -1 -1 99 99

epcgen 6 ! ! ! : #9 mva=0.53 "motorc.p" 3.0 "rsrc" 0 "xsrc" 0 /

"ls" 3 "lp" 0.25 "lpp" 0.22 "ll" 0.08 "tpo" 0.2 "tppo" 0.02 "ra" 0.02 "kq" 0.8 "raq" 0.04 "xcr" 1.5 /

"se1" 0.01 "se12" 0.1 "h" 0.0568 "d" 0.0 "tav" 8 "tload1" 6.0 "flag" 0 "flag2" 0 "flag3" 1

epcgen 7 ! ! ! : #9 mva=0.53 "motorc.p" 3.0 "rsrc" 0 "xsrc" 0 /

"ls" 3 "lp" 0.25 "lpp" 0.22 "ll" 0.08 "tpo" 0.2 "tppo" 0.02 "ra" 0.02 "kq" 0.8 "raq" 0.04 "xcr" 1.5 /

"se1" 0.01 "se12" 0.1 "h" 0.0568 "d" 0.0 "tav" 8 "tload1" 6.0 "flag" 0 "flag2" 0 "flag3" 1

epcgen 8 ! ! ! : #9 mva=0.53 "motorc_Trip.p" 3.0 "rsrc" 0 "xsrc" 0 /

"ls" 3 "lp" 0.25 "lpp" 0.22 "ll" 0.18 "tpo" 0.2 "tppo" 0.02 "ra" 0.02 "kq" 0.8 "raq" 0.04 "xcr" 1.5 /

"se1" 0.01 "se12" 0.1 "h" 0.0568 "d" 0.0 "tav" 8 "tload1" 6.0 "flag" 0 "flag2" 0 "flag3" 1

epcgen 9 ! ! ! : #9 mva=0.74 "motorc.p" 3.0 "rsrc" 0 "xsrc" 0 /

"ls" 3 "lp" 0.25 "lpp" 0.22 "ll" 0.08 "tpo" 0.2 "tppo" 0.02 "ra" 0.02 "kq" 0.8 "raq" 0.04 "xcr" 1.5 /

"se1" 0.01 "se12" 0.1 "h" 0.0568 "d" 0.0 "tav" 8 "tload1" 6.0 "flag" 0 "flag2" 0 "flag3" 1

epcgen 10 ! ! ! : #9 mva=0.74 "motorc.p" 3.0 "rsrc" 0 "xsrc" 0 /

"ls" 3 "lp" 0.25 "lpp" 0.22 "ll" 0.08 "tpo" 0.2 "tppo" 0.02 "ra" 0.02 "kq" 0.8 "raq" 0.04 "xcr" 1.5 /

"se1" 0.01 "se12" 0.1 "h" 0.0568 "d" 0.0 "tav" 8 "tload1" 6.0 "flag" 0 "flag2" 0 "flag3" 1

epcgen 11 ! ! ! : #9 mva=0.74 "motorc_Trip.p" 3.0 "rsrc" 0 "xsrc" 0 /

"ls" 3 "lp" 0.25 "lpp" 0.22 "ll" 0.18 "tpo" 0.2 "tppo" 0.02 "ra" 0.02 "kq" 0.8 "raq" 0.04 "xcr" 1.5 /

"se1" 0.01 "se12" 0.1 "h" 0.0568 "d" 0.0 "tav" 8 "tload1" 6.0 "flag" 0 "flag2" 0 "flag3" 1

epcgen 12 ! ! ! : #9 mva=0.74 "motorc.p" 3.0 "rsrc" 0 "xsrc" 0 /

"ls" 3 "lp" 0.25 "lpp" 0.22 "ll" 0.08 "tpo" 0.2 "tppo" 0.02 "ra" 0.02 "kq" 0.8 "raq" 0.04 "xcr" 1.5 /

"se1" 0.01 "se12" 0.1 "h" 0.0568 "d" 0.0 "tav" 8 "tload1" 6.0 "flag" 0 "flag2" 0 "flag3" 1

epcgen 13 ! ! ! : #9 mva=0.74 "motorc.p" 3.0 "rsrc" 0 "xsrc" 0 /

"ls" 3 "lp" 0.25 "lpp" 0.22 "ll" 0.08 "tpo" 0.2 "tppo" 0.02 "ra" 0.02 "kq" 0.8 "raq" 0.04 "xcr" 1.5 /

"se1" 0.01 "se12" 0.1 "h" 0.0568 "d" 0.0 "tav" 8 "tload1" 6.0 "flag" 0 "flag2" 0 "flag3" 1

epcgen 14 ! ! ! : #9 mva=0.74 "motorc_Trip.p" 3.0 "rsrc" 0 "xsrc" 0 /

"ls" 3 "lp" 0.25 "lpp" 0.22 "ll" 0.18 "tpo" 0.2 "tppo" 0.02 "ra" 0.02 "kq" 0.8 "raq" 0.04 "xcr" 1.5 /

"se1" 0.01 "se12" 0.1 "h" 0.0568 "d" 0.0 "tav" 8 "tload1" 6.0 "flag" 0 "flag2" 0 "flag3" 1

motor1 3 "bus3" 12.47 "2" : #9 mva=0.64 3.0000 0.220000 0.010000 0.3 0.12 2.0000 0.010000 0.100000 0.850000 2.500000 /

0.100000 99.0000 1.000000 99.0000 0.500000 0.20000 0.070000 0.006700 20 1

motor1 4 "bus4" 12.47 "2" : #9 mva=0.64 3.0000 0.220000 0.010000 0.3 0.12 2.0000 0.010000 0.100000 0.850000 2.500000 /

0.100000 99.0000 1.000000 99.0000 0.500000 0.20000 0.070000 0.006700 20 1

motor1   5 "bus5"   12.47 "2" : #9 mva=0.64 3.0000 0.220000 0.010000   0.3 0.12   2.0000 0.010000

0.100000 0.850000 2.500000 /

0.100000 99.0000 1.000000 99.0000 0.500000 0.20000 0.070000 0.006700 20 1

vmetr 1 "bus1" 69 "1 " : #9 0.00000

vmetr 2 "bus2" 69 "1 " : #9 0.00000

vmetr 3 "bus3" 12.47 "1 " : #9 0.00000

vmetr 4 "bus4" 12.47 "1 " : #9 0.00000

vmetr 5 "bus5" 12.47 "1 " : #9 0.00000

imetr 3 ! ! ! 2 ! ! "1 " 1 : #9 0.0000

#imetr 1 ! ! ! 2 ! ! "1 " 1 : #9 0.0000